WASHINGTON UNIVERSITY
SEVER INSTITUTE OF TECHNOLOGY
DEPARTMENT OF CIVIL ENGINEERING

DEVELOPMENT OF A SMART DAMPING SYSTEM FOR AIRCRAFT AVIONICS

by

Suzy M. Hyun

Prepared under the direction of Professor Shirley J. Dyke

A thesis presented to the Sever Institute of
Washington University in the partial fulfillment
of the requirements of the degree of

MASTER OF SCIENCE

December, 2001

Saint Louis, Missouri

WASHINGTON UNIVERSITY
SEVER INSTITUTE OF TECHNOLOGY
DEPARTMENT OF CIVIL ENGINEERING

ABSTRACT

DEVELOPMENT OF A SMART DAMPING SYSTEM FOR AIRCRAFT AVIONICS

by Suzy M. Hyun

ADVISOR: Professor Shirley J. Dyke

December, 2001
Saint Louis, Missouri

This thesis presents the results of research to develop effective control strategies to achieve acceleration reduction in avionics components for high performance aircraft applications. Five control devices described herein: an ideal active device, an ideal semi-active device, a passive device, a variable orifice damper, and a magnetorheological damper. The control techniques considered include: a clipped optimal control algorithm and H_2/ LQG optimal control algorithm.

Dedicated to

Gonçalo Rodrigues Quaresma de Macedo

(1973-1998)

In memoriam

the victims

of the terrorist attacks

9 - 11 - 2001

“However beautiful the strategy,

you should occasionally look at the results.”

-Winston Churchill

Contents

1. Introduction 1

1.1 Research Motivation 1

1.2 Literature Review 3

1.2.1 Passive Control Devices 4

1.2.2 Active Control Devices 5

1.2.3 Semi-Active Control Devices 6

1.3 Summary 9

1.4 Objectives 9

2. Avionics Model 10

2.1 Two Degree of Freedom Avionics Model 10

2.1.1 Equations of Motion 12

2.1.2 Parameters for the Avionics Model 16

2.1.3 State Space System 17

2.2 Properties of the Model 20

2.2.1 Eigenvalues 20

2.3 Summary 23

3. Development of Control Strategies for Avionics System 24

3.1 Controllability 25

3.2 Observability 26

3.3 H/LQG Control Design 27

3.3.1 Linear Quadratic Regulator (LQR) 28

3.3.2 Kalman Filter Estimator 31

3.4 Ideal Control Device Models 32

3.4.1 Ideal Active Control Device Model 32

3.4.2 Ideal Semi-Active Model 33

3.4.3 Passive Case 35

3.5 Control Device Location 36

3.6 Summary 38
4. Ideal Control Device Performance 39
4.1 Parameters 39
4.2 Ideal Active Controller Performance 41
4.2.1 Parameters used for Ideal Active Control 41
4.2.2 Q Matrix Selection: Case Ai 42
4.2.3 Selection of Q Matrix Weighting for Various CG Cases 46
4.2.4 Parametric Study of Control Device Location 50
4.3 Ideal Passive Controller Performance 53
4.3.1 Behavior of Ideal Passive Viscous Damper 53
4.3.2 Damping Coefficient Selection 57
4.3.3 Parametric Study of Control Device Location 58
4.4 Ideal Semi-Active Device Performance 61
4.4.1 Parameters used for Ideal Semi-Active Control 61
4.4.2 Behavior of Ideal Semi Active Control Device 61
4.4.3 Q Matrix Selection: Case Ai 62
4.4.4 Selection of Q Matrix Weighting for Various CG Cases 67
4.4.5 Parametric Study of Control Device Location 69
4.5 Summary 72
5. Semi-Active Device Modeling 74
5.1 MR Damper 75
5.1.1 MR Damper Device Model 76
5.2 Clipped Optimal Control Algorithm 77
5.3 Variable Orifice Damper 79
5.3.1 Variable Orifice Damper 80
5.4 Summary 81
6. Performance of Semi-Active Devices 82
6.1 MR Damper Performance 83
6.1.1 Parameters used for MR Damper Control 83

6.1.2 Behavior of the MR Damper 84
6.1.3 Q Matrix Weighting: Case Ai 87
6.1.4 Parametric Study of Control Device Location 93
6.2 Variable Orifice Damper 97
6.2.1 Parameters used for the Variable Orifice Damper 97
6.2.2 Behavior of the Variable Orifice Damper 98
6.2.3 Q Matrix Weighting: Case Ai 99
6.2.4 Selection of Q Matrix Weightings for Varying CG Cases 100
6.2.5 Parametric Study for Control Device Location 102
6.3 Summary 107
7. Comparison of Performance 108
7.1 Best Overall Performance 109
7.2 Summary of Numerical Study Results 114
8. Final Remarks 116
8.1 Summary 116
8.2 Conclusions 117
8.3 Future Research 118
. VITA 125

Tables

2-1. Parameters used for numerical analysis 16
2-2. Definition of the CG cases 17
3-1. Parameters for the control force locations 37
4-1. Ideal active control system performance: Case Ai 46
4-2. Ideal active control system performance: Case Bi 47
4-3. Ideal active control system performance: Case Ci 47
4-4. Ideal active control system performance: Case Di 48
4-5. Ideal active control system performance: Case A, B, C, D 52
4-6. Passive control system performance: Cases Ai, Bi, Ci and Di 58
4-7. Passive control system performance: Cases A,B,C, and D 59
4-8. ISA control system performance: Case Ai 67
4-9. ISA control system performance: Case Bi 68
4-10. ISA control system performance: Case Ci 68
4-11. ISA control system performance: Case Di 69
4-12. ISA control system performance: Case A, B, C, and D 71
4-13. ISA control system performance:
various control force and CG cases 72
6-1. MR damper performance: Case Ai 91
6-2. MR damper performance: Case Bi 92
6-3. MR damper performance: Case Ci 92
6-4. MR damper performance: Case Di 93
6-5. MR damper performance for different control force location trade study 95
6-6. MR damper control system performance:
fixed controller design 96
6-7. VO Damper Performance: Case Ai 102
6-8. VO damper performance: Case Bi 102
6-9. VO damper performance: Case Ci 103

6-10. VO damper performance: Case Di 103
6-11. VO damper performance for different control force locations 104
6-12. VO damper control system performance 106
6-13. VO damper "best overall" performance 107
7-1. Best overall performance case comparison:
Cases Ai, Bi, Ci, and Di 111

Figures

1-1. a) A highly damped isolator, b) typical avionics mounting configurations for aircraft and helicopter applications .....
i. bulkhead mounting, ii. inverted mounting, and iii. upright mounting
(Photos reproduced from Barry Controls Catalog) 2
2-1. Two degree of freedom model 12
2-2. Top view of avionics plate model 12
2-3. Definition of CG cases considered 17
2-4. Open loop transfer functions for the different CG cases 22
2-5. First and second natural frequencies as the CG varies 22
3-1. General feedback block diagram 24
3-2. Block diagram for LQG control design 28
3-3. Force vs. velocity envelope for ISA device 34
3-4. Block diagram with an ideal semi active controller 34
3-5. Block diagram of avionics with an ideal passive device 36
3-6. Different control force locations 37
3-7. Closed loop transfer functions for the CG cases 38
4-1. Ideal active displacements
RMS vs. weights for Case Ai 42
4-2. Ideal active absolute acceleration
RMS vs. weights for Case Ai 43
4-3. Ideal active maximum control force
RMS vs. weights for Case Ai 44
4-4. Time histories for Case Ai:
uncontrolled and ideal active control
a) displacement, b) absolute acceleration, and c) control force 45

4-5. Demonstration of selection process for best overall performance case
% reduction for displacement and acceleration vs. index
with Case Ai and weight 49
4-6. Demonstration of selection process for best overall performance case
% reduction for displacement and acceleration vs. index
with Case Ai and weight 49
4-7. Control force location vs. i) , ii) , iii) , and iv)
for each CG location case
Note:(CG location denoted by x on origin).....51
4-8. Control Force vs. Velocity of Control Device.....54
4-9. Maximum control force vs. displacement of control device 55
4-10. Time histories for Case Ai:
uncontrolled and ideal passive control
a) displacement, b) absolute acceleration, and c) control force 56
4-11. Control force vs. damping parameter for ideal passive control.....57
4-12. Control force location vs. i) , ii) , iii) , and iv)
for each CG location case
Note:(CG location denoted by x on origin).....60
4-13. Time history of ideal semi-active device for a sinusoid input.....62
4-14. ISA displacement
RMS vs. weights for Case Ai 63
4-15. ISA absolute acceleration
RMS vs. weights for Case Ai 64
4-16. ISA maximum control force
RMS vs. weights for Case Ai 65
4-17. Time histories for Case Ai:
uncontrolled and ideal semi-active control
a) displacement, b) absolute acceleration, and c) control force 66

4-18. Control force location vs. i) , ii) , iii) , and iv)
for each CG location case
Note:(CG location denoted by x on origin).....70
5-1. Block diagram of the System with the MR Damper Model.....74
5-2. Ideal MR damper control force envelopes
a) force vs. displacement
b) force vs. velocity.....75
5-3. Mechanical model of MR damper.....76
5-4. Force vs. velocity envelope of the clipped optimal control algorithm.....78
5-5. Ideal control force envelope for variable orifice damper
a) force vs. displacement
b) force vs. velocity.....79
5-6. Force vs. Velocity of Variable Orifice Damper 81
6-1. Force vs. displacement of MR damper for a sinusoid input
with Vmax = 5 V and Vmin = 0 V.....85
6-2. Force vs. velocity of MR damper for a sinusoid input
with Vmax = 5 V and Vmin = 0 V.....86
6-3. Parametric study results for varying damping parameters of MR damper: i) force vs. displacement and ii) force vs. velocity.....86
6-4. Parametric study results for varying damping parameters of MR damper: i) force vs. displacement and ii) force vs. velocity.....87
6-5. MR damper displacement
RMS vs. weights for Case Ai.....88
6-6. MR damper absolute acceleration
RMS vs. weights for Case Ai.....88
6-7. MR damper maximum control force vs. weights
for Case Ai 89
6-8. Selection of weights for displacement reduction.....90
6-9. Selection of weights for acceleration reduction 91

6-10. Control force location vs. i) , ii) , iii) , and iv)
for each CG location case
Note:(CG location denoted by x on origin).....94
6-11. Force vs. velocity for a sinusoid input
with Vmax = 5 V and Vmin = 0 V.....98
6-12. Force vs. displacement of a variable orifice damper for a sinusoid input
with Vmax = 5 V and Vmin = 0 V.....99
6-13. VO damper displacements
RMS vs. weights for Case Ai.....100
6-14. VO damper absolute acceleration
RMS vs. weights for Case Ai.....101
6-15. VO damper maximum desired control force
RMS vs. weights for Case Ai.....101
6-16. Control force location vs. i) , ii) , iii) , and iv)
for each CG location case
Note:(CG location denoted by x on origin).....105
7-1. Comparison of best overall performance absolute accelerations 110
7-2. PSD for input, uncontrolled and controlled Case Ai:
i. active, passive, and ideal semi-active ii. MR and VO dampers.....112
7-3. PSD for input, uncontrolled and controlled: Case Bi.....113
7-4. PSD for input, uncontrolled and controlled: Case Ci.....113
7-5. PSD for input, uncontrolled and controlled: Case Di.....114
8-1. Experimental apparatus for 2DOF avionics 119

Acknowledgements

"The roots of education are bitter, but the fruit is sweet."

-Aristotle

I would like to thank Dr. Dyke for funding my masters education and research.

A special thank you to Dr. Harmon and Dr. Truman for being on my committee and for their counsel, continual support, and words of encouragement.

I would like to give a very big thank you to Linda Buckingham, Victoria Winn and Juan Caicedo for their kindness and willingness to drop everything to help me. I am very lucky to have friends like them.

Thank you to my fellow graduate students: Fu Yi, Virendra Jadhav, Laura Jansen, Osamu Yoshida, and Diego Giraldo.

I give thanks to Tesha Harris and Pat Harkins for their helpful assistance.

My parents, my sisters, and my friends. If it weren't for their love and support I would not still be standing.

Chapter 1

Introduction

1.1 Research Motivation

“Avionics are the electronics used in aviation” (Lopez, 1995). This broad definition includes, but is not limited to, any electronic instrumentation for military, commercial, helicopter, private aircraft, and spacecraft. The focus of this thesis is on avionics packages for high performance aircraft, but can be adapted for any of the aforementioned vehicles. Aircraft avionics packages are typically housed in avionics bays located beneath the cockpit, and the space in the bay is fixed once the aircraft is built. With rapid advances in technology, more avionics packages are being placed in the limited spaces. In recent years, there has emerged a new overcrowding issue, not critical, but of growing concern.

Avionics have made many advances since the “Liberty Bell”, the first American bomber built in 1917. However, since the 1970’s the avionics technology (Stavridou 1999) and the mounting of avionics packages to the bays have not changed significantly.

High performance aircraft are subject to vibrations over a large frequency range of vibrations. Some examples of contributing factors are vibrations during normal flight

operations due to the engine and wind, large shocks during take-off and landing, vibrations due to weapons firing, and a large dynamic range of motion from steady flight with slower turns to combat situations with quick maneuvers and sharp turns.

An aircraft can instantaneously experience up to 12 g's of acceleration in one turn alone. Currently, avionics packages are made to be very stiff with a natural frequency near 100 Hz. The packages are designed to be symmetric in geometry and mass distribution; which are helpful in apply the technique of vibration isolation with passive mounts. Each package can weigh up to 50 lbs.

There are typically four passive mounts, one on each of the four corners of the package. The mounts are highly damped isolators made of a elastomer or rubber. A typical Barry Controls isolator is shown in Fig. 1-1.a and typical mountings of avionics packages to the bays are shown in Fig. 1-1.b. The passive isolator mounts have fixed dynamic characteristics. These passive devices require the use of ruggedized avionics packages, increasing the weight and size of the boxes.

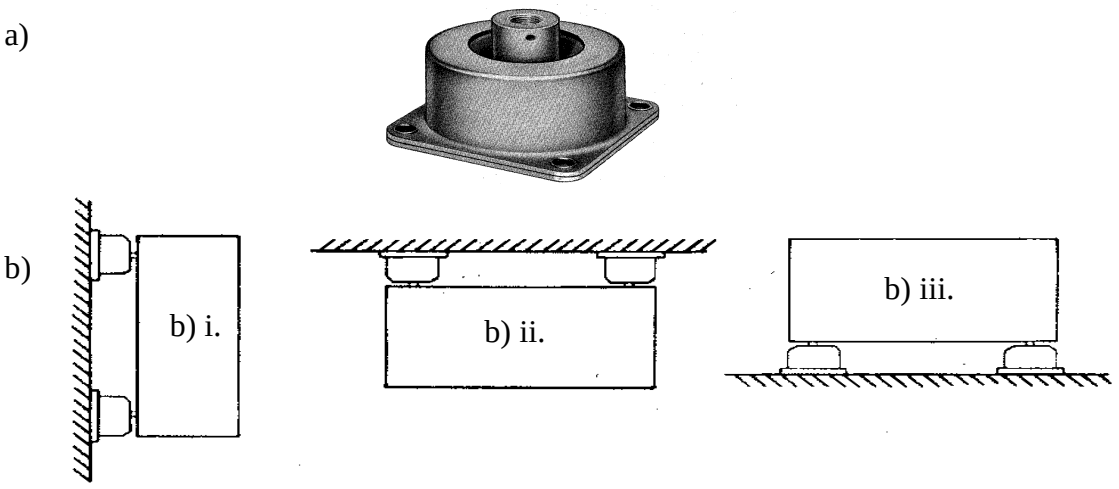

FIGURE 1-1 a) A highly damped isolator, b) typical avionics mounting configurations for aircraft and helicopter applications i. bulkhead mounting, ii. inverted mounting, and iii. upright mounting (Photos reproduced from Barry Controls Catalog)

In the aircraft industry, it is well known that even a small savings in weight can lead to significantly large savings in the fuel costs during the lifetime of the aircraft. Thus, there has always been a desire to use the most modern lighter and smaller electronics in military aircraft applications for new and existing aircraft. Due to the high vibration and shocks imparted to the avionics through the racks upon which they are mounted, the technology to protect the systems has not been available.

This research proposes the implementation of a control system to protect avionics packages by reducing the accelerations experience during take-off, landing, and flight operations. The use of such a controller would allow flexibility in the placement of the center of gravity (CG) location and softer systems with a lower natural frequency of the avionics package, near 10 Hz. This would results in less massive and smaller packages; and inexpensive technology, such as off-the-shelf computer components, can be implemented in new and existing aircraft. Avionics would be able to keep up with fast pace of electrical and software technology, ultimately shortening the process of, or eliminating the need for, ruggedization of the avionics. The reduction in weight can potentially lead to tremendous savings in cost of fuel during the lifetime of the aircraft. Last, but not least, the reduction in size of the packages addresses the overcrowding issues and can potentially allow the addition of many more avionics packages to the limited bay space. However, the approach used to allow avionic packages to have a variable CG and much lower natural frequency, disallows the uncoupling of the modes of vibration and subsequently the use of vibration isolation. The goals in the design of such a control system are to reduce accelerations, maintain acceptably small displacements, and ensure the avionics survival in the harsh aircraft environment.

1.2 Literature Review

Passive devices are purely dissipative devices that cannot input energy into the system. The damping coefficient, or some similar parameter for the system, is fixed. Purely active devices require an external power supply and exhibit superior tracking and control

performance. However, they typically require a significant power supply and associated increase in hardware, such as compressors or pumps. These additional components increase cost and introduce reliability issues due to introduction of more moving parts (Hrovat, 1988). Semi-active control offers the reliability of a passive devices and the versatility and adaptability of active control systems (Spencer et al. 1998). Typical semi-active devices can produce large dynamic control forces, by varying a control device parameter, usually stiffness or damping coefficients (Kurata 1999). These devices have been shown to be effective in response reductions, require low power, and are easily implemented in existing systems, which makes it a good candidate for the avionics controller.

1.2.1 Passive Control Devices

Currently, highly damped elastomeric passive devices are used for avionics vibration isolation through focalization. Vibration isolation and focalization are not a new concepts. The Browne Report, circa, 1937 is an in-house Lord Corporation report on "Predetermination and Control Vibration in Aircraft Originating from the Engine." K.A. Browne presents the idea of "dynamics suspension" for mountings of aircraft engines in order to isolate the aircraft from the vibrations of the engine. He recommends a configuration of springs, in which the stiffness of two axes is retained, allowing little restraint of the third axis on the propeller mounts in order to create a virtual suspension at the CG. This results in decoupling of the translational and rotational modes of vibration, allowing the independent control of the natural frequencies.

In 1975, A. J. Hannibal wrote the report, "Focalization of Semi-Symmetric Systems," in which he "investigates the focalization of a rigid body attached to a rigid foundation through four axi-symmetric isolators." The principle of focalization is defined as the decoupling of translational degrees of freedom from the rotational degrees of freedom with respect to an arbitrary point. The arbitrary point has traditionally been selected as the CG and the isolators have been configured in a rectangular pattern about the CG of the body. It is admitted in the report that focalization is not ideal when the elevation of the

focal plane in the X-Z plane is not the same as the Y-Z plane. In the case, the center of mass and the center of rigidity do not coincide, the rotational and translational motion cannot be decoupled.

If the rotational and translational modes of vibration can be decoupled, isolation and focalization can be implemented for vibration isolation of avionics packages. The general approach is two-fold. First, make the natural frequency of the avionics box high, such that the lower frequencies of vibration experienced during aircraft applications are inconsequential. Next, make the package symmetric about two axes with the CG on or near the center of geometry so the resonant frequency can be damped out by the highly damped isolator mounts.

1.2.2 Active Control Devices

Active control systems can effectively reduce the dynamic response of a system to external disturbances by inputting energy in to the system. Soong and Reinhorn (1993) provide an overview of typical active devices: active tuned mass driver (AMD), active bracing system (ABS), pulse generator, active parameter controller, and aerodynamic appendage. Active controllers have been shown to be very effective in reducing accelerations and displacements in many engineering applications (Soong, 1990, Soong et al., 1991, Fujino et al., 1996). However, they generally are large, demand a large external power supply, increase the complexity of the system, can be difficult to implement, and have many moving parts which introduces reliability issues. The power requirement alone, disqualifies current active control devices for consideration in the avionics application. The necessary external power supply would require too much space and generate heat. Although it is not a viable option for implementation in high performance aircraft applications, active controllers may, in some cases, achieve the best controlled performance. An ideal active control model is included as a baseline comparison.

1.2.3 Semi-Active Control Devices

Semi-active systems are defined as those that cannot input energy into the system being controlled (Housner et al., 1997). Since they cannot add energy to the system, they are inherently stable in the bounded input bounded output (BIBO) sense. Therefore, they do not have the potential to destabilize the system. They offer the reliability of passive devices in that there are no moving parts (Spencer et al., 1998).

Recently, semi-active, or “smart” dampers have shown success in seismic and ambient vibration protection implemented in actual civil engineering application (Kurata et al., 1999). There have been studies that demonstrated potential aerospace applications such as wing flutter vibration reduction (Nitzche et al., 1999, Burnham et al., 2001, and Moses et al., 2001) and in spacecraft vibration reduction applications (Oh et al., 2000, Onoda et al., 1991, 1996, 1997a, b, 2000a, and b). Additionally, semi-active devices have very low power requirements (Spencer et al., 1998). Since they do not require a large amount of power or space, it is feasible to implement these types of controllers in avionics bays.

One semi-active device that has recently received significant attention is the magnetorheological (MR) damper. MR dampers are composed of a controllable fluid with the ability to change reversibly from a free flowing viscous linear fluid to a semi-solid with a controllable yield strength in milliseconds when exposed to a magnetic field (Spencer, 1996). The fluid is comprised of micron-sized soft iron particles suspended in a fluid, typically mineral or silicone oil. It is insensitive to temperature fluctuation from -40 to 150 degrees Celsius and to impurities encountered in manufacturing and usage. A typical MR device can be controlled with a 12-24V power supply with an output of 1-2 amps.

The MR damper is an attractive choice for avionic systems due to its small power supply, high reliability, inherent stability, and its ability to impart high forces to a dynamic system in real time. They have been shown to be successful in civil engineering applications for

response reductions in seismically excited structures and in the alleviation of seismic, wind, and traffic loading on bridges. (Dyke et al., 1996a,b, and 1998, Jansen and Dyke, 2000, Johnson et al., 2000, Ramallo et al., 2000, Yi et al., 2001, and http:// www.rheonetic.com/mrfluid/). In order to apply the MR damper to aerospace applications, parameter modifications must be made in existing models and control algorithms. Earthquakes have large initial transient excitation, but only for a very short duration. An aircraft flight is much longer than an earthquake and the aircraft experiences a higher bandwidth of energy in accelerations and higher shocks during flight, take-off, and landing. Civil structures have typically a fundamental frequency between 0.25 - 2 Hz depending on the size and building type of the structure (shear wall vs. moment frame). The softer avionics packages will be modelled as having a first natural frequency of 20 Hz. The nature of the excitation and the structure to be controlled are the main differences between aerospace and civil engineering applications.

Variable orifice dampers are another type of semi-active device receiving much attention recently. Typical variable orifice devices have a solenoid valve whose diameter can be varied with applied voltage, varying the fluid flow rate, and thereby changing the viscous properties of the device. Solenoids can consume 10-100's of Watts (10-100V at 1-10 A) for AC operation. Variable orifice dampers have been shown to be experimentally successful in simulation analysis of a three story building with a shake table to severe earthquake excitations by Mizuno et al. (1992) and Kawashima (1992). Patten et al. (1998a,b) have developed a damper that has been implemented in a full scale bridge (Kurata et al., 1999). A list of the many current projects in the process of being or recently implemented in full scale structures can be found at www.taylordevices.com/ 3seismic.htm.

These fluid dampers have also been used in shock isolation of military hardware in aerospace applications, in particular the U.S. Air Force's MX missile and B-2 "Stealth" Bomber (http://www.taylordevices.com/3seismic). These devices typically have a valve acutator that controls the flow of fluid through an orifice, changing the properties of the

device. For the B-2 application, the damper was comprised of a silicon oil, a stainless steel piston, a bronze orifice head, a self contained piston displacement accumulator, and there are two chambers in which the fluid flows. The piston motion is translational and as it moves, fluid flows from one chamber to another. The damping force is proportional to the pressure differential in these two chambers (Constantinou and Taylor 1993).

Piezoelectric actuators and piezoelectric interdigitated electrodes are two examples of another type of “smart” control dampers: piezoelectric materials. These materials consist of plates with oppositely poled electrodes placed on opposite faces of the plates. The plates are pole electrically through the thickness or through the plane of the actuator of the plates for the actuators. When a voltage is applied the plates would strain in the direction of the thickness of the plate (or in the plane of the actuator). Recently, a control system using strain actuation to reduce the vibration response due to tail buffeting has been tested on a full scale F/A-18 shown successful in reduction of buffeting vibrations in twin tail aircraft. The results indicated a reduction in response of the tail’s first and second modes (first bending mode near 15 Hz and second tail mode, tip torsion, near 45 Hz) (Nitzsche et al., 1999; Moses and Huttsell, 2000; Burnham, et al., 2001; and Moses et al., 2001). In the initial tests, the piezo electronic wafer used one to three layers of 0.020 inch thick, total weight of acutators was 20 lbs. per tail. The typical piezoelectric pneumatic actuator can consume 100’s of milliwatts of power (100-200 V at 1mA) for AC operation and 100-200V at less than 0.01 mA. They can be less than 0.0250 thick, as indicated in the aircraft application, with a response time of 1ms (http://www.acx.com/lab/cool_fighter).

Three semi-active control devices have been included in this study: an ideal semi-active device, a variable orifice damper, and a magnetorheological damper. The latter is the only model of an actual physical device included in the study to illustrate the difference in performance of the ideal model to an actual device.

1.3 Summary

The goals of this research are to design a control system to reduction the response of high performance aircraft avionics. Five cases are considered in this analysis: an active force actuator, an ideal semi-active device, a linear viscous device, a magnetorheological damper, and a variable orifice device. For these cases, actuator dynamics and structure-controller interactions are neglected. Absolute accelerations will be used for feedback to ensure the control laws are implementable on the physical system. Appropriate control algorithms have been selected for application in the various devices.

1.4 Objectives

- Develop a two-degree of freedom model of an avionics package with a first natural frequency near 20 Hz.
- Model an ideal active, an ideal semi-active, ideal passive, variable orifice damper, and MR damper control device from existing models.
- Develop optimal control algorithms in conjunction with LQG techniques using acceleration feedback.
- Perform parallel numerical studies based on the best overall performance that can be achieved with a maximum of 32 N for of each control device.
- Compare the results and make recommendations for future research.
- Introduce the experimental avionics package apparatus design.

Chapter 2

Avionics Model

In any effective control system, it is crucial to thoroughly understand the dynamics of the physical system, and translate this understanding in the model of the process to design and implement control strategies appropriate for the system. The definitions and assumptions of the model must be clearly stated for readers and future researchers to understand the resulting discussion of the dynamics of the system. In this chapter, the mathematical representation of the two degree of freedom avionics used in the numerical studies is presented.

2.1 Two Degree of Freedom Avionics Model

In this study, the avionics is modeled as a rigid body, supported on springs, with a first fundamental frequency of 20 Hz. Two masses are used to represent the avionics package: a thin plate, m_1, and a rectangular prism, m_2. The total mass of the avionics package, M_1, is the sum of the two masses $M_1 = m_1 + m_2$.

The supports are modeled as lumped visco-elastic supports with stiffness and damping coefficients, k_1, c_1 and k_2, c_2, that are attached a distance of g_1 and g_2 from the left and right ends of m_1. The system is assumed to be lightly damped with a damping ratio, ζ, and equally distributed through out the structure. The damping matrix for the system is determined from the modal damping ratio (Chopra 1995). Mass proportional damping is assumed with a

$$c_d = 2\zeta\omega_n M_1 . \tag{2-1}$$

Since the damping is assumed to be equally distributed, the damping coefficient of each support is half the total damping of the system,

$$c_1 = c_2 = \frac{c_d}{2} . \tag{2-2}$$

A 2-DOF representation of the avionics model is shown in Fig. 2-1. A reference frame is defined with the origin placed at half the length and half the thickness of m_1 denoted as O in Fig. 2-1. The two primary degrees of freedom of interest are vertical translation in the y-direction q_1 and rotation about the z-axis q_2, where z is defined to be positive out of the page. The base acceleration, $\ddot{q}_g$, also referred to as the base excitation, is assumed to be positive in the y-direction. A moveable control force, f(t), is applied to the bottom of m_1, along the y = - 0.0032 line.

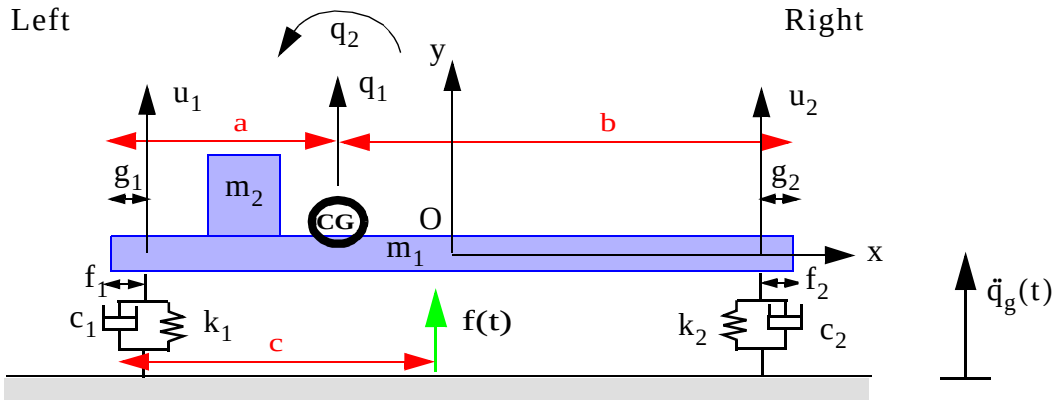

FIGURE 2-1 Two degree of freedom model

The second mass, m_2, is attached to the top of the plate, along the y = 0.0032 shown in Fig. 2-2. It is movable and can be placed at different locations along the length of the plate, thereby allowing for two degree of freedom (2-DOF) motion and variable center of mass locations.

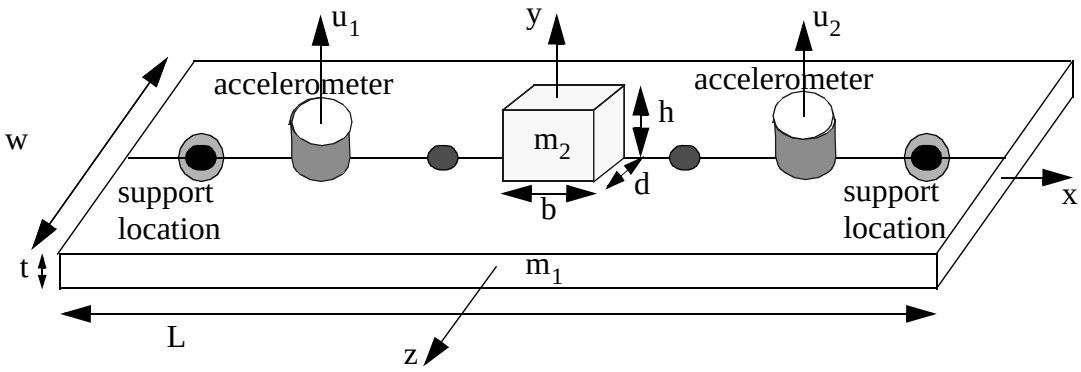

FIGURE 2-2 Top view of avionics plate model m_1

2.1.1 Equations of Motion

The avionics system or the process to be controlled is modeled as a linear system, satisfying the necessary conditions of superposition and homogeneity for the excitation

and response regions of interest (Dorf and Bishop, 1998). It is assumed to be time invariant system. The two equations of motion to describe the linear continuous model of the plant dynamics are given by

$$\begin{aligned}\sum F \;=\; M_1\ddot{q}_1 \;=\; & -k_1q_1 + k_1q_2(a-f_1) - c_1\dot{q}_1 + c_1\dot{q}_2(a-f_1) \\ & - k_2q_1 - k_2q_2(b-f_2) - c_2\dot{q}_1 - c_2\dot{q}_2(b-f_2) + f(t) - M_1\ddot{q}_g(t)\end{aligned} \tag{2-3}$$

and

$$\begin{aligned}\sum M_{CM} \;=\; I_{cm}\ddot{q}_2 \;=\; & (a-f_1)k_1q_1 - k_1q_2(a-f_1)^2 + (a-f_1)c_1\dot{q}_1 - c_1\dot{q}_2(a-f_1)^2 \\ & -(b-f_2)k_2q_1 - k_2q_2(b-f_2)^2 - (b-f_2)c_2\dot{q}_1 - c_2\dot{q}_2(b-f_2)^2 + (c-a)f(t)\end{aligned} \tag{2-4}$$

where I_{cm} is the moment of inertia about the center of gravity (CG). This investigation is for a single control device with a single control force point of application. Further studies should be performed with multiple controllers. For the initial investigation, the mass of the two accelerometers is neglected.

The moment of inertia about the center of mass, I_{cm}, is calculated from the sum the inertial properties of the two homogeneous bodies about the z-axis of m_1 and m_2 $I_{cm} = I_{m1} + I_{m2}$. The parallel axis theorem and each inertial property equation I_{m1} is for a thin plate defined in terms of the properties of the plate length, L, thickness, t, and width, w. The inertial property equation I_{m2} is for a rectangular prism base is defined in terms of its base b, height h, and depth d. The equations are defined by (Greenwood, 1988)

$$I_{m1} \;=\; m_1\left[\frac{(L^2+t^2)}{12} + (0-x_{cm})^2 + (0-y_{cm})^2\right] \tag{2-5}$$

and

$$I_{m2} \;=\; m_2\left[\frac{(b^2+h^2)}{12} + (0-x_{cm})^2 + \left(\left(\frac{t}{2}+\frac{h}{2}\right)-y_{cm}\right)^2\right] \tag{2-6}$$

where the different center of mass locations are calculated depending on a parameter defined as percentage, P, and the following equations

$$x_{cm} = \frac{(m_1 \times 0) + m_2 \times P \times L}{M_1} \tag{2-7}$$

and

$$y_{cm} = \frac{(m_1 \times 0) + m_2\left(\frac{t}{2} + \frac{h}{2}\right)}{M_1} . \tag{2-8}$$

P is a parameters that gives the desired center of gravity location.

Rewriting Eqs. (2-1) and (2-2) in matrix form,

$$\mathbf{M}_s\ddot{\mathbf{x}} + \mathbf{C}_s\dot{\mathbf{x}} + \mathbf{K}_s\mathbf{x} = G\begin{bmatrix}\ddot{q}_q(t)\\ f(t)\end{bmatrix} \tag{2-9}$$

where $\mathbf{x} = [q_1, q_2]^T$,

$$\mathbf{M}_s = \begin{bmatrix}M_1 & 0\\ 0 & I_{cm}\end{bmatrix}, \tag{2-10}$$

$$\mathbf{K}_s = \begin{bmatrix}k_1 + k_2 & -k_1(a-f_1) + k_2(b-f_2)\\ -k_1(a-f_1) + k_2(b-f_2) & k_1(a-f_1)^2 + k_2(b-f_2)^2\end{bmatrix}, \tag{2-11}$$

$$\mathbf{C}_s = \begin{bmatrix}c_1 + c_2 & -c_1(a-f_1) + c_2(b-f_2)\\ -c_1(a-f_1) + c_2(b-f_2) & c_1(a-f_1)^2 + c_2(b-f_2)^2\end{bmatrix}, \tag{2-12}$$

$$\text{and } G = \begin{bmatrix}-M_1 & 1\\ 0 & c-a\end{bmatrix}. \tag{2-13}$$

The control force is located a distance c from the left end of m_1. The parameter c can be varied to consider different control device locations. The velocity at the control force location for feedback purposes is defined as

$$\dot{x}_c = \dot{q}_1 + (c-a)\dot{q}_2 . \tag{2-14}$$

The equations are also in terms of the distance from the left end of m_1 to the center of mass defined as a so the equations can be easily modified to account for the variable center of mass locations.

For feedback purposes, two accelerometers are placed at distances of g_1 and g_2 from the left and right ends of m_1. Therefore, to obtain sensor outputs it is necessary to find the transformation from the coordinates of the model to the coordinates at the sensor locations. The transformation from the translation and rotation at the center of mass, q_1, q_2, to the displacements, u_1, u_2 are given by

$$\begin{bmatrix} u_1 \\ u_2 \end{bmatrix} = \begin{bmatrix} 1 & -(a-g_1) \\ 1 & (b-g_2) \end{bmatrix} \begin{bmatrix} q_1 \\ q_2 \end{bmatrix} = \mathbf{L}\mathbf{x} . \tag{2-15}$$

The absolute accelerations, $\ddot{u}_{1a}, \ddot{u}_{2a}$, at the sensor locations are then given by

$$\begin{bmatrix} \ddot{u}_{1a} \\ \ddot{u}_{2a} \end{bmatrix} = \begin{bmatrix} \ddot{u}_1 + \ddot{q}_g \\ \ddot{u}_2 + \ddot{q}_g \end{bmatrix} = \begin{bmatrix} -\mathbf{L}\mathbf{M}_s^{-1}\mathbf{K}_s & -\mathbf{L}\mathbf{M}_s^{-1}\mathbf{C}_s \end{bmatrix} \begin{bmatrix} x \\ \dot{x} \end{bmatrix} + \left[\mathbf{L}\mathbf{M}_s^{-1}\mathbf{G} + \begin{bmatrix} 1 & 0 \\ 1 & 0 \end{bmatrix} \right] \begin{bmatrix} \ddot{q}_g(t) \\ f(t) \end{bmatrix} \tag{2-16}$$

where

$$\left[\mathbf{L}\mathbf{M}_s^{-1}\mathbf{G} + \begin{bmatrix} 1 & 0 \\ 1 & 0 \end{bmatrix} \right] = \begin{bmatrix} 0 & \dfrac{1}{M_1} - \dfrac{(a-g_1)(c-a)}{I_{cm}} \\ 0 & \dfrac{1}{M_1} + \dfrac{(b-g_2)(c-a)}{I_{cm}} \end{bmatrix} \tag{2-17}$$

2.1.2 Parameters for the Avionics Model

The parameter values of the model are tabulated in Table 2-1. The excitation $\ddot{q}_g$ is

TABLE 2-1 Parameters used for numerical analysis

Parameter	Value
L	304.8 mm
w	76.2 mm
t	6.35 mm
b , h , d	2.54 mm
m_1	1.134 kg
m_2	0.4536 kg
k_1 , k_2	$12\ \frac{kN}{mm}$
ζ	0.01
c_1 , c_2	$1.952\ \frac{kg}{s}$
g_1 , g_2	12.7 mm
f_1 , f_2	38.1 mm

modeled based on military specifications to qualify avionics for non-gunfire random vibration testing levels. The excitation is assumed to be a uniform, identically distributed Gaussian white noise. The military specification used for the power spectral density (PSD) was $0.04\frac{g^2}{Hz}$ for low frequencies 10–2000 Hz with a root mean square (RMS) amplitude of 7.7 g's.

Four cases are considered in which the parameters a and P are varied. Case A corresponds to the case when the CG is located at the origin. For this case, only the first mode of

vibration is excited and the system essentially acts as a single degree of freedom system for vertical excitations. The different center of mass locations selected and the corresponding values of the parameters a and P are given in Table 2-2 and shown in Fig. 2-3.

TABLE 2-2 Definition of the CG cases

	Case A	**Case B**	**Case C**	**Case D**
	$0 \ \frac{L}{2}$	$0.25 \ \frac{L}{2}$	$0.5 \ \frac{L}{2}$	$0.75 \ \frac{L}{2}$
a	0.1524	0.1905	0.2286	0.2667
P	0	0.4375	0.8750	1.3125

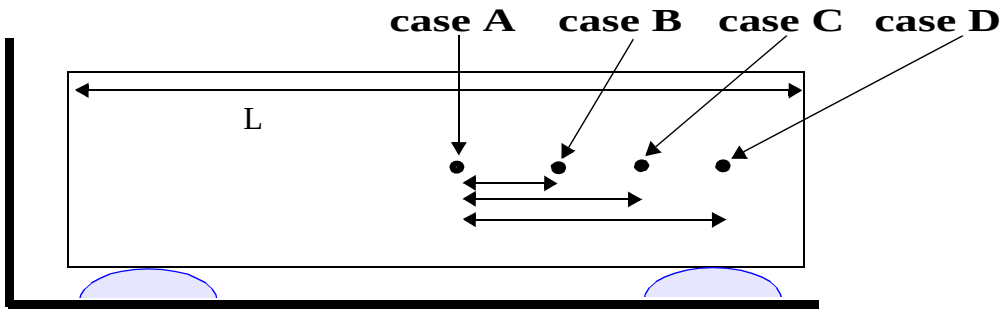

FIGURE 2-3 Definition of CG cases considered

2.1.3 State Space System

State space form is used for ease in numerical analysis and simulations. State space representations are not unique and the definition of the states and the outputs are user defined based on the application. A state space representation of the system in Eq. (2-3) and Eq. (2-4).

$$\dot{\mathbf{x}} = \mathbf{A}\mathbf{x} + \mathbf{B}f(t) + \mathbf{E}\ddot{q}_g(t) \tag{2-18}$$

where $\left[\mathbf{x} \ \dot{\mathbf{x}}\right]^T = [q_1, q_2, \dot{q}_1, \dot{q}_2]^T$ is the state vector, and

$$\mathbf{A} = \begin{bmatrix} \mathbf{0}_{2\times 2} & \mathbf{I}_{2\times 2} \\ -\mathbf{M}_s^{-1}\mathbf{K}_s & -\mathbf{M}_s^{-1}\mathbf{C}_s \end{bmatrix}, \mathbf{B} = \begin{bmatrix} 0 \\ 0 \\ -1 \\ 0 \end{bmatrix}, \mathbf{E} = \begin{bmatrix} 0 \\ 0 \\ \frac{1}{M_1} \\ \frac{(c-a)}{I} \end{bmatrix}.$$

Combining the $\mathbf{B}$ and $\mathbf{E}$ matrices gives the state space in the simplified form

$$\frac{d}{dt}\begin{bmatrix} \mathbf{x} \\ \dot{\mathbf{x}} \end{bmatrix} = \begin{bmatrix} \mathbf{0}_{2\times 2} & \mathbf{I}_{2\times 2} \\ -\mathbf{M}_s^{-1}\mathbf{K}_s & -\mathbf{M}_s^{-1}\mathbf{C}_s \end{bmatrix}\begin{bmatrix} \mathbf{x} \\ \dot{\mathbf{x}} \end{bmatrix} + \begin{bmatrix} \mathbf{0}_{2x2} \\ \mathbf{M}_s^{-1}\mathbf{G} \end{bmatrix}\begin{bmatrix} \ddot{q}_g(t) \\ f(t) \end{bmatrix}. \tag{2-19}$$

The vector of measurements used for feedback is written

$$\mathbf{y} = \mathbf{C}_y\mathbf{x} + \mathbf{D}_y f(t) + \mathbf{F}_y\ddot{q}_g + \mathbf{v}. \tag{2-20}$$

where $\mathbf{v}$ is the vector of uncorrelated measurement noises associated with the measurement devices.

The algebraic equation defining all of the outputs is referred to as the output equation

$$\mathbf{z} = \mathbf{C}_z\mathbf{x} + \mathbf{D}_z f(t) + \mathbf{F}_z\ddot{q}_g(t) \tag{2-21}$$

where $\mathbf{z}$ is the vector of structural responses it is desired to control or also known as the regulated outputs that will be controlled. The outputs are selected to be

$$\mathbf{z} = \begin{bmatrix} q_1 \\ q_2 \\ \ddot{q}_1 \\ \ddot{q}_2 \\ u_1 \\ u_2 \\ \ddot{u}_{1a} \\ \ddot{u}_{2a} \\ \dot{x}_c \end{bmatrix}. \tag{2-22}$$

The C and D matrices resulting from the selection of outputs are given by

$$\mathbf{C} = \begin{bmatrix} \mathbf{I}_{2\times 2} & \mathbf{0}_{2\times 2} \\ -\mathbf{M}_s^{-1}\mathbf{K}_s & -\mathbf{M}_s^{-1}\mathbf{C}_s \\ \mathbf{L} & \mathbf{0}_{2\times 2} \\ -\mathbf{L}\mathbf{M}_s^{-1}\mathbf{K}_s & -\mathbf{L}\mathbf{M}_s^{-1}\mathbf{C}_s \\ \begin{bmatrix} 0 & 0 \end{bmatrix} & \begin{bmatrix} 1 & c-a \end{bmatrix} \end{bmatrix},$$

$$\mathbf{D} = \begin{bmatrix} \mathbf{0}_{6\times 1} \\ \dfrac{1}{M_1} - \dfrac{(a-g_1)(c-a)}{I_{cm}} \\ \dfrac{1}{M_1} + \dfrac{(b-g_2)(c-a)}{I_{cm}} \\ 0 \end{bmatrix}, \text{ and } \mathbf{F} = \begin{bmatrix} \mathbf{0}_{9\times 1} \end{bmatrix}.$$

Combining the $\mathbf{D}$ and $\mathbf{F}$ matrices gives

$$\mathbf{z} = \begin{bmatrix} q_1 \\ q_2 \\ \dot{q}_1 \\ \dot{q}_2 \\ u_1 \\ u_2 \\ \ddot{u}_{1a} \\ \ddot{u}_{2a} \\ \dot{x}_c \end{bmatrix} = \begin{bmatrix} \mathbf{I}_{2\times 2} & \mathbf{0}_{2\times 2} \\ -\mathbf{M}_s^{-1}\mathbf{K}_s & -\mathbf{M}_s^{-1}\mathbf{C}_s \\ \mathbf{L} & \mathbf{0}_{2\times 2} \\ -\mathbf{L}\mathbf{M}_s^{-1}\mathbf{K}_s & -\mathbf{L}\mathbf{M}_s^{-1}\mathbf{C}_s \\ \begin{bmatrix} 0 & 0 \end{bmatrix} & \begin{bmatrix} 1 & c-a \end{bmatrix} \end{bmatrix} \begin{bmatrix} \mathbf{x} \\ \dot{\mathbf{x}} \end{bmatrix} + \begin{bmatrix} \mathbf{0}_{2\times 2} \\ \begin{bmatrix} 0 & 1 \\ 0 & c-a \end{bmatrix} \\ \mathbf{0}_{3\times 2} \\ \mathbf{L}\mathbf{M}^{-1}\mathbf{G} + \begin{bmatrix} 1 & 0 \\ 1 & 0 \end{bmatrix} \\ \mathbf{0}_{1\times 2} \end{bmatrix} \begin{bmatrix} \ddot{q}_g(t) \\ f(t) \end{bmatrix} \qquad (2\text{-}23)$$

or

$$\mathbf{z} = \begin{bmatrix} q_1 \\ q_2 \\ \dot{q}_1 \\ \dot{q}_2 \\ u_1 \\ u_2 \\ \ddot{u}_{1a} \\ \ddot{u}_{2a} \\ \dot{x}_c \end{bmatrix} = \begin{bmatrix} \mathbf{I}_{2\times 2} & \mathbf{0}_{2\times 2} \\ -\mathbf{M}_s^{-1}\mathbf{K}_s & -\mathbf{M}_s^{-1}\mathbf{C}_s \\ \mathbf{L} & \mathbf{0}_{2\times 2} \\ -\mathbf{L}\mathbf{M}_s^{-1}\mathbf{K}_s & -\mathbf{L}\mathbf{M}_s^{-1}\mathbf{C}_s \\ \begin{bmatrix} 0 & 0 \end{bmatrix} & \begin{bmatrix} 1 & c-a \end{bmatrix} \end{bmatrix} \begin{bmatrix} \mathbf{x} \\ \dot{\mathbf{x}} \end{bmatrix} + \begin{bmatrix} \mathbf{0}_{2\times 2} \\ \begin{bmatrix} 0 & 1 \\ 0 & c-a \end{bmatrix} \\ \mathbf{0}_{3\times 2} \\ \mathbf{L}\mathbf{M}_s^{-1}\mathbf{G} + \begin{bmatrix} 1 & 0 \\ 1 & 0 \end{bmatrix} \\ \mathbf{0}_{1\times 2} \end{bmatrix} \begin{bmatrix} \ddot{q}_g(t) \\ f(t) \end{bmatrix}. \qquad (2\text{-}24)$$

2.2 Properties of the Model

2.2.1 Eigenvalues

The eigenvalues of the **A** matrix completely determine the natural frequencies of the system. For this system, there is a full set of eigenvectors and the equations of motions can be uncoupled into two equations describing each of the natural modes of the system (Brogan, 1991). The eigenvalues are calculated by solving the characteristic equation

$$|\mathbf{A} - \mathbf{I}\lambda| = 0. \qquad (2\text{-}25)$$

The distinct roots of Eq. 2-21, λ, are the eigenvalues of the system and correspond to the poles of the transfer function.

For the state space equations Eq. 2-16 and Eq. 2-19, the open loop transfer function, $\mathbf{H}_{ol}$, from the base excitation input, $\ddot{q}_g$ to the outputs in the response vector $\mathbf{z}$ is given by

$$\mathbf{H}_{ol} = \mathbf{C}(s\mathbf{I} - \mathbf{A})^{-1}\mathbf{B} + \mathbf{D} \tag{2-26}$$

The open loop transfer functions from $\ddot{q}_g$ to u_1, u_2, $\ddot{u}_{1a}$, $\ddot{u}_{2a}$ are shown in Figure 2-5 for each of four CG location cases with the control force equal to zero. The first mode shifts to lower frequencies as the CG is moved farther in the positive x-direction and the second mode stays at relatively the same frequency. The exception is Case A, where the second mode is not excited by a base excitation and there is only one peak. The first mode peak increases in magnitude for the displacement of the right end and the acceleration of the right end as the CG is moved further from the center. This will be confirmed in later chapters.

When m_1 is in different locations, the A matrix of the system changes due to relation to the mass location with the I_{cm}, a, b terms in the **A** matrix. Figure 2-4 shows the change in natural frequencies, ω_n, of the first and second modes as the mass is moved to different locations along the x axis. The highest natural frequency occurs when both masses are located at the center of geometry location, P = 0. The CG location cases considered, and the corresponding negative CG locations are denoted by a “o”.

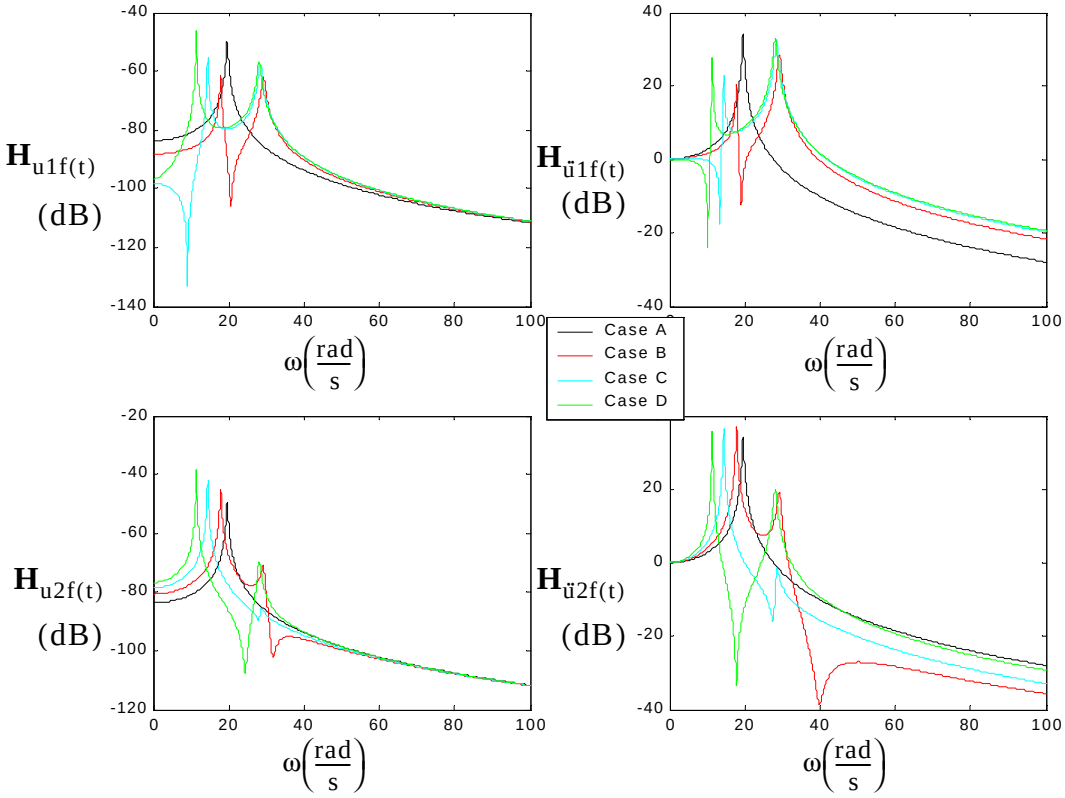

FIGURE 2-4 Open loop transfer functions H_{ol} for the different CG cases

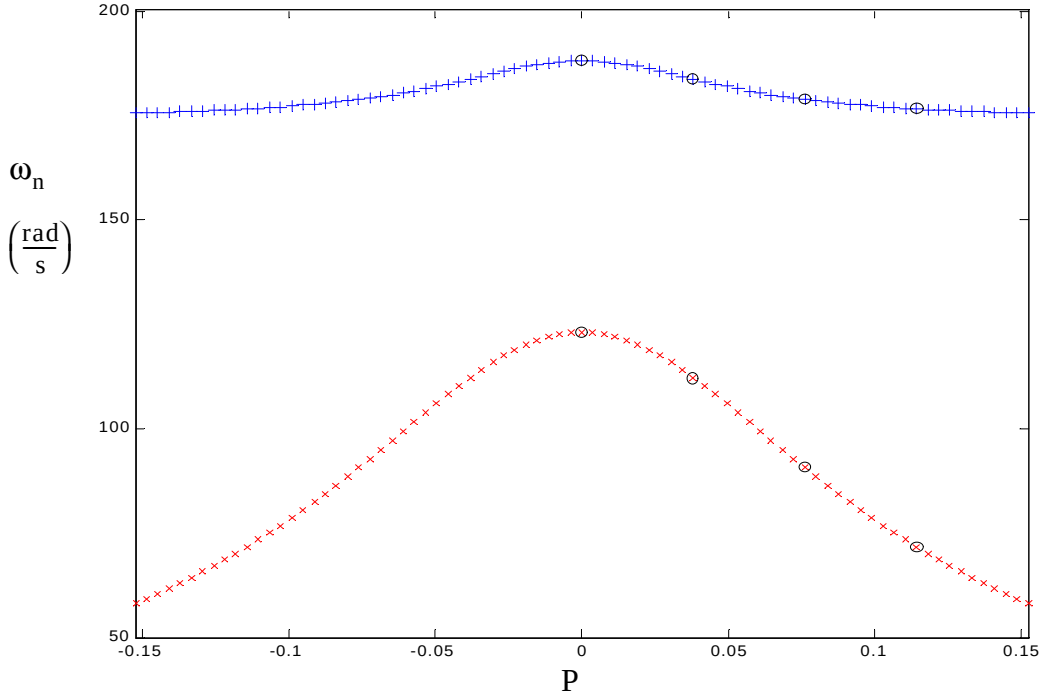

FIGURE 2-5 First and second natural frequencies as the CG varies

2.3 Summary

This chapter details the two degree of freedom mathematical model of the avionics package. The differential equations of motion representing the dynamics of the model and a state space representation are derived. They are also transformed into the state space form. The parameters of the model and the four different CG location cases to be used in subsequent chapters are presented. Lastly, a brief discussion was included on how the adjustable CG parameters of the model lead to subsequent variations in the eigenvalues. The following chapter will derive the control algorithms for the ideal control devices.

Chapter 3

Development of Control Strategies for Avionics System

The block diagram in Fig. 3-1 provides a general feedback control system. For the problem considered in this thesis, the plant represents the avionics model defined in Chapter 2 with the measurement vector, $\mathbf{y}$, and a control device component added to the block diagram. In this chapter, three ideal models will be developed: the ideal active, the ideal semi-active, and the ideal passive controllers. The active and passive models are linear, while the semi-active controller is nonlinear.

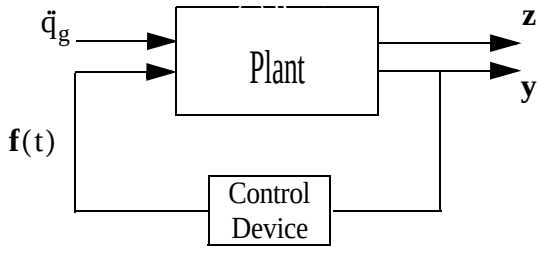

FIGURE 3-1 General feedback block diagram

In this chapter, controllability and observability of the avionics model will be considered to ensure the modes of vibration can be controlled and the states can be estimated. The optimal, time-invariant H_2/Linear Quadratic Gaussian (LQG) control algorithm with be derived for the active control device. The "dissipative constraint equation" will be described for use with the ideal semi-active device. Also, the model for a simple linear viscous damper model will be presented. Finally, different control device locations which will be investigated in the subsequent will be defined.

3.1 Controllability

Before a controller can be designed for a system, the controllability of the system should be checked. The follow issues will be investigated: Is the system controllable, and, if so, how controllable is it? The discussion begins with a look at the open loop transfer function of the plant.

The controllability matrix is defined as

$$\mathbf{C}_M = \left[\mathbf{B} \;\; \mathbf{AB} \;\; \mathbf{A}^2\mathbf{B} \;\; \text{¼} \;\; \mathbf{A}^{n-1}\mathbf{B} \right] \tag{3-1}$$

If $\mathbf{C}_M$ has full rank, n, then the system is controllable and **A**,**B** are a controllable pair. For the avionics system, if n = 4, then C_M is full rank and the system is fully controllable. For Case A and the control force location is at the origin, O,

$$\mathbf{C}_M = \left[\mathbf{B} \;\; \mathbf{AB}\right] = \begin{bmatrix} 0 & 0 & -1 & 0.6299 \\ 0 & 0 & 0 & 0 \\ -1 & 0.6299 & 2.4591 & -1.5489 \\ 0 & 0 & 0 & 0 \end{bmatrix} \tag{3-2}$$

has rank = 2. This implies the first mode is controllable and the states associated with the second mode q_2 are not controllable. This is congruent with the previous discussion of

Case A where only the translation mode of vibration is excited, and not the rotational mode.

For all other cases, when $P \neq 0$, the rank = 4. For example, for Case D and the same control force location at O, Eq. 3-1 now has the value

$$C_M = \begin{bmatrix} 0 & 0 & -1 & 0.6299 \\ 0 & 0 & 0 & -3.8608 \\ -1 & 0.6299 & 2.4591 & -2.6241 \\ 0 & -3.8608 & -15.0722 & 22.7961 \end{bmatrix} \tag{3-3}$$

Since the rank = 4, all four states are controllable. Thus, the system is fully controllable for all modes that are excited.

3.2 Observability

For this system it is not feasible to measure all the states for feedback. Thus, an observer is built to optimally estimate the states. The test for observability is included. The observability matrix is defined as

$$\boldsymbol{O} = \begin{bmatrix} \mathbf{C} \\ \mathbf{CA} \\ \mathbf{CA}^2 \\ \vdots \\ \mathbf{CA}^{n-1} \end{bmatrix} \tag{3-4}$$

where n is the rank of $\mathbf{A}$. If $\boldsymbol{O}$ has a full rank equal to n, then the system is said to be observable, and the state vector can be determined or estimated from the feedback measurement vector $\mathbf{y}$.

For this system n = 4 = rank(**A**), and for Case Ai, Eq. 3-4 is

$$\boldsymbol{O} = \begin{bmatrix} \mathbf{C} \\ \mathbf{CA} \end{bmatrix} = \begin{bmatrix} 1 & 0 & 0 & 0 \\ 0 & 1 & 0 & 0 \\ -1.5117e4 & 0 & -2.4591 & 0 \\ 0 & -3.5371e4 & 0 & -5.7535 \\ 1 & -0.1397 & 0 & 0 \\ 1 & 0.1397 & 0 & 0 \\ -1.5117e4 & 0.4941e4 & -2.4591 & 0.8038 \\ -1.5117e4 & -0.4941e4 & -2.4591 & -0.8038 \\ 0 & 0 & 1 & (c-a) \\ 0 & 0 & 1 & 0 \\ 0 & 0 & 0 & 1 \\ 3.7175e4 & 0 & -1.511e4 & 0 \\ 0 & 2.0350e5 & 0 & -3.5337e4 \\ 0 & 0 & 1 & -0.1397 \\ 0 & 0 & 1 & 0.1397 \\ 3.7175e4 & -2.843e4 & -1.511e4 & 4.9366e3 \\ 3.7175e4 & 2.843e4 & -1.511e4 & -4.9366e3 \\ -1.5117e4 & 0 & -2.4591 & 0 \end{bmatrix}. \quad (3\text{-}5)$$

The rank ($\boldsymbol{O}$) = 4 = n, thus the system is observable regardless of the CG location, and all the states can be estimated.

3.3 H_2/LQG Control Design

Feedback control is the utilization of the output measurements in determining the control action by closing the loop. In most real life applications, all states cannot be measured directly. In order to design a controller that can control each mode, it is necessary to have a full state vector for feedback to determine the control action. Since the system is fully observable, the states can be estimated from the known, thus leading to the full state vector. Accelerometers are inexpensive, light, and reliable. Therefore, accelerations will be used as the known states. The model includes two accelerometers used to directly measure the absolute accelerations $\ddot{u}_{1a}$, $\ddot{u}_{2a}$ at the sensor locations described in Chapter 2. Output acceleration response feedback control strategies based on H_2/LQG methods were developed systematically in Spencer et al., (1991), Suhardjo et al, (1992), and Spencer et al., (1994). The H_2/LQG control law was shown experimentally to be effective in

reducing the response for seismically excited civil engineering structures (Dyke et al., 1996 a, b).

In order to minimize the RMS response it is necessary to choose the optimal gains for the controller $\mathbf{K}_c$ and for the estimator $\mathbf{K}_f$. The H_2/linear quadratic Gaussian (LQG) filter is built using the separation principle. This principle enables the design of the optimal controller using optimal linear quadratic regulator (LQR) techniques and the optimal estimator using a linear Kalman filter estimator independently, and the combination of the resulting systems to form the optimal filter. The block diagram with the H_2/LQG controller added is shown in Fig. 3-2.

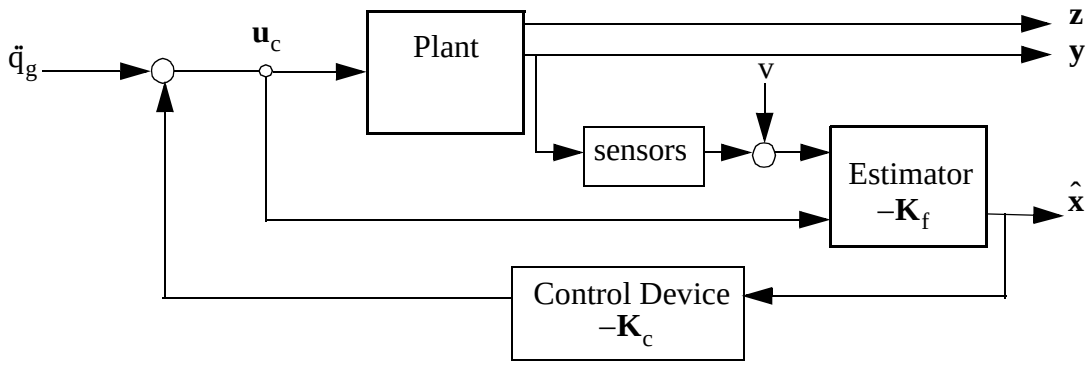

FIGURE 3-2 Block diagram for H_2 LQG control design

3.3.1 Linear Quadratic Regulator (LQR)

The linear quadratic (LQ) optimal control problem can be solved analytically. The quadratic cost function J is defined as

$$J = \int_{t1}^{t2} \left\{ \mathbf{z}^T \mathbf{Q} \mathbf{z} + \mathbf{u}_c^T R \mathbf{u}_c \right\} dt + \mathbf{x}^T \mathbf{N} \mathbf{x} \qquad (3\text{-}6)$$

where $\mathbf{x}^T\mathbf{N}\mathbf{x}$ is called the terminal manifold. Any metric can be minimized using this cost function. For this research, the metric selected to be minimized is a combination of the absolute accelerations and displacements of the left and right ends, i.e. u_1, u_2, $\ddot{u}_{1a}$, $\ddot{u}_{2a}$.

When the operating time is very long compared to the system time constants the infinite horizon problem is considered (Brogan 1991). The goal is to find the control law $\mathbf{u}_c$ that minimizes the cost function for the infinite horizon quadratic cost function, J, given by

$$J_{min} = \lim_{\tau \to \infty} \left[\int_0^{\tau} \left\{ \mathbf{z}^T\mathbf{Q}\mathbf{z} + \mathbf{u}_c^T R \mathbf{u}_c \right\} dt \right] \tag{3-7}$$

Where $\mathbf{N} = \mathbf{0}$ since the upper limit goes to infinity, there is no terminal manifold as the states are forced to zero at infinity. The weighting matrices are $\mathbf{R} = \mathbf{I}$, and $\mathbf{Q}$ is a positive semi-definite matrix.

The $\mathbf{Q}$ matrix is selected to appropriately weight the regulated outputs $\mathbf{z} = [u_1, u_2, \ddot{u}_{1a}, \ddot{u}_{2a}]^T$. The displacements, u_1, u_2, are weighted by a_1 and the absolute accelerations $\ddot{u}_{1a}, \ddot{u}_{2a}$ are weighted by a_2. Thus, the $\mathbf{Q}$ matrix takes the form

$$\mathbf{Q} = \begin{bmatrix} a_1\mathbf{I}_{2\times 2} & \mathbf{0} \\ \mathbf{0} & a_2\mathbf{I}_{2\times 2} \end{bmatrix}. \tag{3-8}$$

Selection of a_1, a_2 are described in later chapters.

From Chapter 2, the state equation and regulated output equation are given by

$$\dot{\mathbf{x}} = \mathbf{A}\mathbf{x} + \mathbf{B}\mathbf{f}(t) + \mathbf{E}\ddot{\mathbf{q}}_{\mathbf{g}} \tag{3-9}$$

$$\mathbf{z} = \mathbf{C}_z\mathbf{x} + \mathbf{D}_z f(t) + \mathbf{F}_z \ddot{q}_g(t) \tag{3-10}$$

where $\mathbf{C}_z, \mathbf{D}_z$ are the rows of the $\mathbf{C}$ and $\mathbf{D}$ matrices associated with the regulated outputs

$$\mathbf{C}_z = \begin{bmatrix} \mathbf{I}_{2\times 2} & \mathbf{0}_{2x2} \\ -\mathbf{M}_s^{-1}\mathbf{K}_s & -\mathbf{M}_s^{-1}\mathbf{C}_s \end{bmatrix} \tag{3-11}$$

$$\mathbf{D}_z = \begin{bmatrix} 0 & \dfrac{1}{M_1} - \dfrac{(a-g_1)(c-a)}{I_{cm}} \\ 0 & \dfrac{1}{M_1} + \dfrac{(b-g_2)(c-a)}{I_{cm}} \end{bmatrix}. \tag{3-12}$$

The optimal control input can be generated through a linear control law for the deterministic linear optimal regulator problem, and takes the form

$$\mathbf{u}_c(t) = -\mathbf{K}_c\hat{\mathbf{x}} \tag{3-13}$$

where $\hat{\mathbf{x}}$ is the Kalman filter estimate of the state vector discussed in the next subsection.

The gain matrix $\mathbf{K}_c$ is the full state feedback gain vector for the optimal time-invariant deterministic linear quadratic regulator (LQR) problem derived by Kwakernaak and Sivan (1972) as

$$\mathbf{K}_c = \mathbf{R}^{-1}\mathbf{B}^T\mathbf{P} \tag{3-14}$$

Since it is an infinite horizon case, the steady state solution of $\mathbf{P}$ is given by the *algebraic* Riccati equation,

$$\mathbf{0} = \mathbf{A}^T\mathbf{P} + \mathbf{P}\mathbf{A} - \mathbf{P}\mathbf{B}\mathbf{R}^{-1}\mathbf{B}^T\mathbf{P} + \tilde{\mathbf{Q}} \tag{3-15}$$

where $\mathbf{P}$ is nonnegative definite and $\tilde{\mathbf{Q}}$ is the nonnegative-definite symmetric matrix

$$\tilde{\mathbf{Q}} = \mathbf{C}^T\mathbf{Q}\mathbf{C} \tag{3-16}$$

Calculations to determine $\mathbf{K}_c$ were done using the MATLAB routine *lqry.m* in the control toolbox.

3.3.2 Kalman Filter Estimator

A Kalman Filter estimator generates an optimal estimate of the states $\hat{\mathbf{x}}$ based on the measured output. Acceleration feedback control has been shown to achieve comparable performance to full state feedback controllers (Dyke et al. 1995). Sensors have noise associated with the measurements and this is included in the model as $\mathbf{v}$. The disturbance and measurement noise are assumed to be an identically distributed, statistically independent, zero mean Gaussian white noise processes with intensity matrices for process or disturbance noise $\mathbf{S}_w = E[ww^T]$, sensor noise $\mathbf{S}_v = E[vv^T]$, and their cross correlation $\mathbf{S}_{wv} = E[wv^T] = \mathbf{0}$.

The goal is to design an observer that estimates the states optimally, such that, the error between the estimated states and the measured states goes to zero. The error is defined as

$$\mathbf{e} = \mathbf{x} - \hat{\mathbf{x}} \tag{3-17}$$

Taking the derivative of the error equation gives

$$\dot{\mathbf{e}} = \dot{\mathbf{x}} - \hat{\dot{\mathbf{x}}} \tag{3-18}$$

Assuming an observer of the form

$$\hat{\dot{\mathbf{x}}} = \mathbf{A}\hat{\mathbf{x}} + \mathbf{B}u(t) + \mathbf{K_f}(\mathbf{y} - \mathbf{C}_y\hat{x} - \mathbf{D}_y u(t)) \tag{3-19}$$

$$\mathbf{y} = \mathbf{C}_y\mathbf{x} + \mathbf{D}_y u(t) + \mathbf{F}_y\ddot{q}_g + \mathbf{v} \tag{3-20}$$

where the feedback vector for the observer is the absolute accelerations measured by the two accelerometers $\mathbf{y} = \begin{bmatrix}\ddot{u}_1 & \ddot{u}_2\end{bmatrix}^T + \mathbf{E}\ddot{q}_g = \begin{bmatrix}\ddot{u}_{1a} & \ddot{u}_{2a}\end{bmatrix}^T$ and $\mathbf{C}_y, \mathbf{D}_y$ are the columns of the $\mathbf{C}$ and $\mathbf{D}$ matrices corresponding to the two feedback accelerations.

$$\mathbf{C}_y = \left[-\mathbf{M}_s^{-1}\mathbf{K}_s \; -\mathbf{M}_s^{-1}\mathbf{C}_s \right] \tag{3-21}$$

$$\mathbf{D}_y = \begin{bmatrix} 0 & \frac{1}{M_1} - \frac{(a-g_1)(c-a)}{I_{cm}} \\ 0 & \frac{1}{M_1} + \frac{(b-g_2)(c-a)}{I_{cm}} \end{bmatrix}. \tag{3-22}$$

The gain matrix that gives the optimal estimates of the states is

$$\mathbf{K}_f = \mathbf{G}\mathbf{C}^T \tag{3-23}$$

where $\mathbf{G}$ is from the solution of the "filter covariance Riccati equation"

$$\mathbf{0} = \mathbf{A}\mathbf{G} + \mathbf{G}\mathbf{A}^T - \mathbf{G}\mathbf{C}^T\mathbf{C}\mathbf{G} + \mathbf{Q}_f \tag{3-24}$$

and $\mathbf{Q}_f$ is

$$\mathbf{Q}_f = \frac{\mathbf{S}_w}{\mathbf{S}_v}\mathbf{E}\mathbf{E}^T \tag{3-25}$$

and the ratio $\frac{\mathbf{S}_w}{\mathbf{S}_v}$ is a positive parameter.

Calculations to determine $\mathbf{K}_f$ were performed using the MATLAB routine *lqew.m* in the control toolbox.

3.4 Ideal Control Device Models

3.4.1 Ideal Active Control Device Model

An active controller can modify the motion of the structure by generating an opposing motion with an external energy supply. An active control device is limited by the actuator

size. Additionally, in a physical device the actuator has dynamics, and those dynamics are linked to the dynamics of the structure to which is it attached.

The active device used in this study is modeled as an ideal force actuator. An ideal actuator is assumed to have the ability to instantaneously and precisely supply the force commanded by the H_2/LQG control command. The model does not include the actuator dynamics or the controller-structure interactions, although it is acknowledged these effects do occur in physical systems (Dyke et at., 1995). This device is also assumed to have unlimited force capacity.

The force provided by the active control device is given by

$$f(t) = u_c(t) \tag{3-26}$$

where $u_c(t)$ is the control force determined using a H_2/LQG control algorithm.

Substituting the control law from Eq. (3-13) and $\mathbf{y}$ from Eq. (3-19) into Eq. (3-20) gives a state space representation for the controller.

$$\hat{\dot{\mathbf{x}}} = (\mathbf{A} - \mathbf{B}\mathbf{K}_c - \mathbf{K}_f\mathbf{C}_y + \mathbf{K}_f\mathbf{D}_y\mathbf{K}_c)\hat{\mathbf{x}} + \mathbf{K}_f(\mathbf{y} + \mathbf{F}_y\ddot{\mathbf{q}}_g) \tag{3-27}$$

3.4.2 Ideal Semi-Active Model

The ideal semi-active device considered is a purely dissipative device. This means the control force is only applied when the signs of the control force and relative velocity at the control force location, have opposing signs. Otherwise, the controller applies zero control force. This algorithm is illustrated in Fig. 3-3. The ideal model assumes the device can apply any force in the second and fourth quadrants of the force-velocity plane.

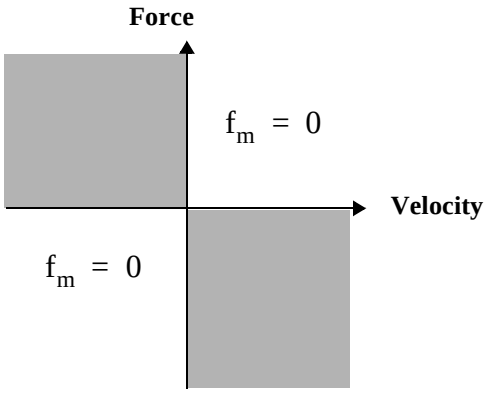

FIGURE 3-3 Force vs. velocity envelope for ISA device

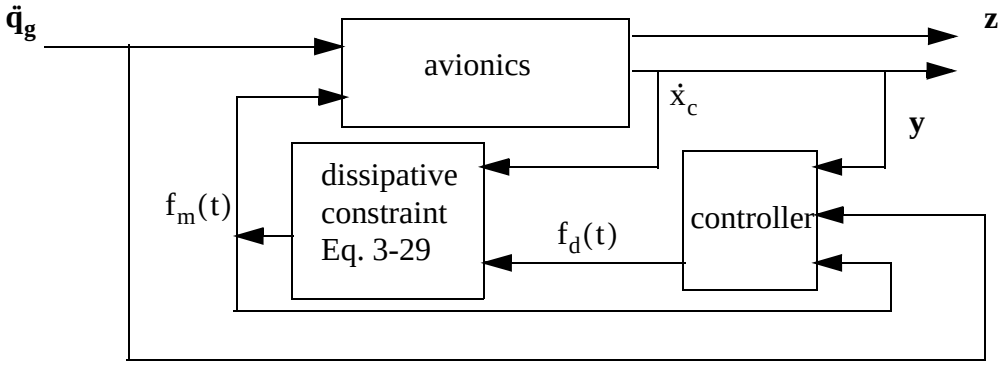

FIGURE 3-4 Block diagram with an ideal semi active controller

The problem is broken in two parts to implement an ideal semi-active control device. A block diagram with the semi-active control system is shown in Fig. 3-4. First, the controller calculates the desired optimal control force, $\mathbf{f}_d(t)$, based on the command force determined using a H_2/LQG control algorithm. The desired force, $\mathbf{f}_d(t)$, provided by the semi-active H_2/LQG controller is given by, *i.e.*,

$$f_d(t) = L^{-1}\left\{-\mathbf{K}_c(s)L\left\{\begin{matrix}\mathbf{y}(t)\\ f_m(t)\end{matrix}\right\}\right\} \tag{3-28}$$

where $L\{\cdot\}$ is the Laplace transform of the output vector, s is the Laplace variable (Merovitch 1986), and $f_m(t)$ is the measured force. Based on the measured structural responses $\mathbf{y} = \left[\ddot{u}_{1a}\ \ddot{u}_{2a}\right]^T$ and the measured control force, $f_m(t)$, applied to the structure is determined by the "dissipative constraint equation" given be

$$f_m(t) = \begin{cases} f_d(t) & \text{when } \dot{x}_c u_c < 0 \\ 0 & \text{otherwise} \end{cases} . \tag{3-29}$$

The desired force, $\mathbf{f}_d(t)$, is the force that would be applied for an active device, as it was in the previous section.

Substituting $f_m(t)$ from Eq. (3-29) into the observer Eq. (3-19) and Eq. (3-20) gives

$$\dot{\hat{\mathbf{x}}} = \mathbf{A}\hat{\mathbf{x}} + \mathbf{B}f_m(t) + \mathbf{K}_f(\mathbf{y} - \mathbf{C}\hat{x}) \tag{3-30}$$

$$\mathbf{y} = \mathbf{C}_y\hat{\mathbf{x}} + \mathbf{D}_y f_m(t) + \mathbf{F}_y\ddot{q}_g \tag{3-31}$$

Substituting $\mathbf{y}$ from Eq. (3-31) gives the Kalman filter optimal estimator for the ideal semi-active case as

$$\dot{\hat{\mathbf{x}}} = \mathbf{A}\hat{\mathbf{x}} + \mathbf{B}f_d + \mathbf{K}_f(\mathbf{y} - \mathbf{C}_y\mathbf{x} - \mathbf{D}_y f_d(t) + \mathbf{F}_y\ddot{\mathbf{q}}_g) \tag{3-32}$$

where $\mathbf{K}_f$ is given by Eq. 3-23.

3.4.3 Passive Case

A passive device is one that cannot add energy into the system. A linear viscous damper is used for the passive control device. In a passive system, the control force applied to the structure is only dependent on the motion of the structure at the point of application. The force is provided by the control device is

$$f(t) = -\alpha\dot{x}_c(t) \tag{3-33}$$

where $\dot{x}_c(t)$ is the relative velocity across the damper and α is the damping coefficient of the damper. The value of α is adjusted to vary the forces provided by the device and selected to provide the desired control force for the application. This device is ideal in that the force depends only on the velocity at the control force location, the properties of the damper are perfectly linear, and the properties of the viscous device do not vary with heat or usage. A block diagram of the ideal semi-active model is provided in Fig. 3-5.

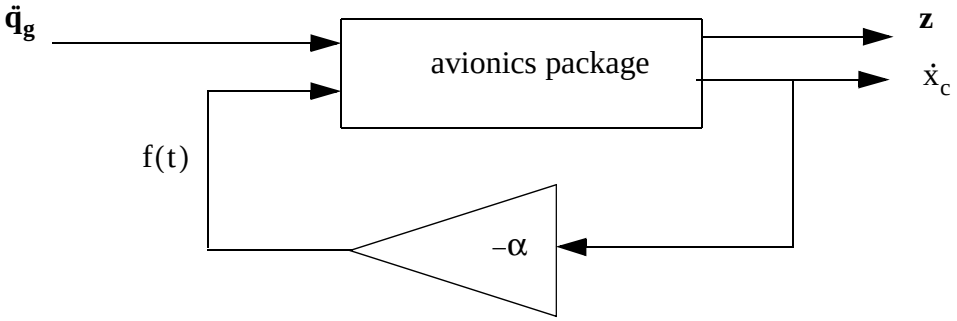

FIGURE 3-5 Block diagram of avionics with an ideal passive device

3.5 Control Device Location

As previously mentioned, this study considers one control device with one point of control force application. The controller placement is strongly tied to the performance of the controller. Four control force locations, were selected based on comparison studies for the best overall reduction of accelerations. A schematic of the avionics box with the locations is found in Fig. 3-6. The locations considered are provided in Table 3-1 with the corresponding c.

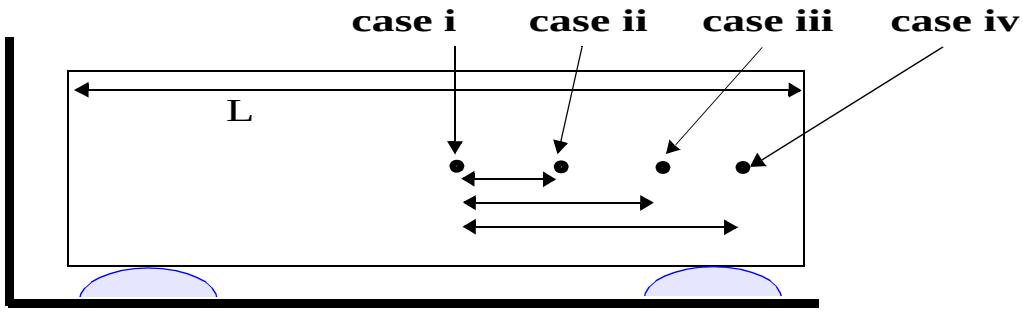

FIGURE 3-6 Different control force locations

TABLE 3-1 Parameters for the control force locations

	Case i	Case ii	Case iii	Case iv
	$0 \ \frac{L}{2}$	$0.25 \ \frac{L}{2}$	$0.50 \ \frac{L}{2}$	$0.75 \ \frac{L}{2}$
c	0.1524	0.1905	0.2286	0.2667

From the state space equations Eq. (2-16) and Eq. (2-19), the transfer functions from the control input $f(t)$ to the outputs in the response vector $\mathbf{z}$ is given by

$$\mathbf{H}_{zf(t)} = \mathbf{C}(s\mathbf{I} - \mathbf{A})^{-1}\mathbf{B} + \mathbf{D} \tag{3-34}$$

The closed loop transfer functions from the control input $f(t)$ to $u_1, u_2, \ddot{u}_{1a}, \ddot{u}_{2a}$ are shown in Fig. 3-7 for each of the CG cases with the control force Case i. The selection of the weights for the control design, a_1 and a_2, for the $\mathbf{Q}$ matrix will be discussed in the next chapter.

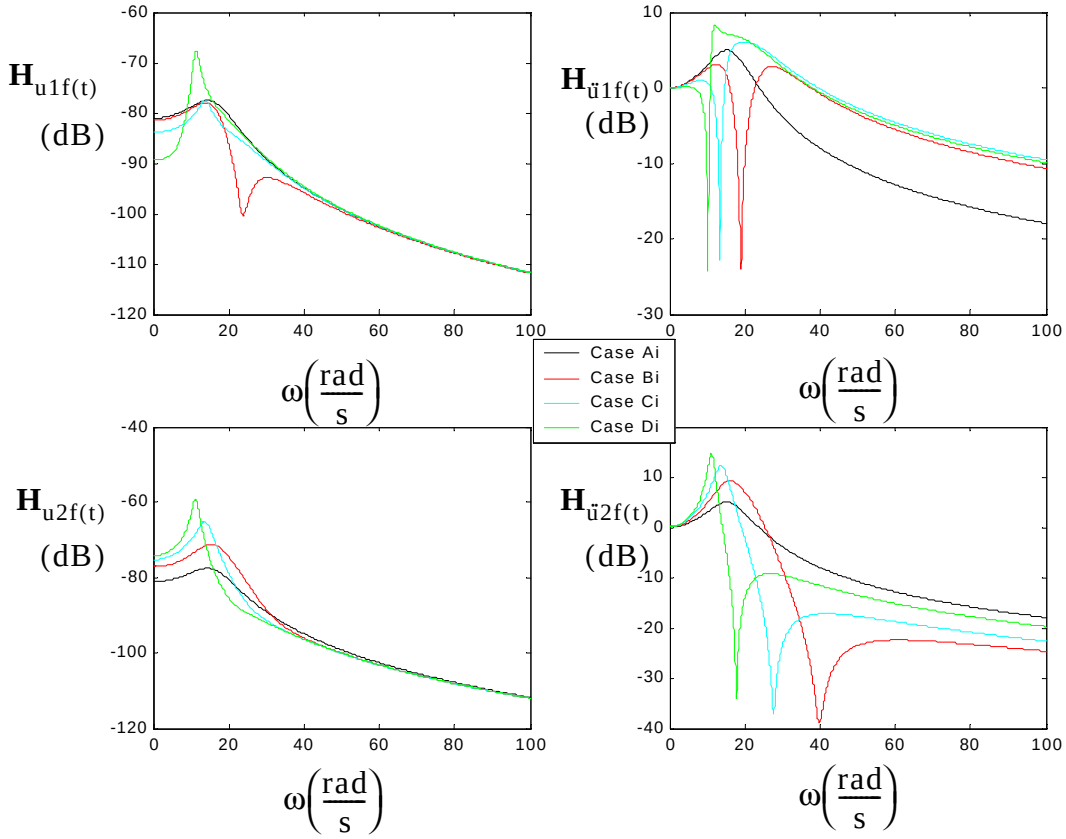

FIGURE 3-7 Closed loop transfer functions $H_{zf(t)}$ for the CG cases

3.6 Summary

In this chapter, the controllability and observability where checked to ensure the avionics model could be fully controlled and all the states could be estimated. Next, the LQR optimal control and Kalman observer were designed separately and combined to form the optimal H_2/LQG controller. Models for an ideal active control device, an ideal semi-active device, and an ideal viscous damper have been presented in this chapter. The "dissipative constraint" control algorithm design for the ideal semi-active controller is also outlined in this chapter. This will be applied to control the magnetorheological (MR) damper and the variable orifice (VO) device in Chapter 6.

Chapter 4

Ideal Control Device Performance

The previous chapter detailed the design of the control algorithms for the ideal active, ideal semi-active, and ideal passive devices for later comparisons with the magnetorheological (MR) damper and variable orifice (VO) device. These ideal models do not include the dynamics of the physical devices. It is assumed the desired force calculated by the controller can be directly applied to the system. It is acknowledged the ideal models are perfect and thus are not indicative of actual device performances. However, it is important to include them in this study as a baseline of the best performance that could ideally be achieved by each device for comparative purposes. The extent of the discrepancies will be apparent in the comparison between the ideal semi-active case and the actual MR and variable orifice damper models.

4.1 Parameters

The parameters and terminology used for the studies presented in the chapter are defined in this section, unless otherwise noted in later sections. The “uncontrolled” case refers to the open loop of the system when a zero force is applied, $f(t) = 0$.

The weights are in reference to the **Q** matrix from the infinite horizon cost function is defined in the previous chapter in Eq. 3-8, where the weights a_1 are on displacements, u_1, u_2, and the weights a_2 are on absolute accelerations, $\ddot{u}_{1a}, \ddot{u}_{2a}$. For comparative purposes, "percent of the uncontrolled" refers to the controlled values (i.e., accelerations and displacements) with respect to the "uncontrolled" case, as in

$$\% \text{ of uncontrolled} = 100 \times \left(\frac{\text{controlled}}{\text{uncontrolled}} \right). \tag{4-1}$$

For similar presentation of results or discussion, the "percent reduction" of the uncontrolled values were tabulated and calculated as

$$\% \text{ reduction} = 100 \times \left(1 - \frac{\text{controlled}}{\text{uncontrolled}} \right). \tag{4-2}$$

Responses are quantified in terms of the standard deviation of the responses, or the root mean squared (RMS) values. The distinction between the RMS and actual values is that the actual values will not be denoted RMS. One such actual value is the maximum control force for the time history studies. Calculations to determine the standard deviations were done using the MATLAB routine *std.m* in the datafun toolbox.

The goal of the research is to minimize the acceleration response while keeping the displacements within reasonable bounds, as discussed in Chapter 1. However, the maximum force the MR damper considered in this study can provide is approximately 32 N. Therefore, this is the limit set for the maximum control force for all control devices considered in this and following chapters. By comparing devices with equal force capacity, the performance from devices of approximately equal size and cost can be compared.

Simulations were performed using a time step of $\Delta t = 10^{-4}$ seconds, a total time for each simulation run, of T_{max} = 60 sec. (unless otherwise noted). The CG locations used in the study were P = [0 0.4375 0.8750 1.3125] with corresponding a = [0.1524 0.1905 0.2286

0.2667], referred to as Case A, Case B, Case C, and Case D, as defined earlier in Chapter 2. Control force locations corresponding to c = [0.1524 0.1905 0.2286 0.2667], are referred to as Case i, Case ii, Case iii and Case iv, defined in Chapter 3. A band-limited, Gaussian excitation was used for each of the simulation inputs with a power spectral density of So = 0.04 $\frac{g^2}{Hz}$ = 0.2513 rad$\frac{g^2}{Hz}$ in accordance with military specifications used in avionics random vibration test levels for non-gunfire endurance and performance testing. The first order filter has a time constant of η = 100 Hz. The intensity matrices for this section are selected as $\mathbf{S}_w = 25$, $\mathbf{S}_v = \mathbf{I}_{2\times 2}$, and $\mathbf{S_{wv}} = \mathbf{0}$.

The responses were obtained for a sinusoidal displacement input to demonstrate the behavior of the devices. The sinusoidal displacement input with an amplitude of 0.01 m, a natural frequency of $\omega = 100\frac{rad}{sec}$, and T_{max} = 5 sec. was used. The velocities were computed from the sinusoidal displacement input in Simulink by using a derivative block. For the clipped optimal controller, the desired force was input as a constant equal to 1. Also, parametric studies were performed to compare the response reduction for different control force locations. The different control force locations are varied by the parameter c. For the study included, the values were c = [0.0152:0.00762:0.2895].

4.2 Ideal Active Controller Performance

4.2.1 Parameters used for Ideal Active Control

The vectors containing many different weights in the **Q** matrix selection were selected for presentation of behavior were $\mathbf{a}_1$ = [0 1 10 100 10^4 10^5 10^6 10^7 10^8 3×10^8 5×10^8 8×10^8 10^9 10^{10}] and $\mathbf{a}_2$ = [0 10^{-2} 10^{-1} 1 2 3 4 5 6 7 8 9 10 20 30 40 50 60 70 80 90 100 10^3 10^4 10^5 10^6 10^7 10^8]. The $\mathbf{a}_2$ used for the ideal active case was truncated to 100, simply because the latter values forces are much larger in magnitude than the 32 N limit.

4.2.2 Q Matrix Selection: Case Ai

For an optimal H_2/LQG controller, a vector of metrics to be minimized are specified in the infinite time horizon cost function. This vector is multiplied by a **Q** matrix containing weights for each of the metrics to be minimized. There are no units for the weightings. The displacements u_1, u_2 are weighted by a_1 and it is clear from Fig. 4-1 that as the value of a_1 increases, the displacement decreases. It is interesting to note that as a_2 varies so do the displacements, although it is the weighting on absolute acceleration. The a_1 that effect the displacements are very large, i.e. 10^{10}, while smaller a_2 seem to minimize the displacements between 1 and 10. The $\log_{10}(a_1)$ and $\log_{10}(a_2)$ were calculated and the values are plotted along with the RMS displacements.

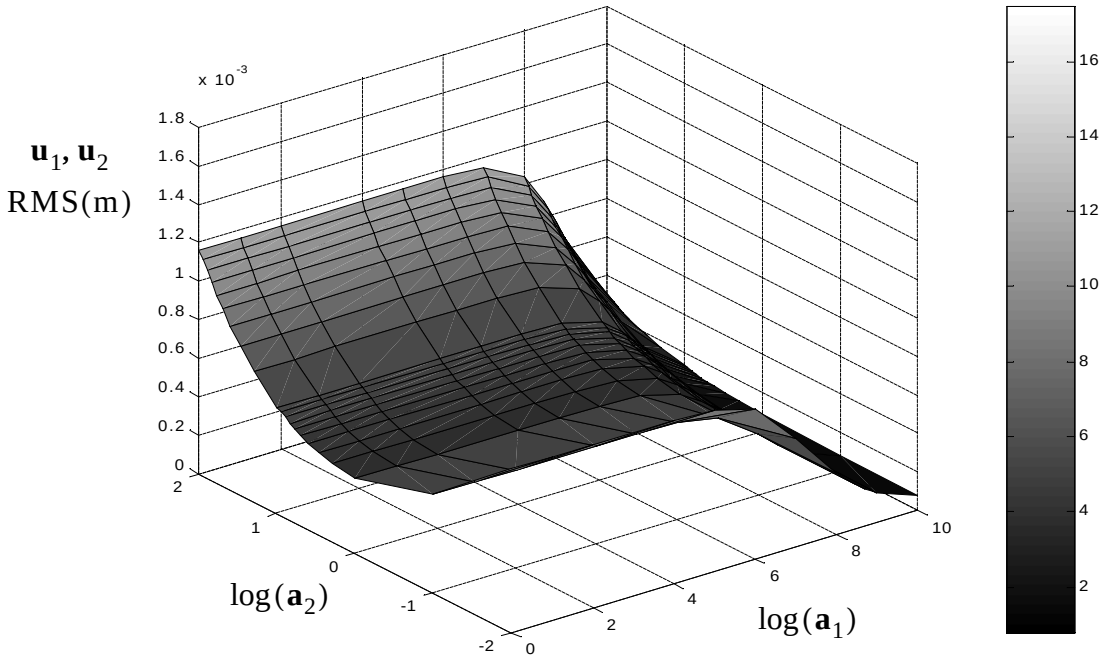

FIGURE 4-1 Ideal active displacements RMS vs. weights a_1, a_2 for Case Ai

The absolute accelerations $\ddot{u}_{1a}, \ddot{u}_{2a}$ are weighted by a_2. In Fig. 4-2, it is shown that the acceleration is minimized for larger a_2. The a_2 weight is limited due to the maximum control force 32 N limit. It is also interesting to note that for the lower values of a_2, the accelerations increase with increasing a_1. The displacements are more heavily weighted than the accelerations as the lower weights of a_1 do not affect the performance of the controller.

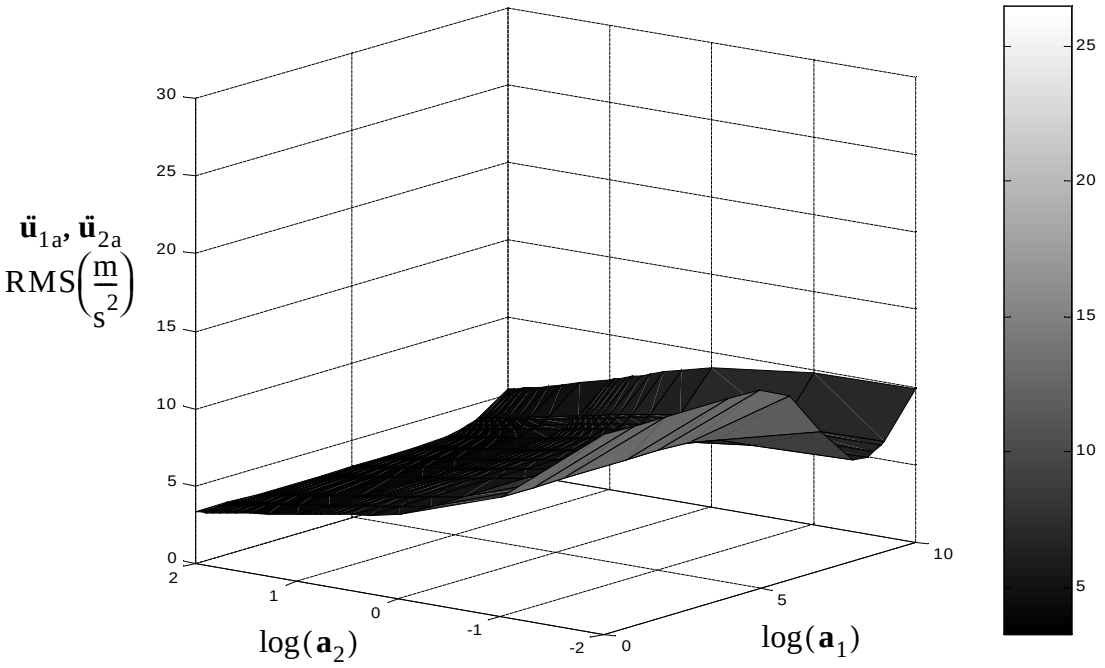

FIGURE 4-2 Ideal active absolute acceleration RMS vs. weights $\mathbf{a}_1, \mathbf{a}_2$ for Case Ai

The maximum control force is plotted vs. the **Q** matrix weights in Fig. 4-3. It is apparent in this figure that the control force varies greatly with small changes in a_2, and not as significantly for changes in a_1. The most interest in this study is when the maximum control force is 32 N. This was selected to be the force limit of the MR damper, to which the ideal controllers performance will be compared in Chapter 7. From the graph it is clear that several weighting combinations (a_1, a_2) at which this maximum occurs.

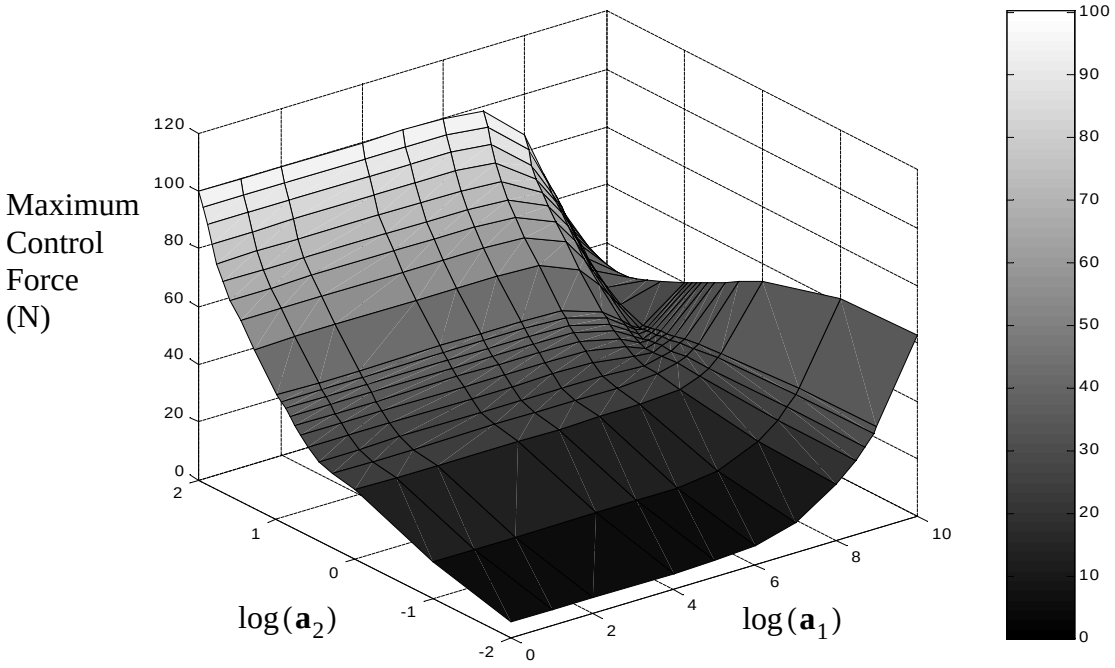

FIGURE 4-3 Ideal active maximum control force RMS vs. weights $\mathbf{a}_1$, $\mathbf{a}_2$ for Case Ai

Further examination is required for the selection of weight combinations that give the best overall performance and are below the maximum control force limit. The uncontrolled (light) and controlled (dark) time histories for displacement, absolute acceleration, and control force representative of the ideal active control system are shown in Fig. 4-4. This is included to show the amount of each reduction for the weighting case $a_1 = 3\times10^8$ and $a_2 = 4$ for 30 sec.

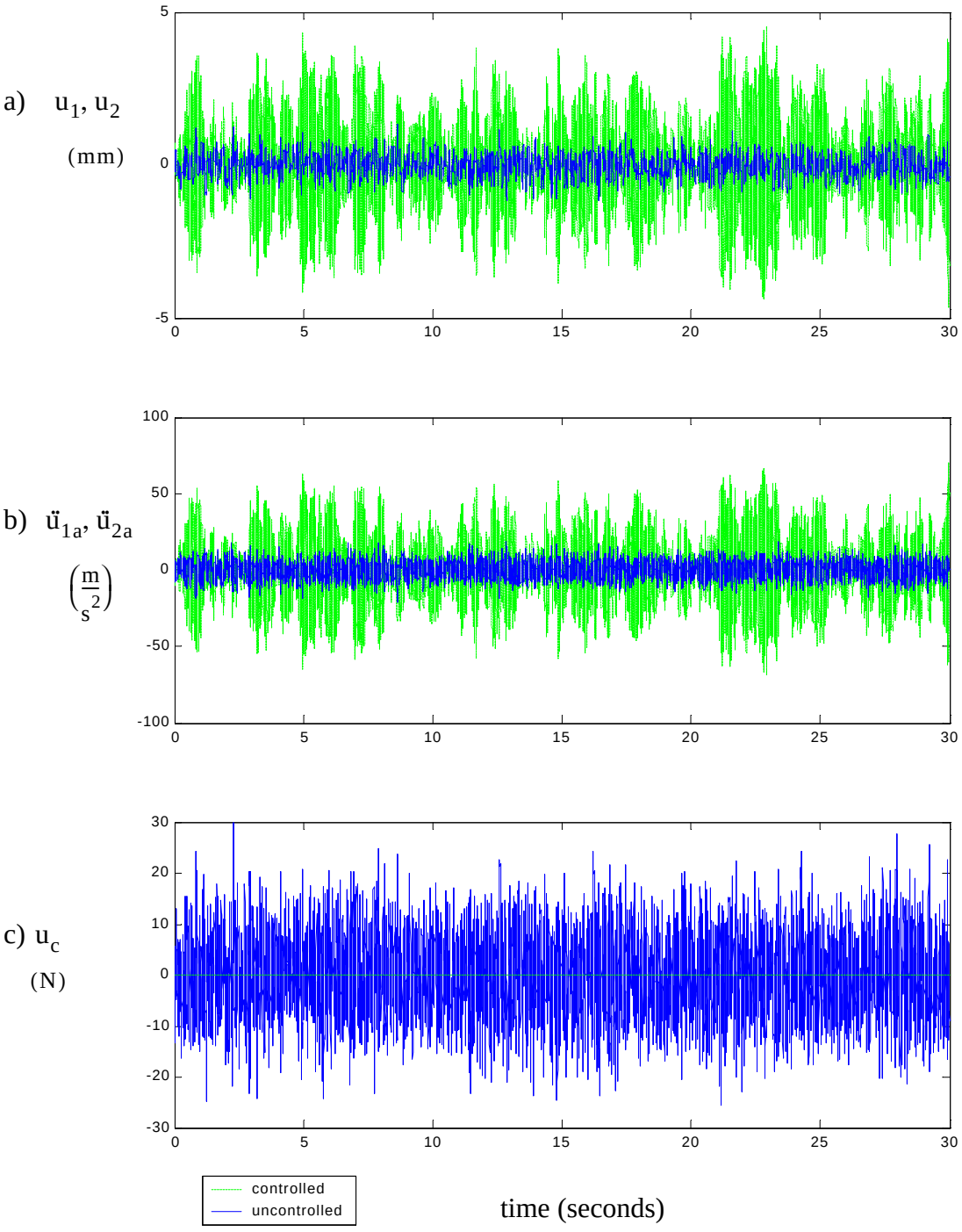

FIGURE 4-4 Time histories for Case Ai:
uncontrolled and ideal active control
a) displacement, b) absolute acceleration, and c) control force

4.2.3 Selection of Q Matrix Weighting for Various CG Cases

In selection of **Q** values for the Cases B, C, and D (in which both modes of vibration are excited) there are new trade-offs that were not an issue for Case A. One trade-off is between the performance of the left end and the right end. A certain combination of weights can give the most reduction in the u_1 performance, but the u_2 performance suffers, and vice-versa. There is another trade-off between the acceleration reduction and the displacement reductions of each variable. The weighting trade-offs are illustrated by numerical examples for Case Ai in Table 4-1, Case Bi in Table 4-2, Case Ci in Table 4-3, and Case Di in Table 4-4. The tables include the weighting case that lead to the most reduction of each of the four metrics (indicated in bold) to be minimized and the final selection case (indicated in *italics*). This "best overall reduction" case will be used in the comparison with other device performance in Chapter 7. The values in the tables are in terms of the RMS except for the maximum control force.

TABLE 4-1 Ideal active control system performance: Case Ai

Case Ai	$\mathrm{Max} u_c$ (N)	u_c (N)RMS	u_1 u_2 q_1 (mm)RMS	$\ddot{u}_{1a}$ $\ddot{u}_{2a}$ $\ddot{q}_{1a}$ $\left(\frac{m}{s^2}\right)$RMS
$a_1 = a_2 = 0$	0	0	1.7492	26.4487
$a_1 = 5\times10^8$, $a_2 = 0$	29.7657	7.4353	**0.1935**	6.6309
$a_1 = 0$, $a_2 = 4$	30.4756	7.5199	0.4427	**4.7174**
$a_1 = 3\times10^8$, $a_2 = 4$	*27.7676*	*6.5162*	*0.3182*	*5.2225*

TABLE 4-2 Ideal active control system performance: Case Bi

Case Bi	u_c (N) MAX	u_c (N) RMS	u_1 (mm) RMS	u_2 (mm) RMS	q_1 (mm) RMS	$\ddot{u}_{1a}$ $\left(\frac{m}{s^2}\right)$RMS	$\ddot{u}_{2a}$ $\left(\frac{m}{s^2}\right)$RMS	$\ddot{q}_{1a}$ $\left(\frac{m}{s^2}\right)$RMS
$a_1 = a_2 = 0$	0	0	0.7881	2.6139	1.8014	23.619	33.702	22.888
$a_1 = 5\times10^8$ $a_2 = 1$	31.588	6.8469	**0.2361**	**0.5099**	0.3660	9.5295	6.6127	5.7002
$a_1 = 0$ $a_2 = 2$	*30.826*	*7.7552*	*0.3947*	*0.7147*	*0.5844*	***5.9511***	*6.3172*	*5.2098*
$a_1 = 5\times10^8$ $a_2 = 7$	31.871	8.210	0.3812	0.6481	0.5335	6.5596	**5.8415**	4.9527
$a_1 = 10^8$ $a_2 = 3$	31.262	7.9429	0.6783	0.6783	0.5562	6.2260	6.0554	5.0525

TABLE 4-3 Ideal active control system performance: Case Ci

Case Ci	u_c (N) MAX	u_c (N) RMS	u_1 (mm) RMS	u_2 (mm) RMS	q_1 (mm) RMS	$\ddot{u}_{1a}$ $\left(\frac{m}{s^2}\right)$RMS	$\ddot{u}_{2a}$ $\left(\frac{m}{s^2}\right)$RMS	$\ddot{q}_{1a}$ $\left(\frac{m}{s^2}\right)$RMS
$a_1 = a_2 = 0$	0	0	1.4025	3.7525	2.7314	37.363	30.786	23.995
$a_1 = 0$ $a_2 = 1$	*26.964*	*6.7588*	***0.3126***	*0.9929*	*0.7756*	***7.6112***	*7.0858*	*5.8152*
$a_1 = 5\times10^8$ $a_2 = 1$	31.888	7.6984	0.3619	**0.6760**	0.5162	11.658	5.5971	5.4609
$a_1 = 8\times10^8$ $a_2 = 3$	31.582	7.9406	0.3604	0.7247	0.5690	10.264	**5.5182**	5.1798
$a_1 = 10^7$ $a_2 = 1$	27.055	6.7892	0.3159	0.9653	0.7540	7.7702	6.9136	5.7074

TABLE 4-4 Ideal active control system performance: Case Di

Case Di	u_c (N) MAX	u_c (N) RMS	u_1 (mm) RMS	u_2 (mm) RMS	q_1 (mm) RMS	$\ddot{u}_{1a}$ $\left(\frac{m}{s^2}\right)$RMS	$\ddot{u}_{2a}$ $\left(\frac{m}{s^2}\right)$RMS	$\ddot{q}_{1a}$ $\left(\frac{m}{s^2}\right)$RMS
$a_1 = a_2 = 0$	0	0	2.0538	4.0119	3.5100	39.965	22.420	21.399
$a_1 = 10^6$ $a_2 = 1$	*31.579*	*6.6131*	***0.5361***	*1.3055*	*1.1565*	*8.2600*	***6.5875***	*6.0643*
$a_1 = 10^8$ $a_2 = 0.1$	31.901	7.5585	0.5602	**0.8531**	0.7507	12.620	**5.4612**	5.5853
$a_1 = 0$ $a_2 = 1$	31.439	6.5862	0.5378	1.3159	1.1655	**8.2433**	6.6358	6.1033

One method used in the selection of the "best overall reduction" case is explained in detail here and the other method used will be demonstrated in section 6.1.4. First, the percent reduction for the displacements and accelerations were plotted along with the maximum control force vs. a_2 indices (with $a_1 = 0$) in Fig. 4-5. It is clear that the best reductions occur at index 14, but the maximum control force is near 60 N. Thus, the best performance, without exceeding the 32 N limit is $a_2(7) = 4$. Next, holding $a_2(7) = 4$ constant, a plot of the performance vs. a_1 is shown in Fig. 4-6. It is clear from the figure, the control force is within the limit, and the best reduction for both variables is achieved using $a_1(10) = 3\times10^8$.

For this study, the control force location is at the origin, Case i. In the next section, the performance of the controller at different locations will be discussed. Notice when the center of mass is moved in the positive x-direction, the uncontrolled acceleration and displacements, $u_1, \ddot{u}_1$, are larger than those of $u_2, \ddot{u}_2$. These findings confirm the behavior expected from the open loop bode plots done in Chapter 2. However, if the center of mass were moved in the negative x-direction, the reverse would be true.

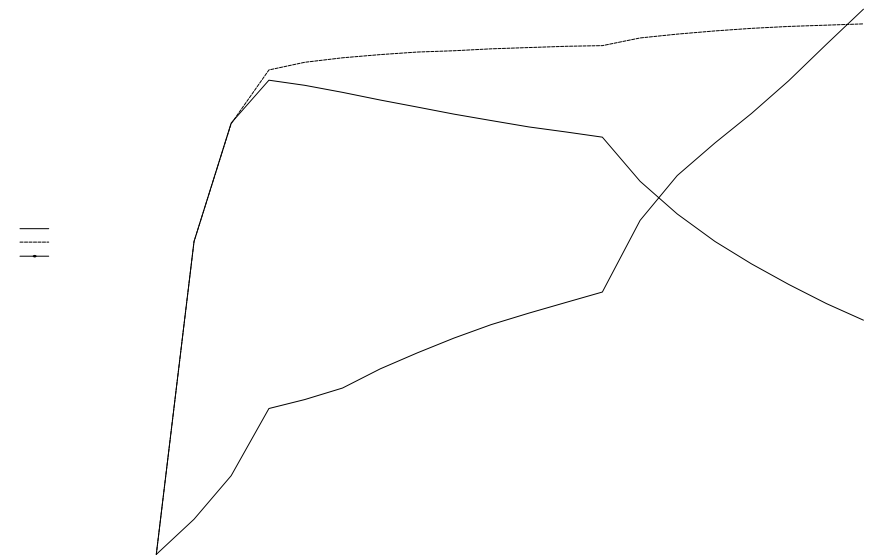

a_2 index

FIGURE 4-5 Demonstration of selection process for best overall performance case % reduction for displacement and acceleration vs. a_2 index with Case Ai and weight $a_1 = 0$

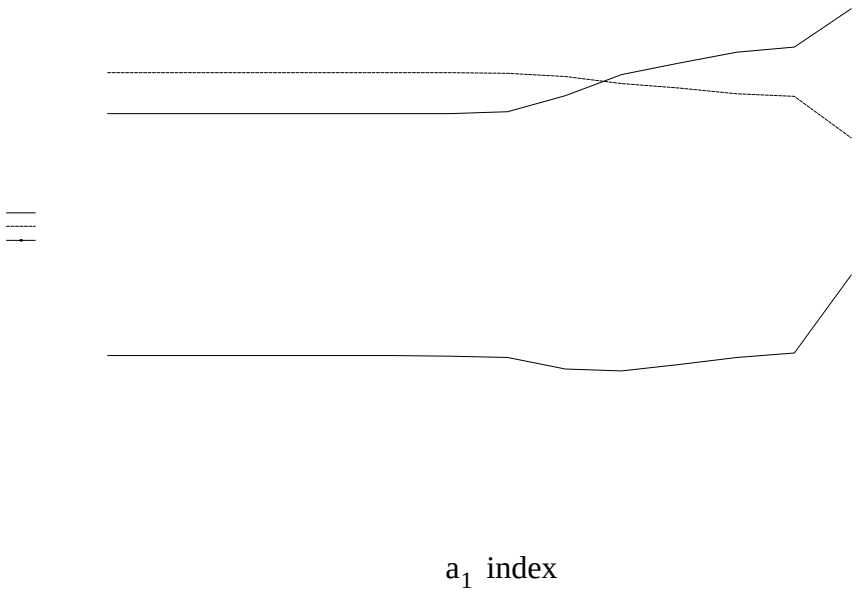

a_1 index

FIGURE 4-6 Demonstration of selection process for best overall performance case % reduction for displacement and acceleration vs. a_1 index with Case Ai and weight $a_2(7) = 4$

4.2.4 Parametric Study of Control Device Location

As is expected for Case A, the optimal control location is Case i when the control force is applied at O in Fig. 4-7. However, it was not clear if this was the optimal control force location for the cases where both modes of vibration were excited Cases B,C, and D. The control force location decision for each controller was made based on the acceleration reductions of both ends for various control force locations. One controller was designed and used in the study to find the best control force location for the active force actuator. The controller design with weights $a_1 = 10^7$ and $a_2 = 1.8$. It was selected based on the results in the previous section and a more refined search. This control design ensured the control force did not exceed the 32 N limit, even for the higher acceleration cases with the CG further from the origin.

There are several trade-offs in control force location selecction. For instance, there is a trade-off between the left and right displacement and acceleration reduction, between the displacement reduction as opposed to the acceleration reduction, and the most acceleration or displacement reduction as opposed to the collective “best overall” performance. It is important to realize when overall performance is examined, that better reductions can be achieved for each individual regulated output and it may be achieved in overall performance when multiple controllers are researched. However, this thesis only investigates one control device and thus it is important to discuss typical overall performance that can be expected by each controller, but to also note typical and good performance of each variable for future studies.

The trade-off is shown, in examining Fig. 4-7 i) and iii), between the displacement reduction at the right end and at the left end of the avionics package. The absolute accelerations of both ends are in Fig. 4-7 ii and iv. The u_1, u_2, and $\ddot{u}_{1a}$ are minimized when the controller is near or at the CG location, i.e. Case Ai, Case Bii, Case Ciii, and Case Div. However, $\ddot{u}_{2a}$ is minimized for Case Ai and when the control force is at Case ii for the rest of the CG locations.

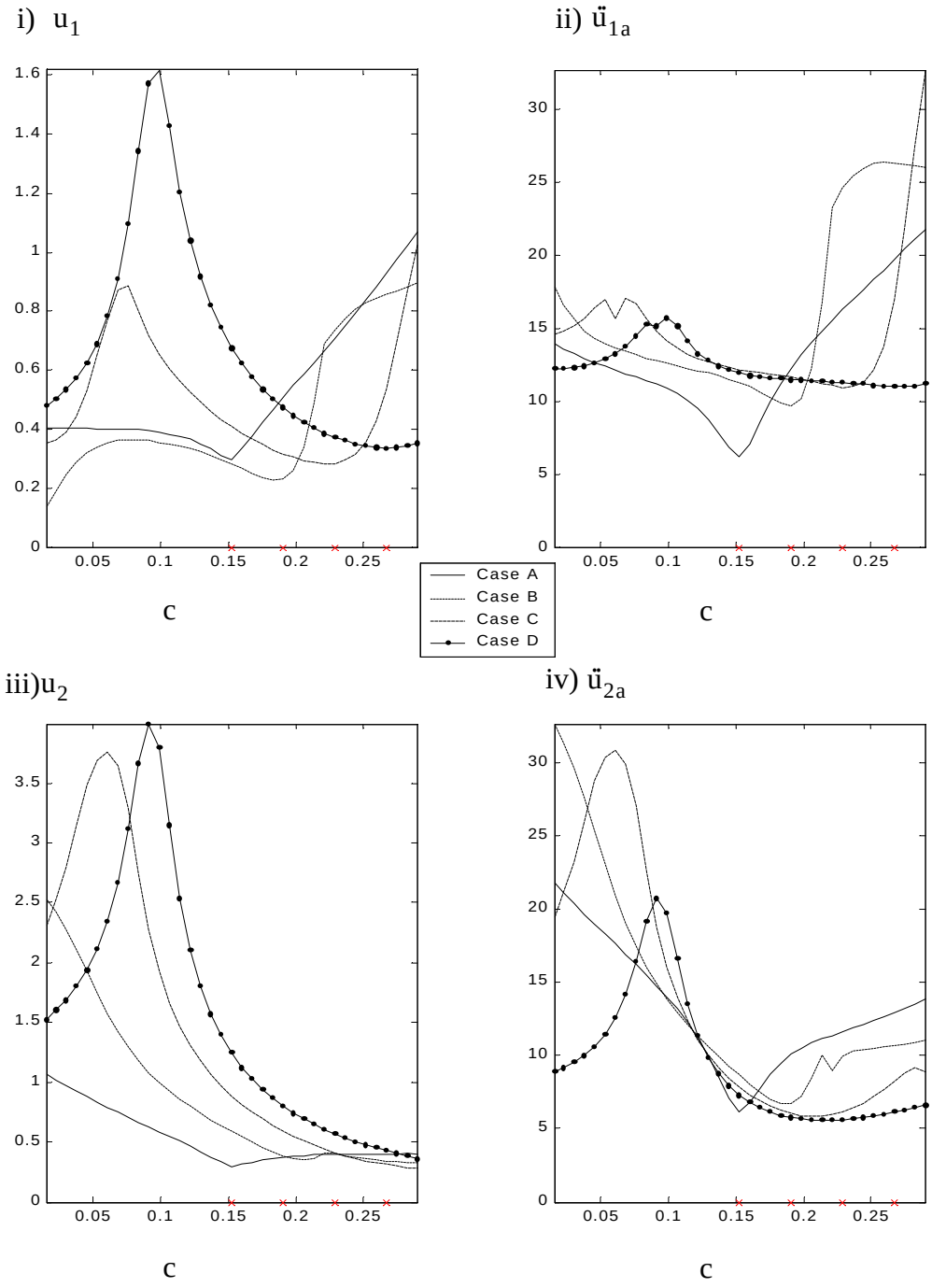

FIGURE 4-7 Control force location vs. i) u_1, ii) $\ddot{u}_{1a}$, iii) u_2, and iv) $\ddot{u}_{2a}$ for each CG location case
Note:(CG location denoted by x on origin)

In summary, the overall performance can be achieved with the control force located either at Case i, Case ii, or somewhere in between. Possibly in further studies using multiple controllers, the sacrifice of performance in one variable for the minimization of another variable, may not be so great and better performance of each variable may be achievable simultaneously.

TABLE 4-5 Ideal active control system performance: Case A, B, C, D

	c	u_c (N) MAX	u_1 (mm) RMS	u_2 (mm) RMS	$\ddot{u}_{1a}$ $\left(\frac{m}{s^2}\right)$RMS	$\ddot{u}_{2a}$ $\left(\frac{m}{s^2}\right)$RMS
Case A a = 0.1524	c(19) = 0.1524	25.1152	**0.3165**	**0.3165**	**5.5174**	**5.5174**
Case B	c(23) = 0.1828	29.9328	**0.1893**	0.4737	7.5859	**5.7769**
a = 0.1905	c(26) = 0.2057	33.2851	0.2644	**0.3642**	9.9455	7.3239
	c(14) = 0.1143	24.7835	0.4845	0.7399	**7.0518**	8.5480
Case C	c(27) = 0.2133	29.4047	**0.2039**	0.5440	8.9629	5.3391
a = 0.2286	c(35) = 0.2743	41.2944	0.4048	**0.3153**	13.2871	9.2976
	c(7) = 0.2364	19.6390	0.5068	3.6863	**7.1727**	30.2596
	c(14) = 0.1983	27.6536	0.2126	0.6194	9.0113	**5.2763**
Case D	c(36) = 0.2798	31.0892	**0.2798**	0.4049	9.1676	6.0541
a = 0.2667	c(38) = 0.2971	33.7505	0.2895	**0.3528**	9.3669	6.5717
	c(1) = 0.0152	22.3476	0.6510	0.9633	**7.4287**	6.0555
	c(25) = 0.1983	29.5330	0.3628	0.7366	9.5830	**4.8148**

4.3 Ideal Passive Controller Performance

Current avionics mounts are passive devices. These mounts (isolators) are composed of highly damped elastomeric materials. Since these isolators are the mounts currently used in vibration isolation of the avionics, an ideal passive control device is included in this study for comparative purposes.

4.3.1 Behavior of Ideal Passive Viscous Damper

The passive device in this study is assumed to be ideal in that it does not include the dynamics that are involved with this type of device. Examples are the exclusion of variations in the elastomeric properties with heat and loading and unloading conditions. The force is assumed to be perfectly linear, have no stiffness, and was defined in Eq. (3-33).

For the sinusoid studies the damping coefficient used was $\alpha = 30$. The linear relationship between the control force and the velocity can be seen in Fig. 4-8 when a sinusoid used as the ground excitation a frequency of ω as

$$u(t) = u_o \sin(\omega t - \phi). \tag{4-3}$$

Taking the derivative of Eq. (4-3) with respect to time and substituting the resulting time rate of change of displacement into Eq. (3-33) results in the force due to the viscous damper

$$f_d = -c\dot{u}(t) = -c\omega u_o \cos(\omega t - \phi) \tag{4-4}$$

Equation (4-4) combined with the trigonometric identity

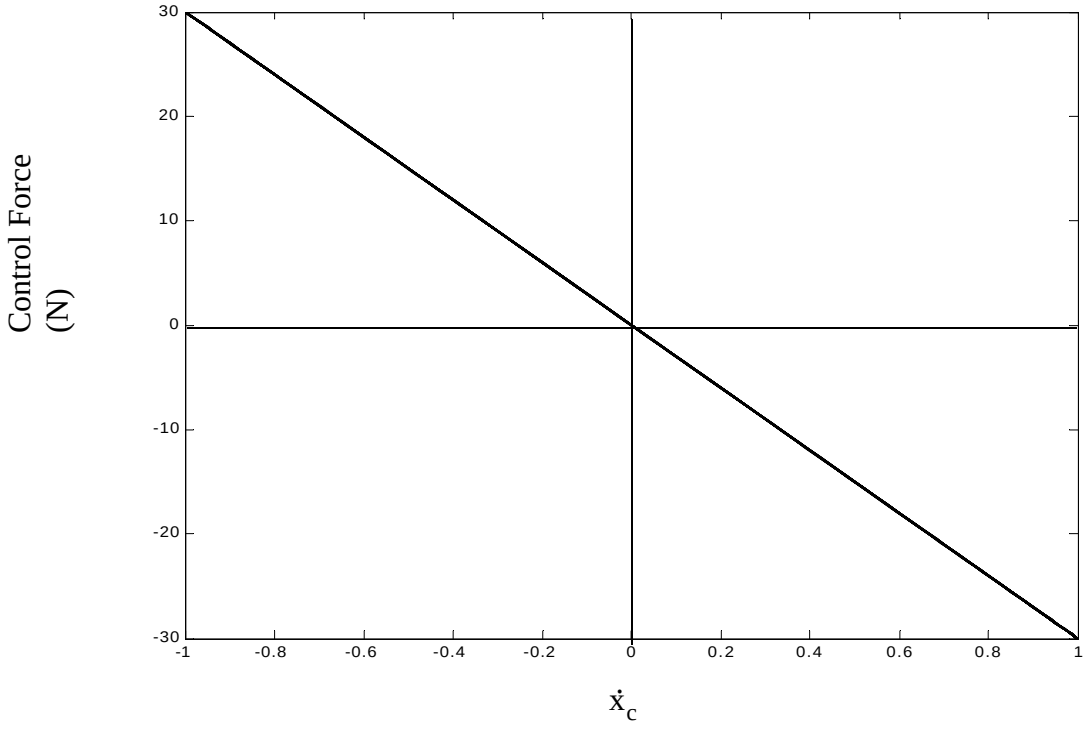

FIGURE 4-8 Control Force vs. Velocity $\dot{x}_c$ of Control Device

$$1 = (\cos(\omega t - \phi))^2 + (\sin(\omega t - \phi))^2 \tag{4-5}$$

gives

$$f_d = -c\omega\sqrt{u_o^2 - u_o^2(\sin(\omega t - \phi))^2} \tag{4-6}$$

and finally gives

$$f_d = -c\omega\sqrt{u_o^2 - [u(t)]^2}. \tag{4-7}$$

Rearranging the equation and equating to one gives the equation of an ellipse

$$\left(\frac{u}{u_o}\right)^2 + \left(\frac{f_d}{c\omega u_o}\right)^2 = 1. \tag{4-8}$$

The preceding was derived by Chopra (1995) who also derived the energy dissipated by the viscous damper in one cycle of harmonic vibration as

$$E_D = \int_0^{\frac{2\pi}{\omega}} f_d du \tag{4-9}$$

using a change in variables and substituting in Eq. (3-33) and derivative of Eq. (4-3)

$$E_d = \int_0^{\frac{2\pi}{\omega}} (c\dot{u})\dot{u}dt = \int_0^{\frac{2\pi}{\omega}} c\dot{u}^2 dt = c\int_0^{\frac{2\pi}{\omega}} [\omega u_o \cos(\omega t - \phi)]^2 dt \tag{4-10}$$

$$E_d = \pi c \omega u_o^2 \tag{4-11}$$

which is the area enclosed by the ellipse. The amount of energy dissipated by damping is the area of the ellipse in the force vs. displacement hysteresis loops for the viscous damper in Fig. 4-9 (Chopra 1995).

Representative time histories for the passively controlled and uncontrolled avionics system corresponding to Case Ai with $\alpha = 298.736$ are in Fig. 4-10.

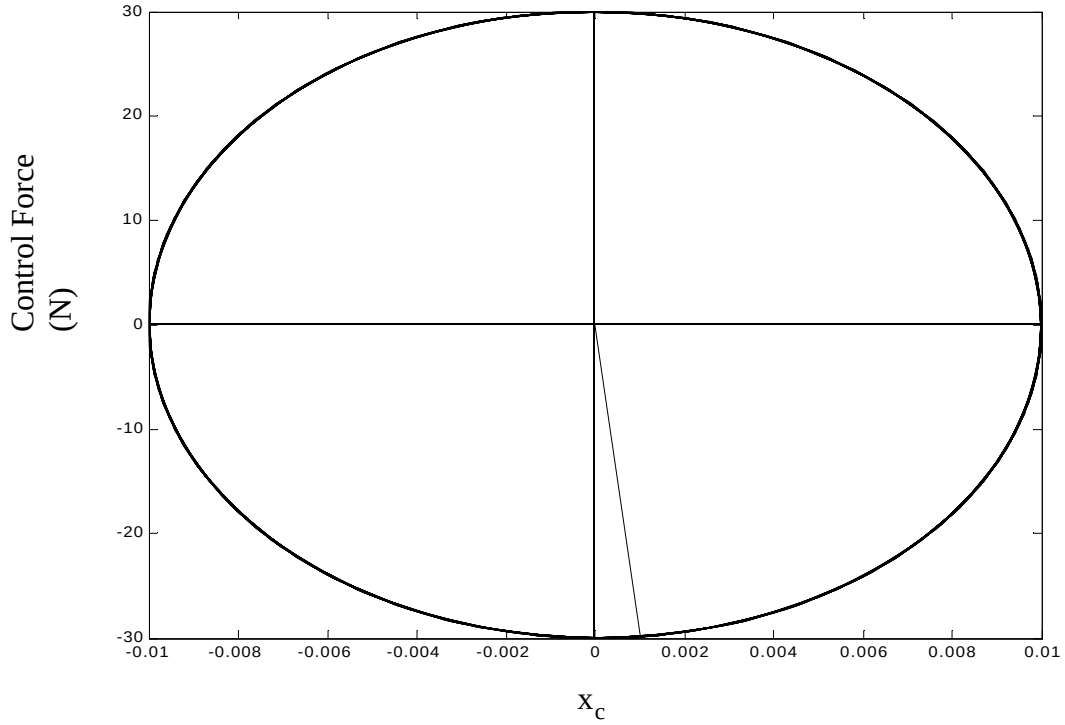

FIGURE 4-9 Maximum control force vs. displacement x_c of control device

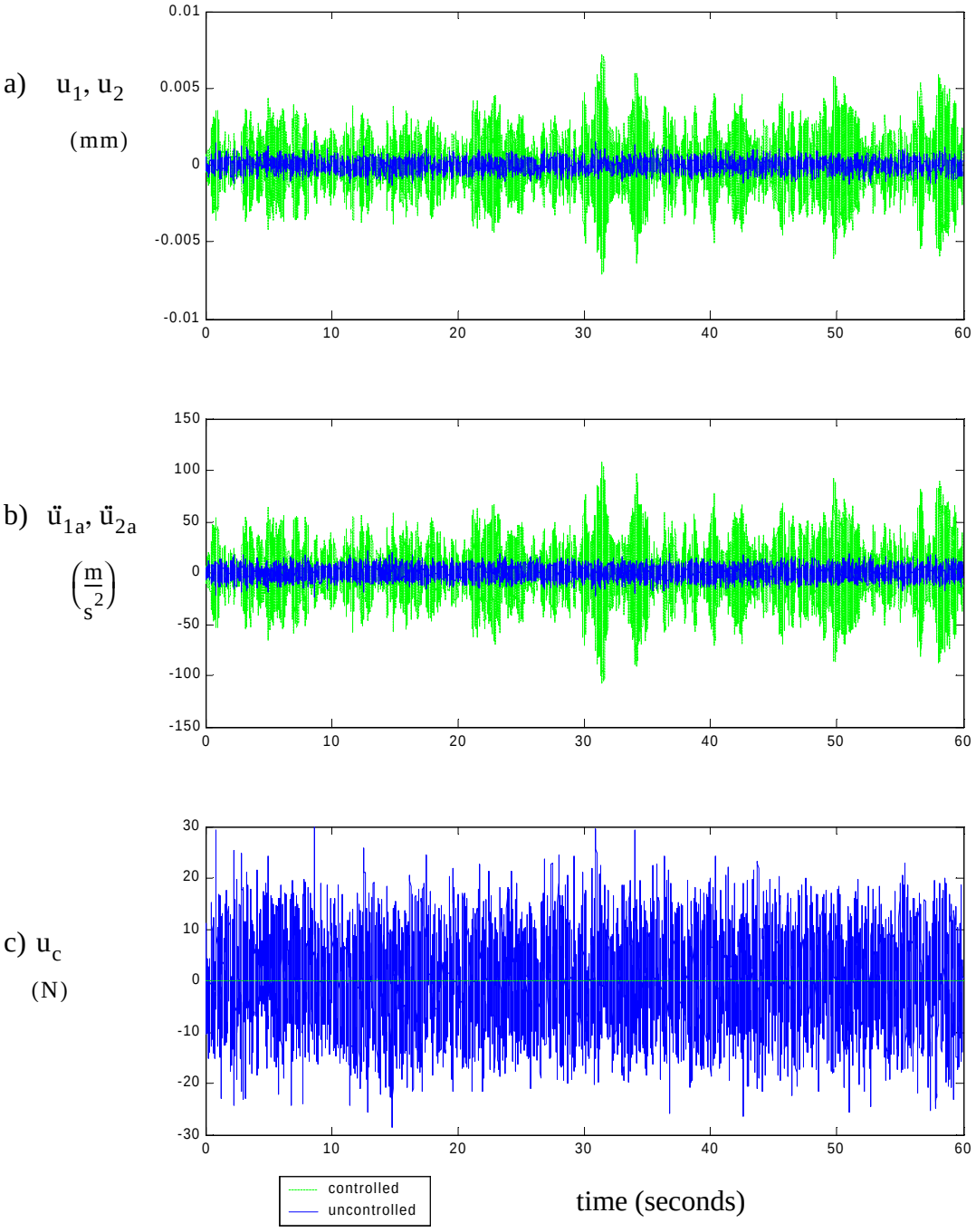

FIGURE 4-10 Time histories for Case Ai:
uncontrolled and ideal passive control
a) displacement, b) absolute acceleration, and c) control force

4.3.2 Damping Coefficient α Selection

In passive control, the damping properties of the device are assumed to be fixed once the device is built. It is assumed the device is a viscous and linear damper within the range of application. The viscous control force varies linearly with the velocity at the damper location with respect to a coefficient related to the amount of damping α in Fig. 4-11. The control force of interest for this application, 32 N, is emphasized with a circle. The parameter used in the study to find the desired damping coefficient was α = [0:10:500].

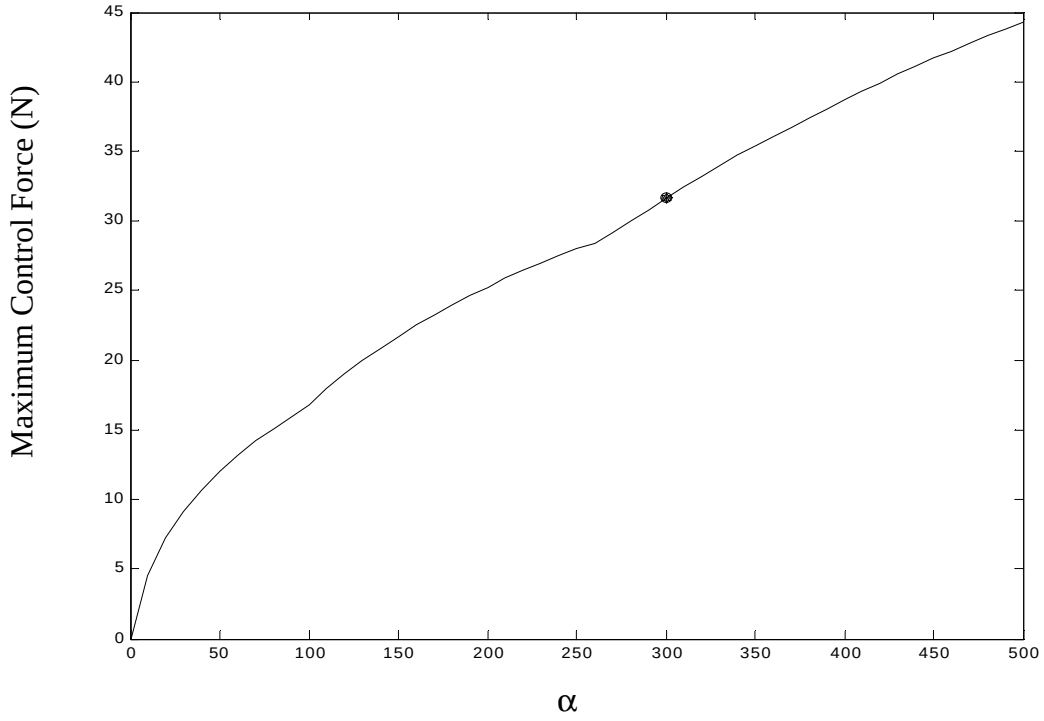

FIGURE 4-11 Control force vs. damping parameter α for ideal passive control

The performance of the system with a viscous device are in Table 4-6 for Case Ai, Bi, Ci and Di. The damping coefficient was selected based on the maximums control force 32 N limit. The coefficient could be manipulated to find the exact case that would lead to a maximum control force of 32 N, but it was elected not to do so in order to vary the passive

case. The case with a control force closes to 32 N is the best overall performance case. It is listed in *italics* and will be included in the comparison.

TABLE 4-6 Passive control system performance: Cases Ai, Bi, Ci and Di

	u_c (N) MAX	u_c (N) RMS	u_1 (mm) RMS	u_2 (mm) RMS	q_1 (mm) RMS	$\ddot{u}_{1a}$ $\left(\frac{m}{s^2}\right)$RMS	$\ddot{u}_{2a}$ $\left(\frac{m}{s^2}\right)$RMS	$\ddot{q}_{1a}$ $\left(\frac{m}{s^2}\right)$RMS
Case Ai $\alpha = 0$	0	0	1.7492	1.7492	1.7492	26.449	26.449	26.449
$\alpha = 300$	*31.624*	*7.8807*	*0.2102*	*0.2102*	*0.2102*	*5.9802*	*5.9802*	*5.9802*
Case Bi $\alpha = 0$	0	0	0.7881	2.6139	1.8014	23.619	33.702	22.888
$\alpha = 300$	*31.707*	*7.7176*	*0.3301*	*0.4829*	*0.2719*	*12.410*	*8.7746*	*5.9618*
Case Ci $\alpha = 0$	0	0	1.4025	3.7525	2.7314	37.363	30.786	23.995
$\alpha = 290$	*31.970*	*7.6053*	*0.4715*	*0.7521*	*0.5057*	*12.180*	*7.4365*	*6.2045*
Case Di $\alpha = 0$	0	0	2.0538	4.0119	3.5100	39.965	22.420	21.399
$\alpha = 350$	*31.599*	*8.3423*	*0.7452*	*1.0816*	*0.9233*	*12.433*	*7.0195*	*6.7055*

4.3.3 Parametric Study of Control Device Location

A study was performed to find the location of the passive damper that would give the best overall performance for the passive device. Thirty-six different control force locations were examined for each of the four CG locations. Figure 4-12 is a graph of the various performance for each of the four metrics to be minimized. Results for all four CG cases are presented for various control force locations in Table 4-7. As is expected, for the CG Case A, the optimal control location is Case i when the control force is applied at O, when c = 0.1524, in Fig. 4-12. The damping coefficient was selected to be $\alpha = 290$ for the

study, because it was the lowest coefficient that would guarantee a damping force of less than 32 N for all four CG locations.

TABLE 4-7 Passive control system performance: Cases A,B,C, and D

	c	u_c (N) MAX	u_1 (mm) RMS	u_2 (mm) RMS	$\ddot{u}_{1a}$ $\left(\frac{m}{s^2}\right)$RMS	$\ddot{u}_{2a}$ $\left(\frac{m}{s^2}\right)$RMS
Case A a = 0.1524	c(1) = 0.0152	25.6416	**0.1861**	1.4522	11.0946	29.1866
	c(37) = 0.2895	25.6621	1.4513	**0.1861**	29.1748	11.0942
	c(19) = 0.1524	17.7848	0.2137	0.2138	**5.9396**	**5.9374**
Case B	c(1) = 0.0152	17.5603	**0.1050**	2.5480	12.3408	32.7126
a = 0.1905	c(38) = 0.2971	28.3266	1.0613	**0.2094**	30.0257	8.2049
	c(23) = 0.1828	30.6415	0.2509	0.3373	**10.3781**	**6.5182**
Case C	c(1) = 0.0152	19.5743	**0.1545**	2.6113	11.9959	22.0721
a = 0.2286	c(38) = 0.2971	28.2718	1.1472	**0.2410**	36.6576	6.2138
	c(27) = 0.2133	35.1892	0.2886	0.3718	**5.4299**	10.8942
	c(26) = 0.2057	35.5128	0.2917	0.3948	10.9641	**5.4136**
Case D	c(1) = 0.0152	27.2697	**0.2878**	1.9515	11.3258	11.3258
a = 0.2667	c(38) = 0.2971	34.6187	0.4371	**0.2941**	13.4310	6.0153
	c(31) = 0.2438	35.2539	0.3092	0.3842	**10.4224**	5.4433
	c(26) = 0.2057	24.4821	0.3838	0.5238	10.8142	**5.2474**

From Fig. 4-12 and Table 4-7, it is clear there is trade-off between reduction for each individual response vs. the best overall performance. The best control force location is at the corresponding CG location, i.e., Case Ai, Case Bii, Case Ciii, and Case iv, except for the acceleration of the left end, $\ddot{u}_{2a}$, which is minimized for Case Ai, Bii, Cii, Dii. This will be used a consideration in the overall performance consideration.

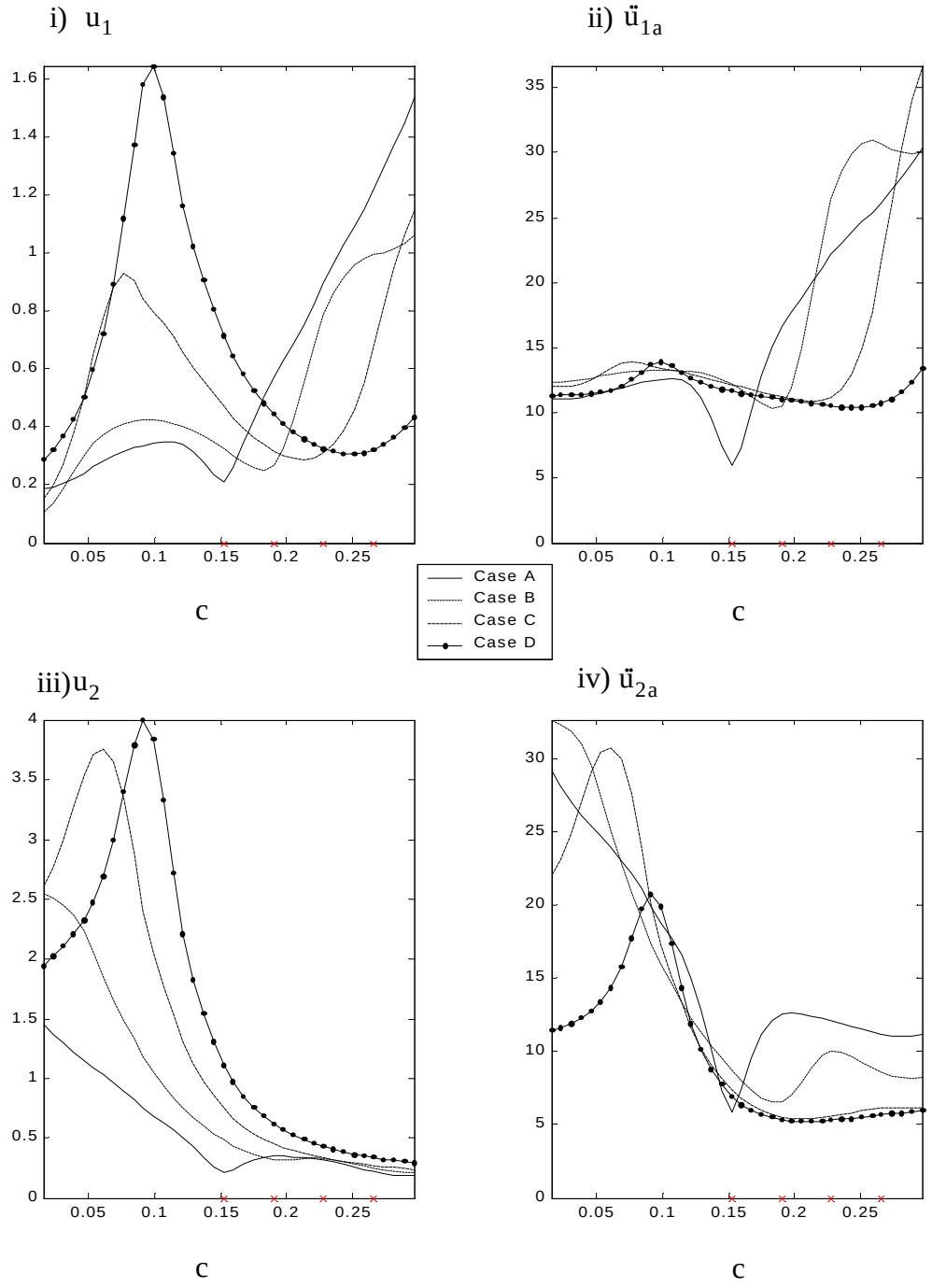

FIGURE 4-12 Control force location vs. i) u_1, ii) $\ddot{u}_{1a}$, iii) u_2, and iv) $\ddot{u}_{2a}$ for each CG location case
Note:(CG location denoted by x on origin)

4.4 Ideal Semi-Active Device Performance

In this section, an ideal model of a semi-active device is considered. Semi-active devices are typically highly nonlinear in nature. The results are indicative of typical results that can be expected from such devices. However, the performance of ideal models is better than the actual device results, and in this sense the results presented herein represent an ideal situation. This discussion is useful in understanding the behavior of the devices relative to one another, and comparing the performance of a real device models (MR and VO dampers) in Chapter 6 to the results of an ideal device model.

4.4.1 Parameters used for Ideal Semi-Active Control

The vectors containing many different weights in the **Q** matrix were selected for presentation of behavior: $\mathbf{a}_1$ = [0 1 10 100 10^4 10^5 10^6 10^7 10^8 3×10^8 5×10^8 8×10^8 10^9 10^{10}] and $\mathbf{a}_2$ = [0 10^{-2} 10^{-1} 1 2 3 4 5 6 7 8 9 10 20 30 40 50 60 70 80 90 100 10^3 10^4 10^5 10^6 10^7 10^8].

4.4.2 Behavior of Ideal Semi Active Control Device

A study illustrating the dissipative nature of the ideal semi-active control device was included. The controller response to a sinusoidal displacement input to the device and a constant positive desired force shows when the control force is applied and when it is zero. It can only apply a control force when the velocity at the control force location and the measured force have opposite signs. Therefore, the measured force (solid line), the desired force (dashed line), and the velocity (dash-dot line) are included in the graph in Fig. 4-13. Also, it is important to notice how the force applied is curved with a gradual roll off from the “off” position to the desired force due to the first order filter applied to the ideal semi-active device. The first order filter is given by

$$\dot{f}_m = -\tau(f_m - f_d) \tag{4-12}$$

where $\tau = \frac{100}{\text{sec}}$ is the time constant associated with the first order filter. If there were no filter, the controller would jerk from the zero to the desired control force, and this can result in large transient responses in the accelerations.

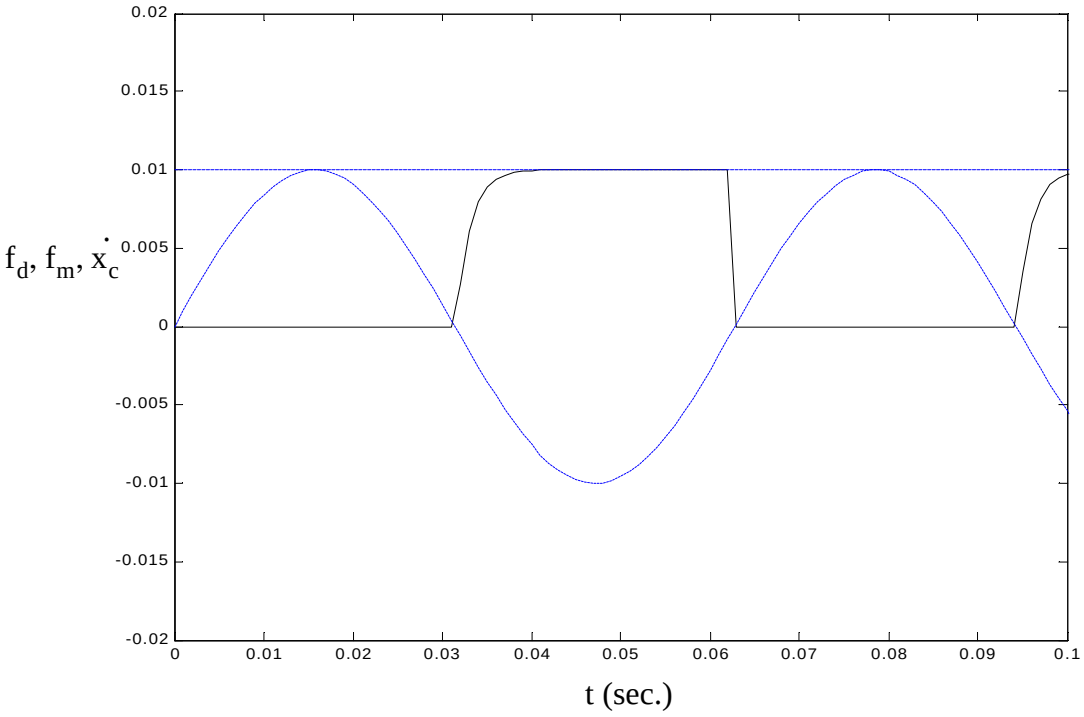

FIGURE 4-13 Time history of ideal semi-active device for a sinusoid input

4.4.3 Q Matrix Selection: Case Ai

The **Q** matrix from the infinite horizon cost function is defined in the previous chapter in Eq. (3-8) where the weights a_1 are on displacements, u_1, u_2, and the weights a_2 are on absolute accelerations, $\ddot{u}_{1a}, \ddot{u}_{2a}$. First, studies were performed by varying a_1, a_2 for Case Ai, in which only the first mode of vibration is excited and the control force is located at O. Since the value of the weights was so varied, the base 10 log of the weights were

calculated. The $\log_{10}(\mathbf{a}_1)$, $\log_{10}(\mathbf{a}_2)$, and RMS values are in Fig. 4-14 for displacement, Fig.4-15 for acceleration, and Fig. 4-16 for maximum control force.

The displacements u_1, u_2 are weighted by a_1 .It is clear from Fig. 4-14 that, as the value of a_1 increases, the displacement decreases. It is interesting to note that as a_2 increases the displacement decreases from 1-100, but then it starts to increase. It adversely affects the displacement as it is the weighting for acceleration and there will be a trade-off between minimizing displacements and reducing accelerations as was the case for the ideal active controller.

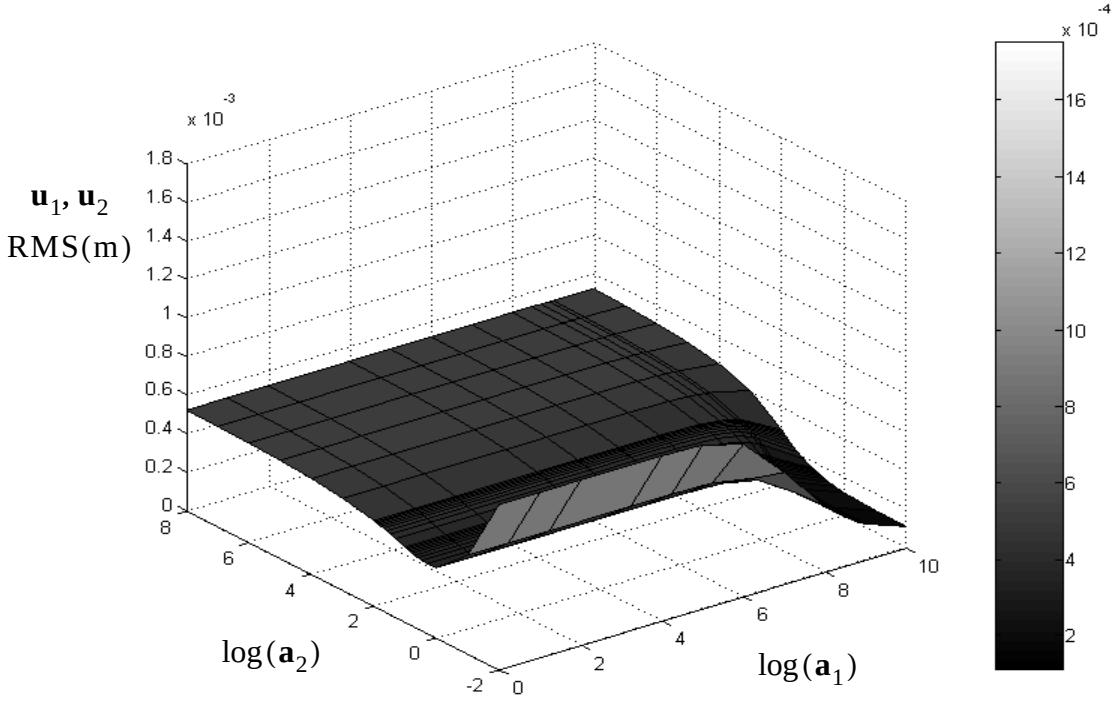

FIGURE 4-14 ISA displacement RMS vs. weights $\mathbf{a}_1, \mathbf{a}_2$ for Case Ai

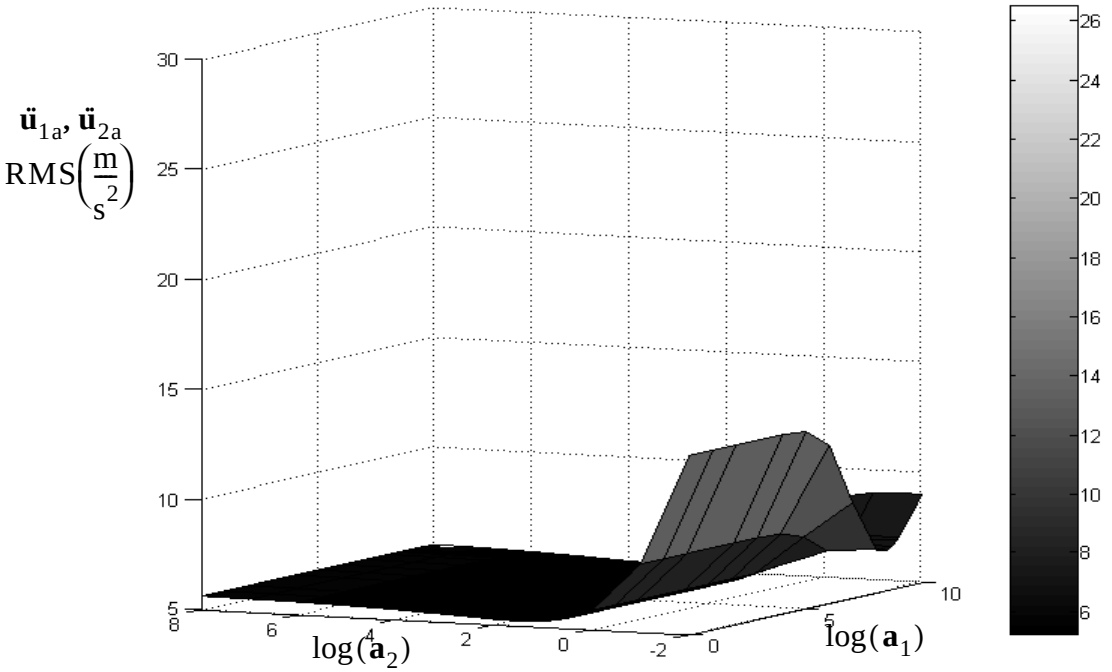

FIGURE 4-15 ISA absolute acceleration RMS vs. weights $\mathbf{a}_1, \mathbf{a}_2$ for Case Ai

The absolute accelerations $\ddot{u}_{1a}, \ddot{u}_{2a}$ are weighted by a_2 and in Fig. 4-15 it is shown that the acceleration is very high for low values of a_2. The acceleration decreases for larger a_2 values, where it seems to plateau. For the lower values of a_2 increasing, the weight on displacement, a_1, increases the absolute accelerations. However, it does not seem to be the case for the higher values larger than 10.

The maximum control force is plotted vs. the **Q** matrix weights in Fig. 4-16. Once again, a_2 is limited due to the maximum control force limit.The desired maximum control force is set to 32 N. It is apparent from this figure that the control force varies greatly with small changes in a_2, and not as significantly for changes in a_1, except for very large values above 10^{10}, where it suddenly effects the force dramatically. From the graph it appears there are several locations where this limit occurs.

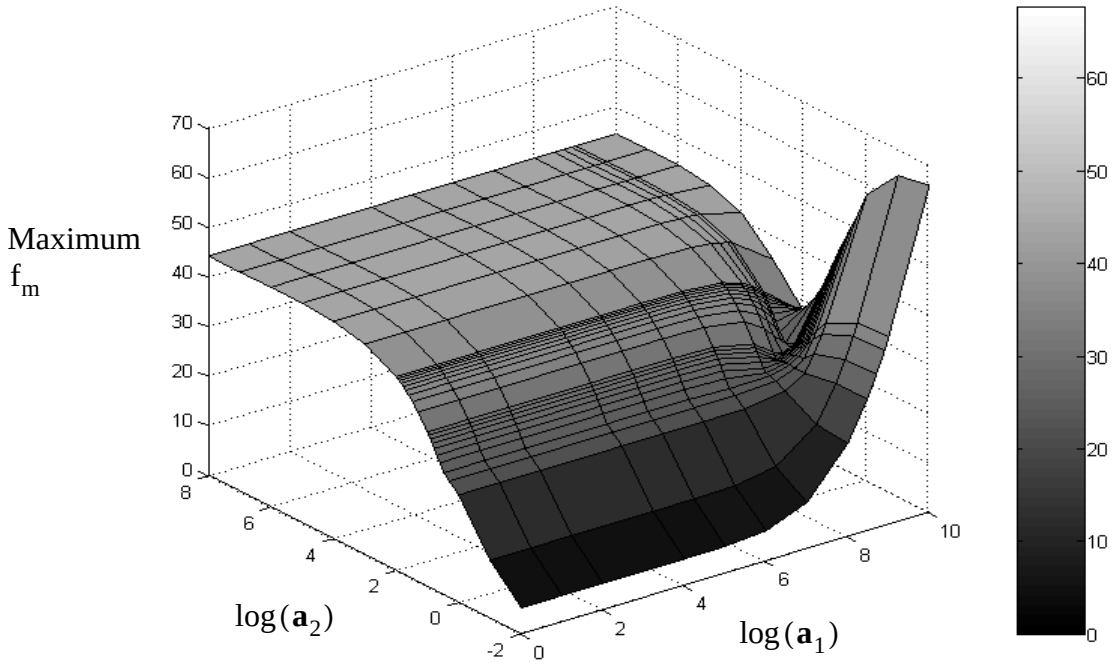

FIGURE 4-16 ISA maximum control force RMS vs. weights $\mathbf{a}_1$, $\mathbf{a}_2$ for Case Ai

The three dimensional graphs in Fig. 4-14, Fig. 4-15, and Fig. 4-16 show the performance trends as the weightings vary, but the best combination of a_1 and a_2 for Case Ai cannot be determined by the figures. The approach used is outlined in Sections 4.2.3 and Section 6.1.4. Time histories for the controlled and uncontrolled acceleration, displacement, and control forces for Case Ai are plotted in Fig. 4-17 with a controller $a_1 = 8\times10^8$ and $a_2 = 50$.

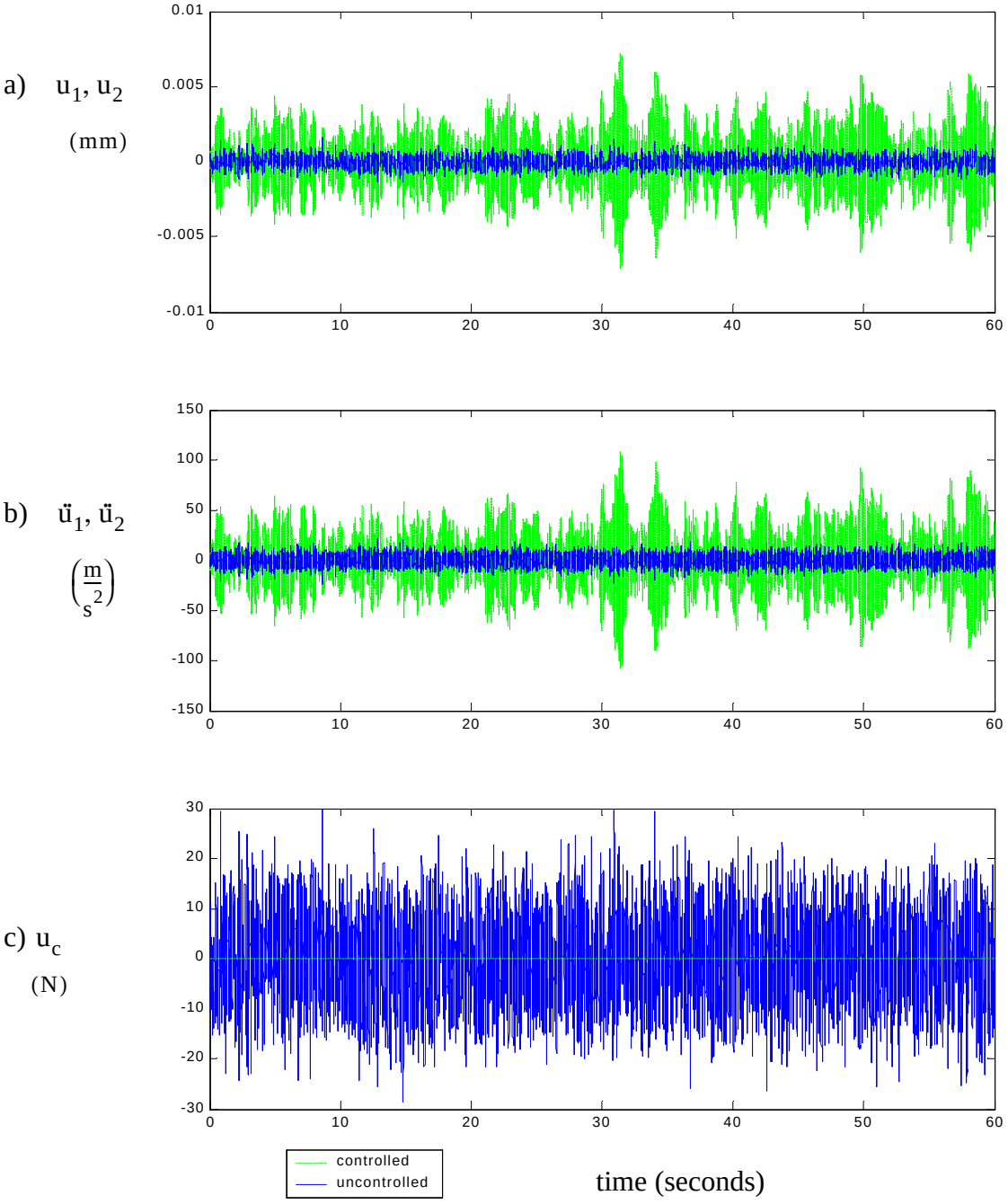

FIGURE 4-17 Time histories for Case Ai:
uncontrolled and ideal semi-active control
a) displacement, b) absolute acceleration, and c) control force

4.4.4 Selection of Q Matrix Weighting for Various CG Cases

In selecting the **Q** matrix for the cases in which both modes of vibration are excited, there are trade-offs that were not an issue for Case Ai in Table 4-8. The trade-off is between the performance at the left end and the right end. A certain combination of weights can give reduction in u_1, but u_2 suffers, and vice versa. The weighting trade-offs are illustrated by numerical examples for Cases Bi in Table 4-9, Case Ci in Table 4-10, and Case Di in Table 4-11. The highest reduction case is in bold for the four weighted responses, u_1, u_2, $\ddot{u}_{1a}$, $\ddot{u}_{2a}$. The methods used in the process for selecting the "best overall reduction" case are detailed in Section 4.2.3 and in Section 6.1.4 The "best overall" cases are indicated in *italics* and are used for comparison in Chapter 7.

TABLE 4-8 ISA control system performance: Case Ai

Case Ai	$\mathrm{Max} u_c$ (N)	u_c (N)RMS	u_1 u_2 q_1 (mm)RMS	$\ddot{u}_{1a}$ $\ddot{u}_{2a}$ $\ddot{q}_{1a}$ $\left(\frac{m}{s^2}\right)$RMS
$a_1 = a_2 = 0$	0	0	1.7492	26.4487
$a_1 = 10^9$, $a_2 = 2$	31.6231	7.4306	**0.2163**	6.6443
$a_1 = 8\times10^8$, $a_2 = 50$	*31.4435*	*7.0943*	*0.3794*	***5.2870***

TABLE 4-9 ISA control system performance: Case Bi

Case Bi	u_c (N) MAX	u_c (N) RMS	u_1 (mm) RMS	u_2 (mm) RMS	q_1 (mm) RMS	$\ddot{u}_{1a}$ $\left(\frac{m}{s^2}\right)$RMS	$\ddot{u}_{2a}$ $\left(\frac{m}{s^2}\right)$RMS	$\ddot{q}_{1a}$ $\left(\frac{m}{s^2}\right)$RMS
$a_1 = a_2 = 0$	0	0	0.7881	2.6139	1.8014	23.619	33.702	22.888
$a_1 = 5\times10^8$ $a_2 = 1$	31.353	6.6955	**0.2526**	0.5225	0.3583	11.123	7.3062	6.1011
$a_1 = 3\times10^8$ $a_2 = 0$	31.634	6.9211	0.2995	**0.4951**	0.3161	13.833	7.7927	6.4922
$a_1 = 0$ $a_2 = 1$	27.259	5.2840	0.2777	0.6906	0.5061	**8.1767**	8.1425	6.2298
$a_1 = 10^{10}$ $a_2 = 50$	31.749	6.7178	0.2667	0.5545	0.4031	9.7081	**6.9885**	5.8133
$a_1 = 10^7$ $a_2 = 1$	27.152	5.3270	0.2756	0.6806	0.4980	8.2572	8.0682	6.1844

TABLE 4-10 ISA control system performance: Case Ci

Case Ci	u_c (N) MAX	u_c (N) RMS	u_1 (mm) RMS	u_2 (mm) RMS	q_1 (mm) RMS	$\ddot{u}_{1a}$ $\left(\frac{m}{s^2}\right)$RMS	$\ddot{u}_{2a}$ $\left(\frac{m}{s^2}\right)$RMS	$\ddot{q}_{1a}$ $\left(\frac{m}{s^2}\right)$RMS
$a_1 = a_2 = 0$	0	0	1.4025	3.7525	2.7314	37.363	30.786	23.995
$a_1 = 10^5$ $a_2 = 6$	31.394	6.4058	**0.3282**	1.0437	0.7996	9.3229	7.8569	6.4690
$a_1 = 10^8$ $a_2 = 0$	29.620	6.1647	0.4512	**0.7594**	0.5444	14.419	6.8261	6.3339
$a_1 = 0$ $a_2 = 6$	*31.396*	*6.4051*	*0.3283*	*1.0439*	*0.7997*	***9.3225***	*7.8284*	*6.4702*
$a_1 = 10^{10}$ $a_2 = 17$	31.819	7.1697	0.3668	0.7689	0.5806	11.269	**6.2825**	5.7153
$a_1 = 10^9$ $a_2 = 6$	31.196	6.4197	0.3288	1.0349	0.7928	9.3355	7.7663	6.4284

TABLE 4-11 ISA control system performance: Case Di

Case Di	u_c (N) MAX	u_c (N) RMS	u_1 (mm) RMS	u_2 (mm) RMS	q_1 (mm) RMS	$\ddot{u}_{1a}$ $\left(\frac{m}{s^2}\right)$RMS	$\ddot{u}_{2a}$ $\left(\frac{m}{s^2}\right)$RMS	$\ddot{q}_{1a}$ $\left(\frac{m}{s^2}\right)$RMS
$a_1 = a_2 = 0$	0	0	2.0538	4.0119	3.5100	39.965	22.420	21.399
$a_1 = 3\times10^8$ $a_2 = 7$	31.998	7.2120	**0.5369**	1.1287	0.9977	10.242	6.1484	5.8833
$a_1 = 10^8$ $a_2 = 4$	30.266	6.8622	0.5749	**1.0552**	0.9253	11.066	6.0946	5.8893
$a_1 = 0$ $a_2 = 7$	*31.201*	*6.5356*	*0.5641*	*1.3836*	*1.2227*	***9.5869***	*7.1705*	*6.6607*
$a_1 = 3\times10^8$ $a_2 = 4$	31.781	7.3174	0.5465	1.0586	0.9336	10.701	**5.9672**	5.7753
$a_1 = 10^8$ $a_2 = 6$	31.55	6.8428	0.5456	1.2335	1.0900	9.8582	6.5419	6.1641

4.4.5 Parametric Study of Control Device Location

The previous studies were all performed and presented with the ideal semi-active controller placed at the origin, O. Naturally, the question arises if this is the best location for the acceleration and displacement reductions, and if the same performance be achieved with a lower control force at different locations? If yes, then what are the penalties, if any, for the different control locations. A study was performed to try to answer these questions.

In Fig. 4-18 four plots are presented to illustrate the trade-offs for different controller locations. For each of the four CG location cases, the controller was moved from near the left end, in even increments in the positive x-direction to near the right end of the avionics package. The weights used in the study were selected as $a_1 = 10^7$ and $a_2 = 1.8$ based on the results in the previous section and a more refined search.

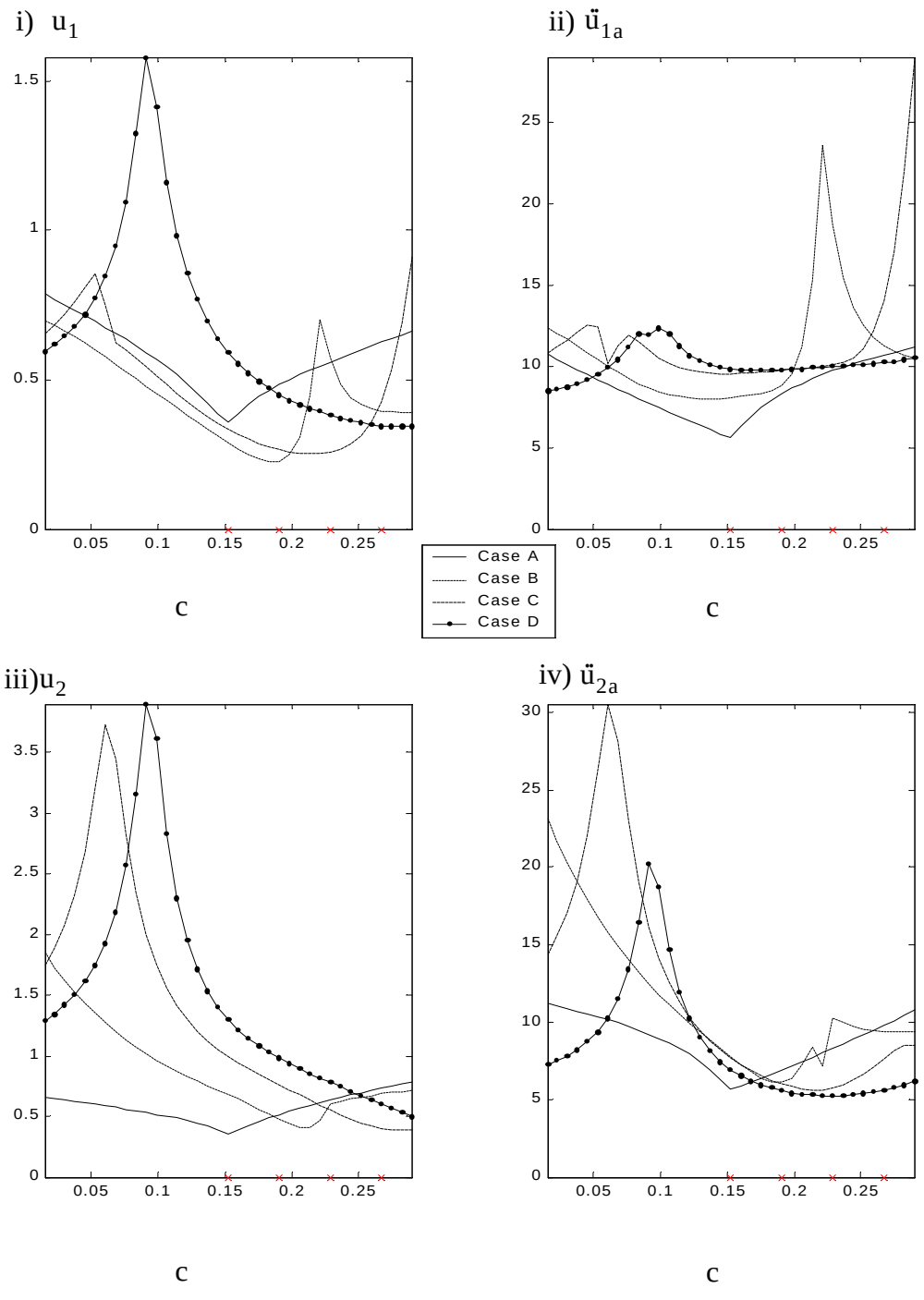

FIGURE 4-18 Control force location vs. i) u_1, ii) $\ddot{u}_{1a}$, iii) u_2, and iv) $\ddot{u}_{2a}$ for each CG location case
Note:(CG location denoted by x on origin)

Both displacements u_1 and u_2 and the acceleration of the right end $\ddot{u}_{2a}$, are minimized when the control force is located at or near the CG location. For example, Cases Ai, Bii, Ciii, and Div. However, this is not the case for the acceleration of the left end $\ddot{u}_{1a}$. The accelerations are minimized when the control force location is at the center. The results for the highest reduction of each individual weighted outputs are tabulated in Table 4-12. Notice, there are great reductions, but for large maximum control forces over the 32 N limit. Only those results below the 32 N limit will be included in the control force location comparison. The cases with the control force and the CG in the same location are tabulated in Table 4-13. The most reduced response is in **bold**.

TABLE 4-12 ISA control system performance: Case A, B, C, and D

	c	u_c (N) MAX	u_1 (mm) RMS	u_2 (mm) RMS	$\ddot{u}_{1a}$ $\left(\frac{m}{s^2}\right)$RMS	$\ddot{u}_{2a}$ $\left(\frac{m}{s^2}\right)$RMS
Case A a = 0.1524	c(19) = 0.1524	**23.2068**	**0.3452**	**0.3452**	**5.6684**	**5.6684**
Case B a = 0.1905	c(23) = 0.1828	30.5403	**0.2236**	0.5192	8.5463	6.1235
	c(26) = 0.2057	33.1575	0.3083	**0.4133**	11.2343	7.2211
	c(17) = 0.1371	30.6018	0.3359	0.7520	**8.0059**	8.8365
	c(24) = 0.1905	30.5109	0.2258	0.4770	8.8656	**6.0771**
Case C	c(27) = 0.2133	30.1943	**0.2517**	0.6354	9.9450	**5.6173**
a = 0.2286	c(35) = 0.2819	41.9679	0.5309	**0.3874**	17.0954	8.1197
	c(19) = 0.1524	25.1884	0.3353	0.9892	**9.5508**	7.6911
	c(27) = 0.2133	30.1943	**0.2517**	0.6354	9.9450	**5.6173**
Case D	c(35) = 0.2743	31.8633	**0.3427**	0.5660	10.3065	5.7899
a = 0.2667	c(37) = 0.2895	36.0384	0.3462	**0.5024**	10.5600	6.2017
	c(1) = 0.0152	16.0225	0.5930	1.2849	**8.4876**	7.2448
	c(27) = 0.2286	25.2076	0.4046	0.8537	9.9227	**5.2412**

TABLE 4-13 ISA control system performance: various control force and CG cases

	u_c (N) MAX	u_1 (mm) RMS	u_2 (mm) RMS	$\ddot{u}_{1a}$ $\left(\frac{m}{s^2}\right)$RMS	$\ddot{u}_{2a}$ $\left(\frac{m}{s^2}\right)$RMS
Case Ai	23.2068	0.3452	0.3452	5.6684	5.6684
Case Bi	*31.2769*	*0.2894*	*0.6782*	***8.0782***	*7.7862*
Case Bii	31.5109	**0.2258**	**0.4770**	8.8656	**6.0771**
Case Biii	30.9427	0.5706	0.5965	18.7742	10.2878
Case Biv	17.5235	0.3962	0.6860	11.3141	9.3872
Case Ci	25.1884	0.3353	0.9892	**9.5508**	7.6911
Case Cii	26.9070	0.2657	0.7596	9.7686	6.0063
Case Ciii	31.9962	**0.2573**	0.5534	10.1057	**5.7402**
Case Civ	39.5613	0.4269	**0.3985**	14.0239	7.6209
Case Di	25.8891	0.5913	1.2981	9.8364	6.9400
Case Dii	25.0271	0.4503	0.9781	9.7953	**5.5723**
Case Diii	25.7225	0.3818	0.7786	10.0085	**5.2412**
Case Div	29.8479	**0.3452**	**0.6000**	10.2342	5.6247

4.5 Summary

The performance of the ideal active, ideal passive and ideal semi-active control systems were presented herein. Although, the controllers are very different in dynamics and performance, the presentation of the material was done in a uniform manner. The purpose of this study was to understand the behavior of the control device and to find good overall performance cases for each device so there can be a fair basis for comparison. Four CG location cases, and four control device location were considered in studies of each controller. The 32 N maximum control force was used as a limitation for results presented. If better results were achieved at lower control forces, they were, of course, included. The

results of the performance of each of the controller were summarized at the end of each subsection. Instead of going into great detail in the comparison of the controllers here, discussion will be deferred until Chapter 7, after the other control models and results are presented in Chapters 5 and 6.

Chapter 5

Semi-Active Device Modeling

Two semi-active device models are considered in this chapter. The first is a magnetorheological (MR) damper and the second is a variable orifice (VO) damper. Both of these devices are used in conjunction with a clipped optimal control algorithm. A block diagram for a general control system with a clipped optimal controller is shown in Fig. 5-1. The clipped optimal controller has two parts: the nominal controller with inputs of measured accelerations and forces with outputs for the optimal controller, and a decision block that sends the appropriate control voltage to produce the optimal control force (Dyke et al., 1986 a,b, Jansen and Dyke, 2000, Ramallo et al., 2000,Yi, et al., 2001).

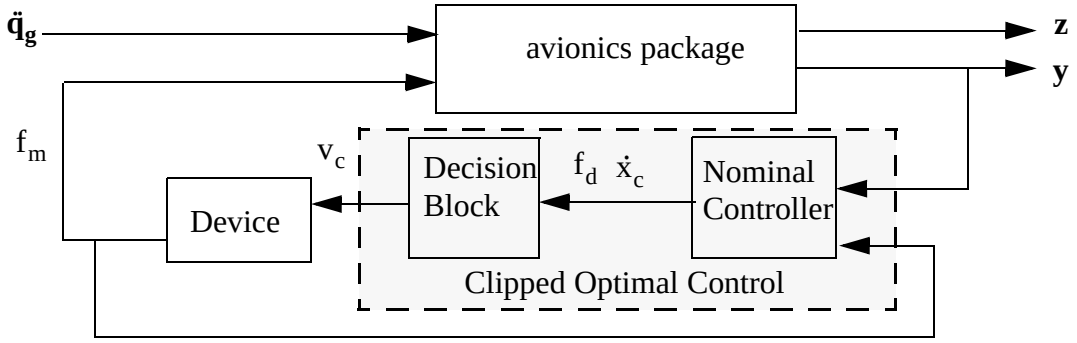

FIGURE 5-1 Block diagram of the System with the MR Damper Model

In this chapter, models of the two semi-active devices are presented. The MR damper model is based on experimental data (Yi et. al, 2001) The variable orifice model includes an ideal model of the device. Both control systems use an H_2/LQG optimal control algorithm based on absolute acceleration measurements and measured forces to determine the optimal desired control force. Note that both of these devices can only apply a control force when the desired control force and the control velocity have opposite signs.

5.1 MR Damper

A prototype of a 7 lb (31.137 N) magnetorheological (MR) damper from Lord corporation has been successfully tested, modeled, and verified in the Washington University Structural Control and Earthquake Engineering Laboratory by Yi and Dyke 2001 for Seismic Response Control in Civil Engineering Applications. The limiting maximum control force for this study was selected based on this device. The device will be used in later experimental verification of the numerical studies. The ideal force vs. displacement and force vs. velocity envelopes for an MR damper are shown in Fig. 5-2. Notice the force and velocity envelope of the MR damper is different from the ideal semi active controller in it does not cover the entire second and fourth quadrants.

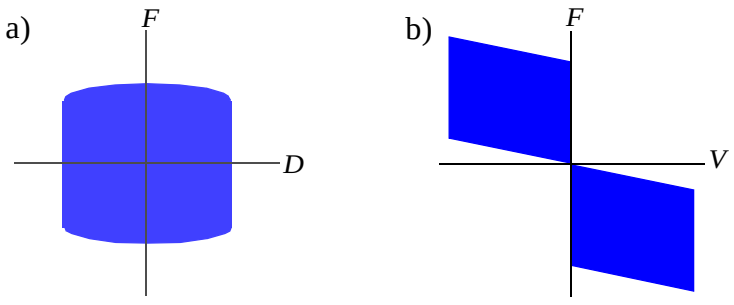

FIGURE 5-2 Ideal MR damper control force envelopes
a) force vs. displacement
b) force vs. velocity

5.1.1 MR Damper Device Model

The MR damper model used in this research is based on a physical device, a parallel plate, shear mode damper. The model was experimentally verified by Yi et al. (Nov. 2001). This model was based on the first phenomenological model of the MR damper (Spencer 1997a). An MR damper is highly nonlinear. The phenomenological model is based on a Bouc-Wen hysteresis model in parallel with a dashpot added for a nonlinear "roll-off" effect c_c as shown in Fig. 5-2. The force of the system is given by

$$f = -(c_c\dot{x}_c + \alpha z) \tag{5-1}$$

where $\dot{x}_c$ is the velocity of the damper. The parameters were defined based on their linear dependence with voltage, and are expressed as

$$\alpha = \alpha(v_c) = \alpha_a + \alpha_b v_c \tag{5-2}$$

$$\text{and } c_c = c_a + c_b v_c . \tag{5-3}$$

The command voltage, v_c, and the evolutionary variable z is governed by

$$\dot{z} = -\gamma|\dot{x}_c|z|z|^{n-1} - \beta\dot{x}_c|z|^n + \Omega\dot{x}_c \tag{5-4}$$

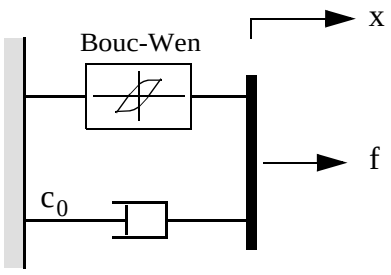

FIGURE 5-3 Mechanical model of MR damper

The model includes a first order filter for the dynamics due to the MR power circuit is given as

$$\dot{v}_c = -\eta(v_c - v_a) \tag{5-5}$$

where v_a is the applied voltage and η is the time constant associated with the first order filter.

5.2 Clipped Optimal Control Algorithm

In this initial study, a hybrid avionics control system design is studied with one control force point of application in parallel with two lightly damped isolators. This hybrid approach has been found to be successful in previous hybrid control studies by Yoshioka et al. (2001) and Ramallo et al. (2001). Although this investigation considers the single controller scenario, multiple control force locations will be considered for further study. In light of this, it would be best to choose the control algorithm with the flexibility to consider the multiple control forces.

The controller determines the voltage to apply to the MR damper based on the control algorithm selected. Many control algorithms have been developed for semi-active systems. In recent studies considering both single-input and multi-input controllers, the performance of a semi-active system was found to be highly dependent on the control law selection (Dyke and Spencer, 1997; Jansen and Dyke, 1999). In these studies the clipped-optimal controller (Sack et al., 1994; Yi et al. 1999; Dyke et al, 1996a,b, 1998) was found to achieve high performance with a semi-active system. Jansen and Dyke (1999) performed a comparative study on control strategies for MR dampers. The results indicated in multiple control force situations, the reductions in absolute acceleration were highest with a clipped optimal control algorithm and a force feedback loop. Thus, the clipped optimal control algorithm was selected for this study.

There are two components to the clipped optimal controller: the decision block and the nominal controller. Based on its success in previous studies, an H_2/LQG control algorithm is selected as the controller. The H_2/LQG controller calculates the estimates of the states based on the inputs: the measured accelerations, the measured force exerted by the controller and the ground excitation. The output of the H_2/LQG controller is a desired control force. This desired force is fed in the decision block along with the velocity at the control force location to "decide" what command voltage to send.

The command to the MR damper from the controller is not a force, but a voltage. Thus, the relationship between the desired force, f_d, the measured control force, f_m, and the command voltage, v_c, is the control law given by Dyke et al. (1996) as

$$v_c = V_{max} H\{(f_d - f_m) f_m\} \tag{5-6}$$

where H is the Heaviside step function and V_{max} is the maximum voltage associated with force saturation of the MR device. An illustration of the selection of the command signal described by Eq. (5-6) is shown in Fig. 5-4.

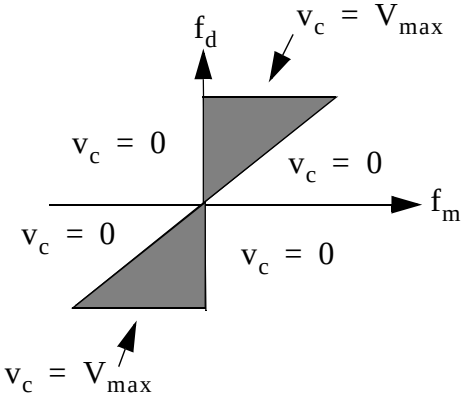

FIGURE 5-4 Force vs. velocity envelope of the clipped optimal control algorithm

The nominal linear optimal H_2/LQG controller is designed that calculates the desired control force based on the measured structural response vector $\mathbf{y}$ and the measured control

force, $f_m(t)$. Although the controller can be obtained from a variety of methods, H_2/LQG strategies were selected due to the stochastic nature of ground motions of the avionics bays and the successful application in other civil engineering structural control applications (Dyke et al., 1996 a, b).

The nominal controller, $\mathbf{K}_c(s)$, determines the control action based on the measured structural responses, $\mathbf{y}$, and the measured control force, $\mathbf{f}_m$, applied to the structure. This gives the desired force, $\mathbf{f}_d(t)$, as the relationship

$$\mathbf{f}_d(t) = L^{-1}\left\{-\mathbf{K}_c(s)L\left\{\begin{matrix}\mathbf{y}(t)\\ \mathbf{f}_m(t)\end{matrix}\right\}\right\} \tag{5-7}$$

where $L\{\cdot\}$ is the Laplace transform of the output vector and the measured control force.

5.3 Variable Orifice Damper

A variable orifice damper is typically composed of a fluid that is free flowing when a solenoid control valve is open (Symans et al. 1995). The ideal control force envelopes for an variable orifice device is in Fig. 5-5.

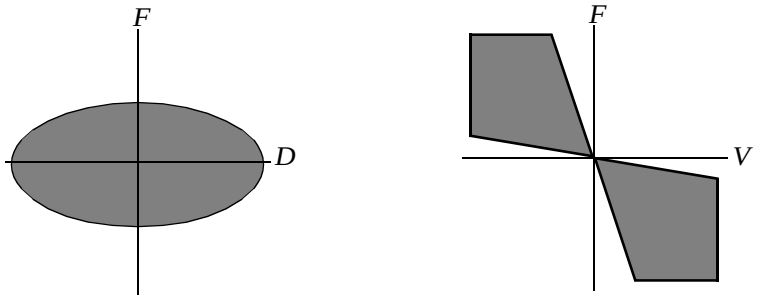

FIGURE 5-5 Ideal control force envelope for variable orifice damper
a) force vs. displacement
b) force vs. velocity

5.3.1 Variable Orifice Damper

The variable orifice damper included in the study is assumed to be ideal and varies linearly with the velocity at the control force location and two coefficients of damping. The linear relationship between the control force and the velocity at the control device location, $\dot{x}_c(t)$, for the variable orifice damper is

$$f_d = -c_o(v_c)\dot{x}_c(t) \tag{5-8}$$

where $c_o(v_c)$ is a damping coefficient that depends on the voltage command from the controller, v_c, described by

$$c_o(v_c) = c_L + c_H v_c \tag{5-9}$$

where the two coefficients of damping correspond to the high damping, c_H, and low damping coefficients, c_L.

The input to the variable orifice damper is a command voltage from the decision block or the clipped optimal controller discussed in the previous sections. Either a command voltage of V_{max} or zero is commanded to the device. Equation (5-8) then becomes

$$f_d = -c_L(v_c)\dot{x}_c(t) \tag{5-10}$$

for a zero command, $v_c = 0$, or

$$f_d = -c_o(v_c)\dot{x}(t) = -(c_L + c_H v_c)\dot{x}(t) \tag{5-11}$$

for the maximum voltage command, $v_c = V_{max}$.

The selection of the damping coefficients, c_L and c_H, are based on the highest absolute value of velocity expected to be experienced by this system and the maximum and minimum control force values expected from the MR damper. Figure 5-6 illustrates the two linear force vs. velocity relationships in relationship to the command voltage.

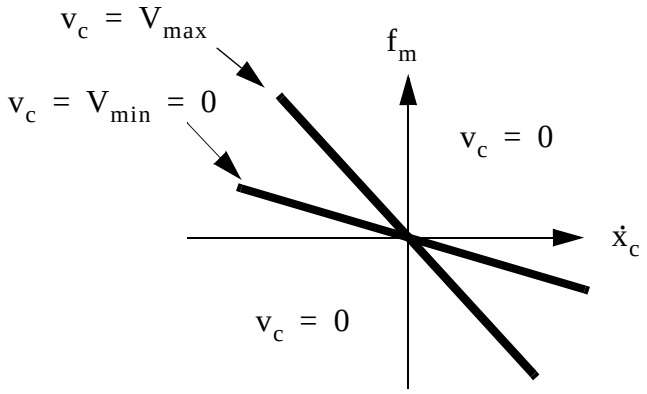

FIGURE 5-6 Force vs. Velocity of Variable Orifice Damper

The model includes a first order filter for the dynamics due to the power circuit is given as

$$\dot{v}_c = -\eta(v_c - v_a) \tag{5-12}$$

where v_a is the applied voltage and η is the time constant associated with the first order filter.

5.4 Summary

A detailed description of magnetorheological (MR) and the variable orifice (VO) damper models and the clipped optimal control algorithm were presented in this chapter. The parameter selection, behavior, and performance of the two devices will be discussed in detail in Chapter 6. Finally in Chapter 7, the results will be compared for overall and best performance that is typical of each type of ideal and actual control device models.

Chapter 6

Performance of Semi-Active Devices

In the previous chapter, two device models were introduced containing the physical characteristics of the actual devices. These models were selected in order to perform realistic numerical studies for the acceleration reduction of the avionics model detailed in Chapter 2. Both systems require the use of a clipped optimal controller to determine the control action. In this chapter, the behavior and performance of the MR and VO dampers will be presented.

The devices presented in this chapter differ from the models presented in Chapters 3 and 4, in that the plant and the control device are separate entities. The first semi-active controller considered is a magnetorheological (MR) damper. It is an existing model of an actual 7 lb Lord Corporation MR damper, was selected for this application. The second device considered in this chapter is a variable orifice (VO) damper designed specifically to match the MR damper control force ranges of interest, based on the highest velocities in the numerical simulations.

The individual performance of the controllers will be examined in the same manner as the ideal controllers were in Chapter 4. Once again, the goal is to find a set parameters that leads to good overall performance, indicative of the type of results that can be expected

from each controller. The results must also be formulated in the same manner as the ideal controller results to have a basis for comparison. As mentioned previously, the goal is to find the best overall performance of each controller, but to not use a control force that exceeds the set 32 N maximum control force limit.

To design an appropriate controller for avionics, there are key parameters to modify in existing controller models. The following are considered in this chapter: i) the effect of varying parameters in the MR and VO damper behavior; ii) the effect of different weightings for the H_2/LQG control algorithm with the control force fixed at the origin; iii) outlining the selection criteria for control force point of application for different center of mass locations; and iv) the trade studies performed in the selection of the best performance of each controller for comparison with the other control device in the next chapter.

6.1 MR Damper Performance

6.1.1 Parameters used for MR Damper Control

The ten parameters for the 7 lb. MR damper were obtained by constrained nonlinear optimization performed by Yi, et al (2001) as: $\alpha_a = 27.3\frac{N}{cm}$, $\alpha_b = 26.5\frac{N}{cmV}$, $c_a = 0.0032\frac{N\,sec}{cm}$, $c_b = 0.002\frac{N\,sec}{cmV}$, $\eta = \frac{80}{sec}$, $\Omega = 120$, $\beta = \frac{300}{cm}$, and $\gamma = \frac{300}{cm^3}$ and n = 1. Simulations of the MR and VO studies were performed using a time step of $\Delta t = 10^{-4}$ seconds, a total time for each simulation run, T_{max} = 60 second (unless otherwise noted).

A sinusoidal displacement input was used to examine the behavior of the devices with an amplitude of 0.01 m, a natural frequency of $\omega = 100\frac{rad}{sec}$, and T_{max} = 5 seconds. The

velocities were computed from the sinusoidal displacement input in Simulink using a derivative block.

In these studies, the "passive-off" case is achieved when a constant voltage of 0 V is commanded to the MR damper. The maximum command voltage is 5 V and the minimum command voltage is 0 V. The vectors containing many different weights tested for the **Q** matrix selection were selected for presentation were $\mathbf{a}_1$ = [0 1 10 100 10^4 10^5 10^6 10^7 10^8 3×10^8 5×10^8 8×10^8 10^9 10^{10}] and $\mathbf{a}_2$ = [0 10^{-2} 10^{-1} 1 2 3 4 5 6 7 8 9 10 20 30 40 50 60 70 80 90 100 10^3 10^4 10^5 10^6 10^7 10^8]. For the control force location studies the different control force locations considered were c = [0.0152:0.00762:0.2895]. A band limited, Gaussian excitation was used for each of the simulation inputs with a power spectral density of So = 0.04 $\frac{g^2}{Hz}$ = 0.2513 rad$\frac{g^2}{Hz}$ in accordance with military specifications used in avionics random vibration test levels for non-gunfire endurance and performance testing.

6.1.2 Behavior of the MR Damper

A sinusoidal displacement is used to excite the MR damper and obtain a better understanding of the behavior of the device. Figure 6-1 is a graph of the resulting control force vs. displacement and Fig. 6-2 is the control force vs. velocity. The graphs illustrate the behavior of the MR damper model when the controller is "on" and "off". The maximum control force is 5.7801 N for the 0 V command (dashed light line) and 33.2807 N for the 5 V command (solid dark line). Two important things to notice. First, in Fig. 6-1, there is clearly a rectangle bounded by the maximum force vs. displacement loop at about 31 N. This is the damping due to the Bouc-Wen element in the MR model. Recall, in the MR damper, there is a Bouc-Wen hysteresis model in parallel with a linear viscous damper. The viscous damper, in turn, accounts for the damping outside the rectangle. Notice, in Fig. 6-2, the MR damper exerts a dissipative force when in the second and fourth quadrants as expected.

.

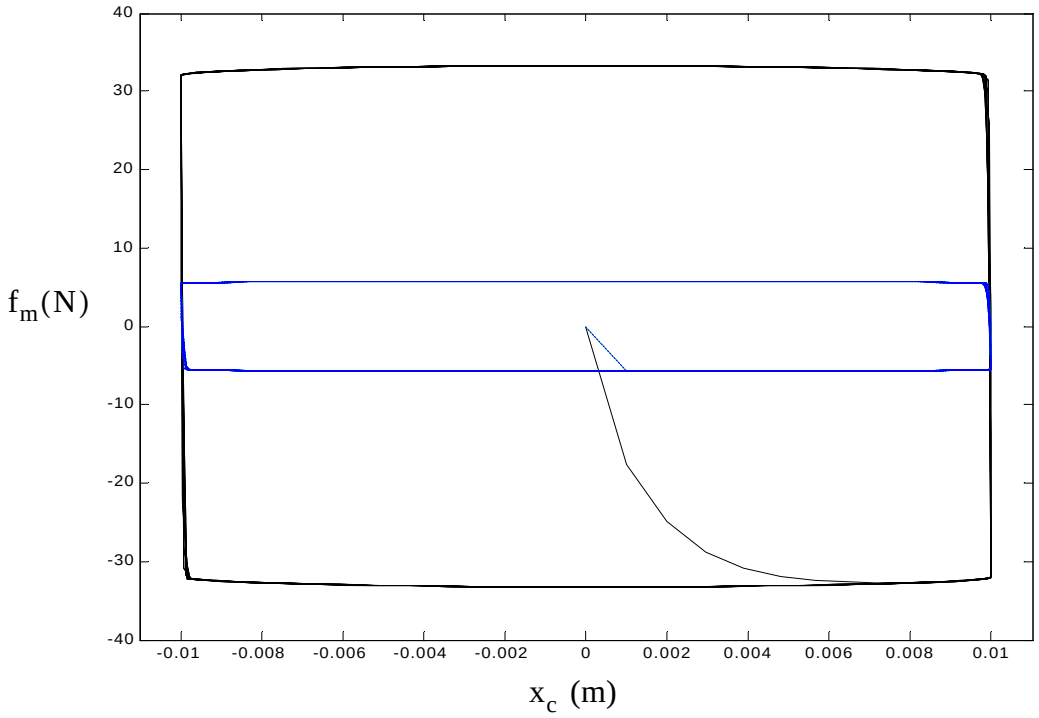

FIGURE 6-1 Force vs. displacement of MR damper for a sinusoid input with Vmax = 5 V and Vmin = 0 V

When the parameters c_a, c_b are varied the maximum amount of control force is affected. If they are increased by a factor of 10, i.e. $c_a = 0.032\frac{N\sec}{cm}$ and $c_b = 0.02\frac{N\sec}{cmV}$, the maximum control force increases as shown in Fig. 6-3 for a constant input of 5 V. When α_a, α_b are increased by a factor of 2 there is an associated increase in the slope of the force vs. velocity curve. See Fig. 6-4. where the resulting behavior from changing the original parameters (light lines) to the new parameters (dark lines).

Finally, according to Yi et. al. (2001), γ, β, Ω, n, control the linearity in the unloading and the smoothness of the pre-yield and post-yield regions.

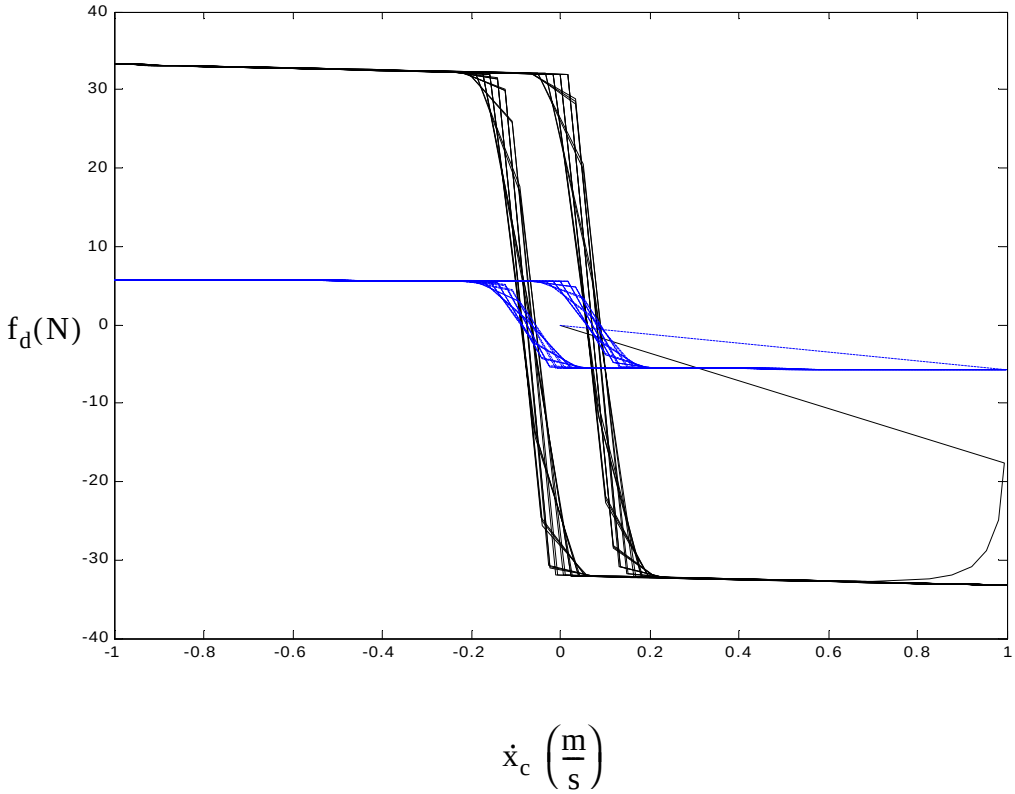

FIGURE 6-2 Force vs. velocity of MR damper for a sinusoid input with Vmax = 5 V and Vmin = 0 V

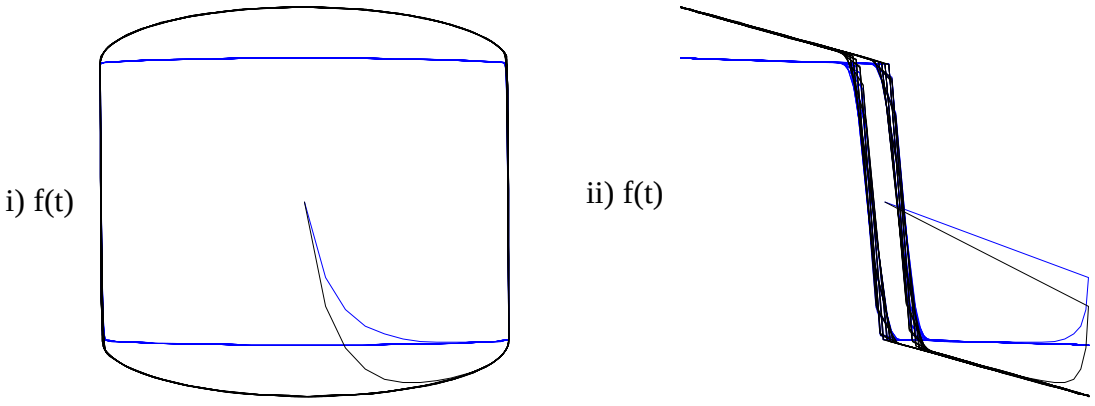

FIGURE 6-3 Parametric study results for varying damping parameters of MR damper: i) force vs. displacement and ii) force vs. velocity

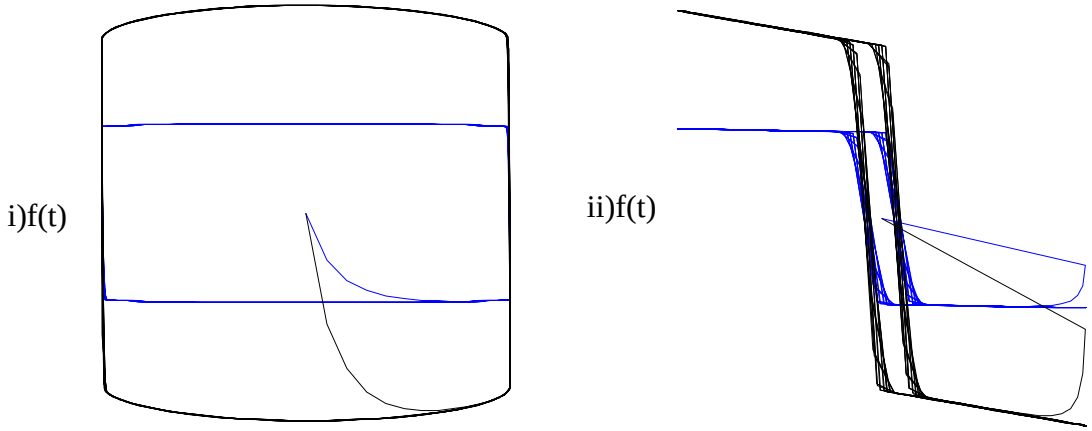

FIGURE 6-4 Parametric study results for varying damping parameters of MR damper: i) force vs. displacement and ii) force vs. velocity

6.1.3 Q Matrix Weighting: Case Ai

The **Q** matrix from the infinite horizon cost function is defined in Chapter 3 in Eq. 3-8 where the weights a_1 are on displacements, u_1, u_2, and the weights a_2 are on absolute accelerations, $\ddot{u}_{1a}, \ddot{u}_{2a}$. The unweighted case for the MR damper, $a_1 = a_2 = 0$ results in the "passive off" case with $f(t) \neq 0$. Various weights a_1 and a_2 were selected to illustrate the trends in performance as the values are varied. The $\log_{10}(a_1)$ and $\log_{10}(a_2)$ are calculated and plotted vs. RMS values. Graphs of the response for various weights are in Fig. 6-5 for displacement, Fig. 6-6 for acceleration, Fig. 6-7 and for maximum desired control force for the MR damper Case Ai.

It can be seen in Fig. 6-5, the displacements are effected more by variations weighted by a_1 than a_2. In fact, the largest values of $a_1 \approx 10^{10}$, give the largest reduction in displacement for the MR damper, while the best displacements are achieved with an a_2 weight seem to be closer to 10. This is expected because a_1 was selected to weight the displacements. In Fig. 6-6, the accelerations are minimized for values for a_2 = 10-100. The larger a_1 seem to effect the accelerations adversely. The best choice for a_1 seems to be near 10^5. The maximum control forces are higher for a_2 values. This indicates that

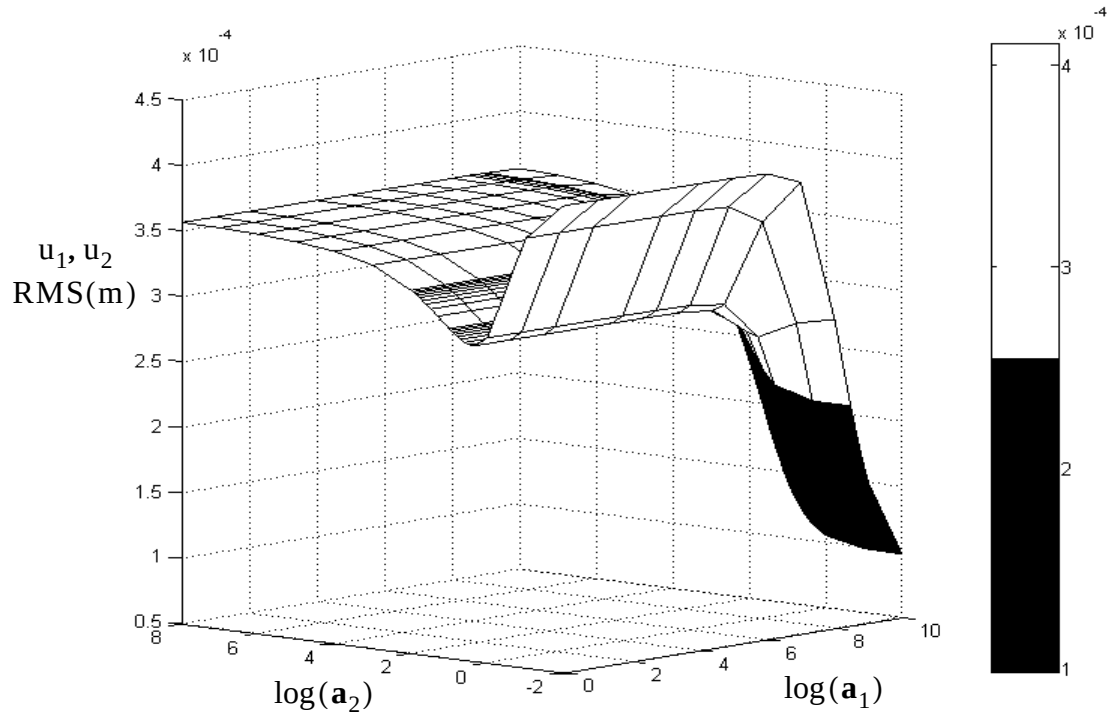

FIGURE 6-5 MR damper displacement RMS vs. weights a_1, a_2 for Case Ai

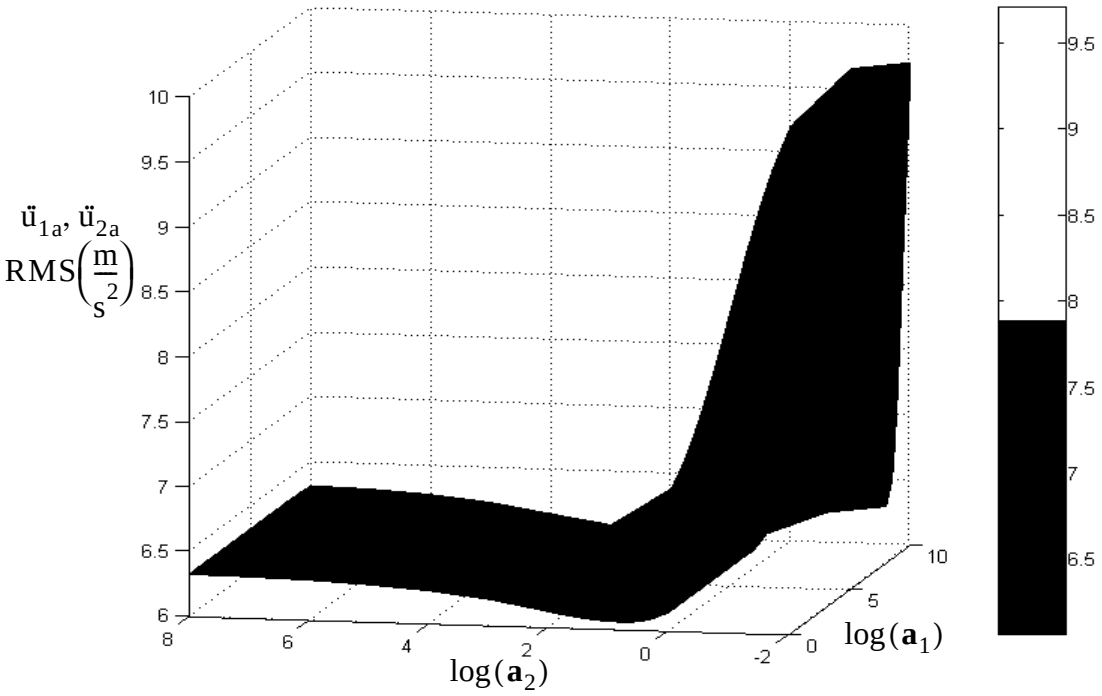

FIGURE 6-6 MR damper absolute acceleration RMS vs. weights a_1, a_2 for Case Ai

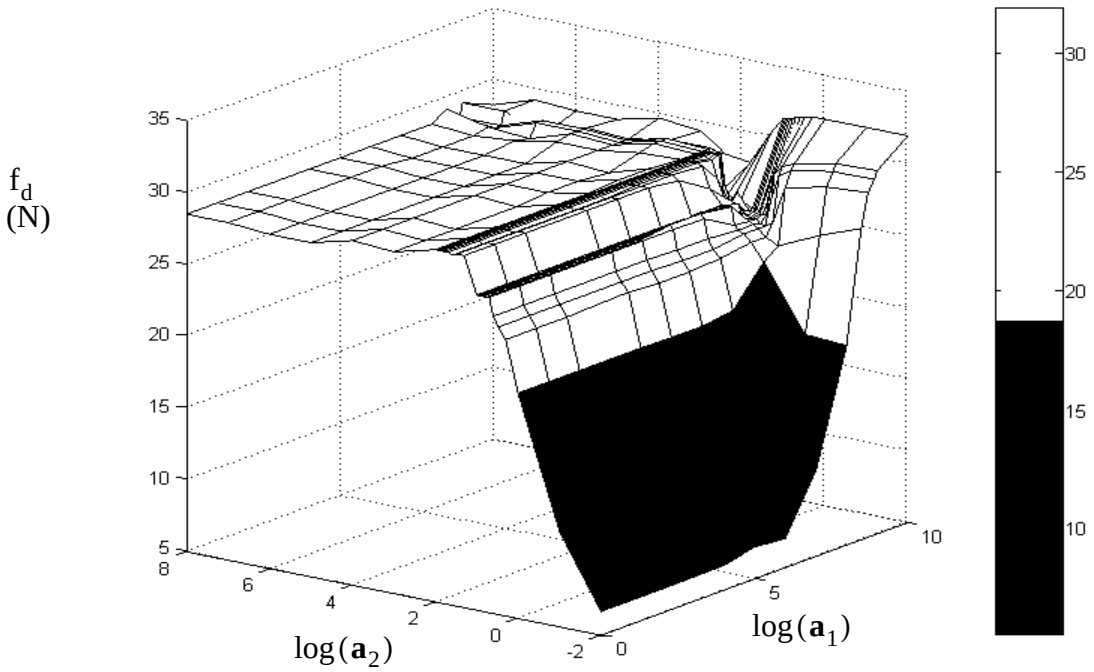

FIGURE 6-7 MR damper maximum control force vs. weights $\mathbf{a}_1$, $\mathbf{a}_2$ for Case Ai

more control force is needed to weight the accelerations than the displacements. Notice the maximum control force achieved by the MR damper is around 32 N, as expected.

The second method to select appropriate weights for the "best overall" performance case is demonstrated in this section. The previous method was described in Section 4.2.3. The method requires the calculation of the "percent reduction" from the "uncontrolled" values using

$$\%\ \text{reduction of uncontrolled case} = 100 \times \left(1 - \frac{\text{controlled}}{\text{uncontrolled}}\right). \qquad (6\text{-}1)$$

First the minimum values of all four weighted output is determined. Next, the percent reduction is systematically and uniformly reduced in small increments until a pair of weights gives the most reduction for the displacements and accelerations of the left and right ends that can be achieved at once. For each weight combination achieving the

specified “percent reduction” of displacement and acceleration, the graph is marked with an “x” for the left end and an “o” for the right end. Also, if the maximum control force was less than the selected control force value, 32 N, then an “+” was marked. The weight indices and the selection for u_1, u_2, and maximum control force are shown in Fig. 6-8 and for $\ddot{u}_{1a}$, $\ddot{u}_{2a}$, and maximum control force in Fig. 6-9. The first pair of weights giving the most reduction for all four variables and staying below 32 N, is emphasized with an arrow in each of the figures. So from the figure, the index for a_1 is 11 and a_2 is 12 with corresponding values of $a_1(11) = 5\times10^8$ and $a_2(12) = 9$.

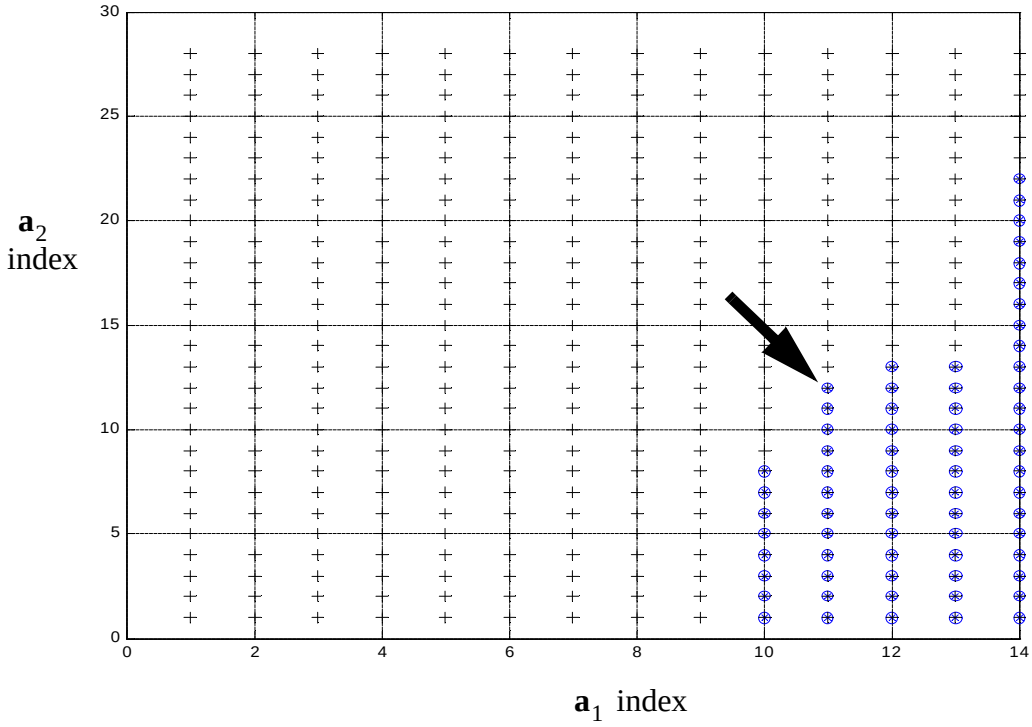

FIGURE 6-8 Selection of weights for displacement reduction

The best reduction for each weighted output, u_1, u_2, $\ddot{u}_{1a}$, $\ddot{u}_{2a}$, are listed in the Table 6-1 for Case Ai, Table 6-2 for Case Bi, Table 6-3 for Case Ci, and Table 6-4 for Case Di. Also included in the tables are the weighting pairs leading to the highest reduction for each individual parameter. This gives an indication of the type of performance that may be achieved simultaneously with multiple controllers.

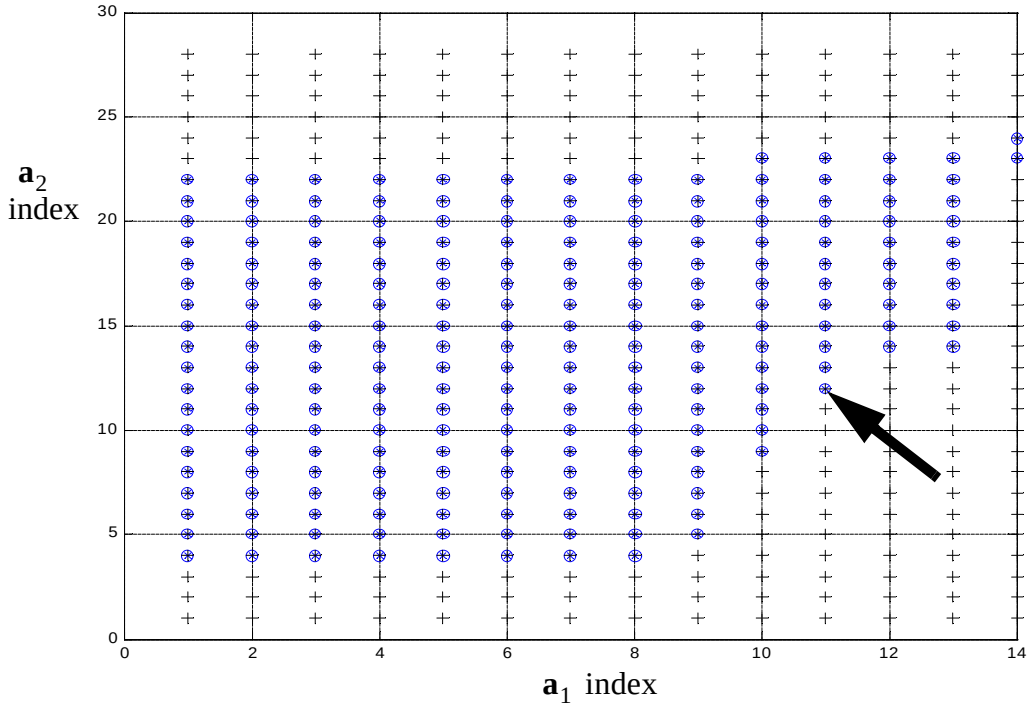

FIGURE 6-9 Selection of weights for acceleration reduction

TABLE 6-1 MR damper performance: Case Ai

Case Ai	$\mathrm{Max}u_c$ (N)	u_c (N)RMS	$u_1\ u_2\ q_1$ (mm)RMS	$\ddot{u}_{1a}\ \ddot{u}_{2a}\ \ddot{q}_{1a}$ $\left(\frac{m}{s^2}\right)$RMS
"passive-off"	5.5401	4.9702	0.4095	7.3214
$a_1 = 10^{10}$, $a_2 = 2$	31.8702	14.1875	**0.0985**	9.7056
$a_1 = 10^{6}$, $a_2 = 7$	*26.8863*	*7.3623*	*0.2976*	***6.0608***
$a_1 = 5\times10^{8}$, $a_2 = 9$	25.6284	7.7851	0.2593	6.1923

TABLE 6-2 MR damper performance: Case Bi

Case Bi	u_c (N) MAX	u_c (N) RMS	u_1 (mm) RMS	u_2 (mm) RMS	q_1 (mm) RMS	$\ddot{u}_{1a}$ $\left(\frac{m}{s^2}\right)$RMS	$\ddot{u}_{2a}$ $\left(\frac{m}{s^2}\right)$RMS	$\ddot{q}_{1a}$ $\left(\frac{m}{s^2}\right)$RMS
"passive-off"	5.537	4.945	0.361	0.736	0.4853	13.048	10.665	7.2514
$a_1 = 3\times10^8$ $a_2 = 2$	28.753	7.6916	**0.2780**	0.5322	0.3456	11.911	8.1828	6.4526
$a_1 = 10^{10}$ $a_2 = 0.1$	31.835	14.069	0.3546	**0.4105**	0.2036	20.540	8.9227	9.5494
$a_1 = 0$ $a_2 = 1$	25.841	6.8445	0.2826	0.5878	0.3880	11.252	8.6653	6.4681
$a_1 = 10^9$ $a_2 = 20$	30.303	7.4783	0.2849	0.5667	0.3782	11.478	**8.3461**	6.4681
$a_1 = 10^4$ $a_2 = 1$	*25.841*	*6.8470*	*0.2828*	*0.5879*	*0.3388*	*11.255*	*8.6679*	*6.4684*

TABLE 6-3 MR damper performance: Case Ci

Case Ci	u_c (N) MAX	u_c (N) RMS	u_1 (mm) RMS	u_2 (mm) RMS	q_1 (mm) RMS	$\ddot{u}_{1a}$ $\left(\frac{m}{s^2}\right)$RMS	$\ddot{u}_{2a}$ $\left(\frac{m}{s^2}\right)$RMS	$\ddot{q}_{1a}$ $\left(\frac{m}{s^2}\right)$RMS
"passive-off"	5.5419	4.9221	0.4767	1.142	0.8194	13.521	9.7695	7.8877
$a_1 = 10^9$ $a_2 = 30$	28.005	7.197	**0.3994**	0.8685	0.6291	12.384	7.582	6.6113
$a_1 = 10^{10}$ $a_2 = 1$	32.016	12.892	0.5063	**0.6087**	0.3974	20.945	7.4708	8.7098
$a_1 = 10^4$ $a_2 = 1$	*24.140*	*6.7243*	*0.4093*	*0.8850*	*0.6334*	*12.165*	*7.8193*	*6.6409*
$a_1 = 10^{10}$ $a_2 = 20$	29.768	9.0843	0.4365	0.6809	0.4755	14.948	**6.7908**	6.7232

TABLE 6-4 MR damper performance: Case Di

Case Di	u_c (N) MAX	u_c (N) RMS	u_1 (mm) RMS	u_2 (mm) RMS	q_1 (mm) RMS	$\ddot{u}_{1a}$ $\left(\frac{m}{s^2}\right)$RMS	$\ddot{u}_{2a}$ $\left(\frac{m}{s^2}\right)$RMS	$\ddot{q}_{1a}$ $\left(\frac{m}{s^2}\right)$RMS
"passive-off"	5.5408	4.8902	0.8206	1.7105	1.4890	12.965	9.4589	8.7254
$a_1 = 10^9$ $a_2 = 20$	30.255	7.8969	**0.6180**	1.1005	0.9586	12.677	6.7769	6.6250
$a_1 = 10^{10}$ $a_2 = 10$	31.924	11.105	0.6671	**0.8483**	0.6671	17.350	7.1419	7.5300
$a_1 = 10^5$ $a_2 = 1$	*23.357*	*6.8157*	*0.6771*	*1.2465*	*1.0820*	***11.893***	*7.3260*	*6.9346*
$a_1 = 10^{10}$ $a_2 = 70$	31.077	8.7398	0.6213	0.9901	0.8594	13.648	**6.5784**	6.5925

6.1.4 Parametric Study of Control Device Location

The results for the MR damper presented thus far have been for all four CG locations (Cases A, B, C, and D) with the control force applied at the origin (Case i). The different cases for the control force location will be examined here and the trade-offs between the different locations will be discussed. A study was performed varying the control force location for the four CG locations in Fig. 6-10. Thirty-six different control force locations were considered for this study by varying the parameter c. For clarity, the control force location is c, and the four CG locations are marked on the axis with an x as a point of reference. The weights $a_1 = 10^4$ and $a_2 = 1$ were selected for the study, because they gave the best overall performance for Case Ci in Table 6-3.

Recall, Case A corresponds to the situation in which the CG is at the origin. In cases B, C, and D, the CG is moved out 25% of one half the total length, of m_1, in the positive x-direction by varying the parameter P and subsequently the variable a. When c = 0.1524 m, the center of mass is at the origin. Moving the control force in the negative x-direction

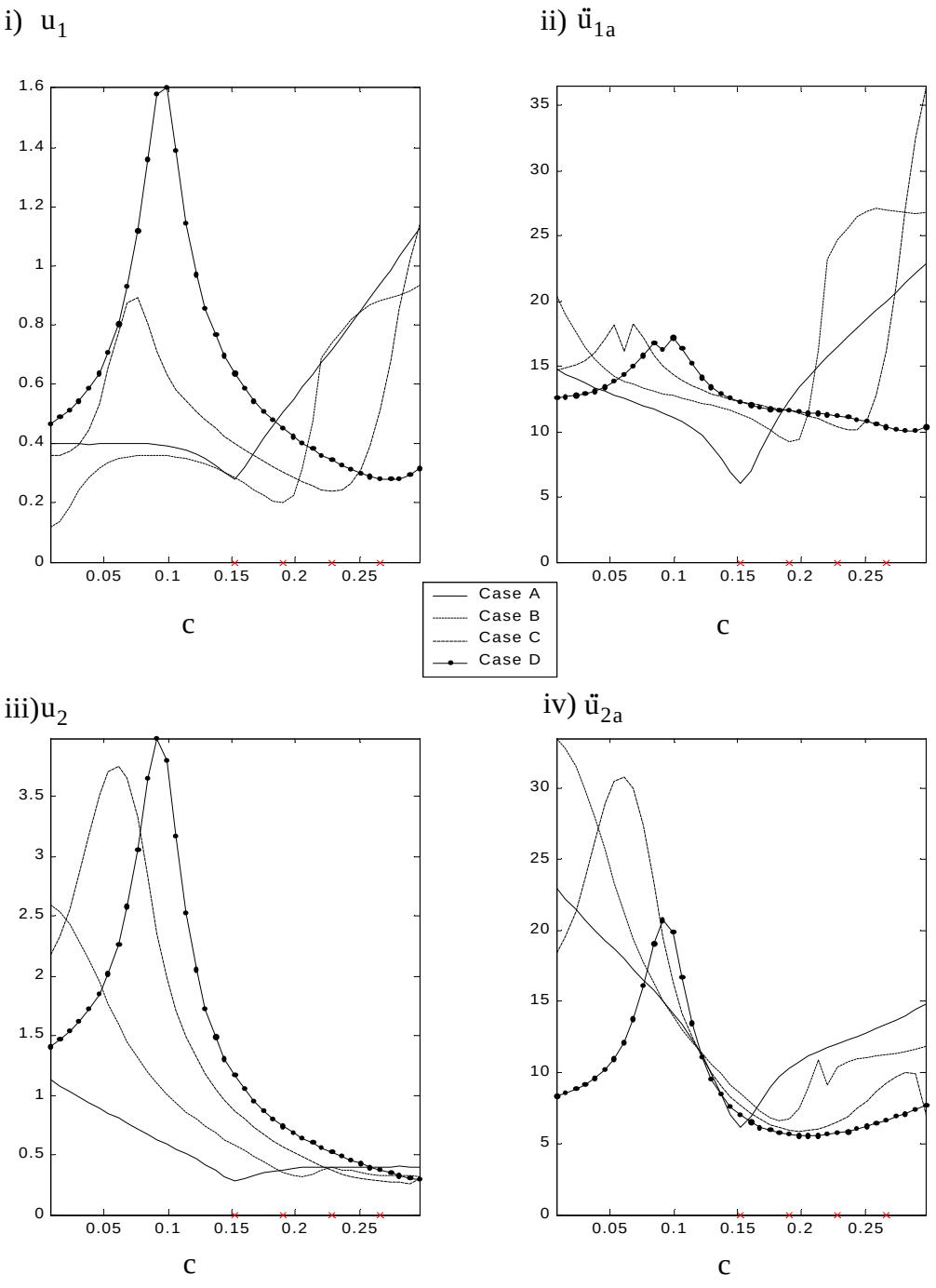

FIGURE 6-10 Control force location vs. i) u_1, ii) $\ddot{u}_{1a}$, iii) u_2, and iv) $\ddot{u}_{2a}$ for each CG location case
Note:(CG location denoted by x on origin)

TABLE 6-5 MR damper performance for different control force location trade study

	c	u_c (N) MAX	u_1 (mm) RMS	u_2 (mm) RMS	$\ddot{u}_{1a}$ $\left(\frac{m}{s^2}\right)$RMS	$\ddot{u}_{2a}$ $\left(\frac{m}{s^2}\right)$RMS
Case A a = 0.1524	c(20) = 0.1524	**26.8863**	**0.2976**	**0.2976**	**6.0608**	**6.0608**
Case B a = 0.1905	c(1) = 0.0076	17.2367	**0.1186**	2.5962	20.3351	33.5342
	c(27) = 0.2057	31.4873	0.3107	**0.3217**	11.4061	8.9688
	c(25) = 0.1905	31.1605	0.2009	0.3552	**9.2397**	6.7219
	c(24) = 0.1829	30.5509	0.2076	0.3939	9.6736	**6.5886**
Case C a = 0.2286	c(30) = 0.2286	30.1395	**0.2393**	0.3743	10.3452	6.5513
	c(38) = 0.2895	31.7548	1.0183	**0.2557**	32.4696	9.8910
	c(31) = 0.2362	30.3840	0.2438	0.3441	**10.1201**	6.9545
	c(26) = 0.1981	28.4894	0.2863	0.5256	11.4630	**5.8904**
Case D a = 0.2667	c(36) = 0.2743	30.4197	**0.2791**	0.3516	10.1447	6.8655
	c(39) = 0.2972	31.6768	0.3184	**0.2918**	10.3371	7.6568
	c(37) = 0.2821	30.5951	0.2821	0.3301	**10.0115**	7.1152
	c(28) = 0.2133	26.8824	0.3811	0.6009	11.3778	**5.5995**

from the origin creates a negative moment, and moving the control force to in the positive x-direction from the origin creates a positive moment. Since the CG is moving in the positive x-direction, it is also generating a negative moment. A positive moment is desired to counter balance the negative moment generated by the CG.

In Case A, the best reduction is achieved with the control force Case i for all four responses of interest. For the other three cases, the best reductions vary depending on the CG location, the control force location, and the variable and they are tabulated in Table 6-5. The best overall performance for the CG locations is when the control force is located

near or at the CG, i.e., Case Ai, Case Bii, Case Ciii, Case iv, with the exception of $\ddot{u}_2$ for Cases C and D which are minimized with a control force at or near Case ii. For performance comparison, this result will be a consideration for the best overall case presented for comparison. The controller was designed with weights $a_1 = 10^4$ and $a_2 = 1$.

TABLE 6-6 MR damper control system performance: fixed controller design

	u_c (N) MAX	u_1 (mm) RMS	u_2 (mm) RMS	$\ddot{u}_{1a}$ $\left(\frac{m}{s^2}\right)$RMS	$\ddot{u}_{2a}$ $\left(\frac{m}{s^2}\right)$RMS
Case Ai	20.6694	**0.2982**	**0.2982**	**6.1431**	**6.1431**
Case Bi	25.8406	0.2828	0.5879	11.2553	8.6679
Case Bii	28.9720	**0.2301**	0.3839	**9.7185**	**6.7514**
Case Biii	29.9583	0.7385	0.4029	24.5747	9.9681
Case Biv	31.3995	0.8591	**0.3414**	26.3109	10.6861
Case Ci	24.1396	0.4093	0.8850	12.1654	7.8193
Case Cii	24.7694	0.3161	0.5935	11.6074	**6.0534**
Case Ciii	28.5416	**0.2848**	0.4141	**10.9501**	6.1551
Case Civ	31.7533	0.5381	**0.3138**	16.9800	8.2838
Case Di	23.6574	0.6769	1.2459	11.8946	7.3236
Case Dii	22.1008	0.4733	0.7996	11.4872	5.7655
Case Diii	25.0381	0.3725	0.5720	11.2640	**5.6083**
Case Div	26.7544	**0.3353**	**0.4273**	**10.9624**	6.1191

6.2 Variable Orifice Damper

6.2.1 Parameters used for the Variable Orifice Damper

The highest velocity expected in the passive off case was 0.2685 $\frac{m}{sec}$. The low and high coefficient were calculated using Eqs. 5-10 and 5-11 based on the high expected velocity, the maximum control force and the passive off control force as $c_L = 20.5570\frac{kg}{sec}$ and $c_H = 20.5847\frac{kg}{sec\,V}$ respectively. Simulations of the MR and VO studies were performed using a time step of $\Delta t = 10^{-4}$ seconds, a total time for each simulation run, T_{max} = 60 second (unless otherwise noted).

A sinusoidal displacement input was used to examine the behavior of the devices with an amplitude of 0.01 m, a natural frequency of $\omega = 100\frac{rad}{sec}$, and T_{max} = 5 seconds. The velocities were computed from the sinusoidal displacement input in Simulink using a derivative block.

In these studies, the "passive-off" case is achieved when a constant voltage of 0 V is commanded to the VO damper. The maximum command voltage is 5 V and the minimum command voltage is 0 V. The vectors containing many different weights tested for the **Q** matrix selection were selected for presentation of behavior were $\mathbf{a}_1$ = [0 1 10 100 10^4 10^5 10^6 10^7 10^8 3×10^8 5×10^8 8×10^8 10^9 10^{10}] and $\mathbf{a}_2$ = [0 10^{-2} 10^{-1} 1 2 3 4 5 6 7 8 9 10 20 30 40 50 60 70 80 90 100 10^3 10^4 10^5 10^6 10^7 10^8]. A band limited, Gaussian excitation was used for each of the simulation inputs with a power spectral density of So = 0.04 $\frac{g^2}{Hz}$ = 0.2513 rad$\frac{g^2}{Hz}$ in accordance with military specifications used in avionics random vibration test levels for non-gunfire endurance and performance testing.

6.2.2 Behavior of the Variable Orifice Damper

A sinusoidal displacement is used as an input to the VO damper for a better understanding of the behavior of the device. Figure 6-11 is a graph of the resulting control force vs. displacement and Fig. 6-12 is the control force vs. velocity. The graphs illustrate the behavior of the VO damper model when the control command voltage is “low” or “high”. The slope with the smaller rise is the for the zero volts command (light dashed) and the slope with the higher rise is for the V_{max} command (dark). The force vs. displacement hysteresis loops in Fig. 6-12 for both voltage cases are elliptical. This is a characteristic of linear viscous damping. The maximum control force exerted by the “passive-off” case was selected as 6.1401 N to be the same as the MR damper. The maximum control force for the “high” voltage command is selected as the maximum control force of the MR damper of 34.1496 N and the maximum control force for the passive off case, 5.5401 N can be seen as the intercept of the maximum expected velocity at 0.2695 $\frac{m}{sec}$ in Fig. 6-11.

.

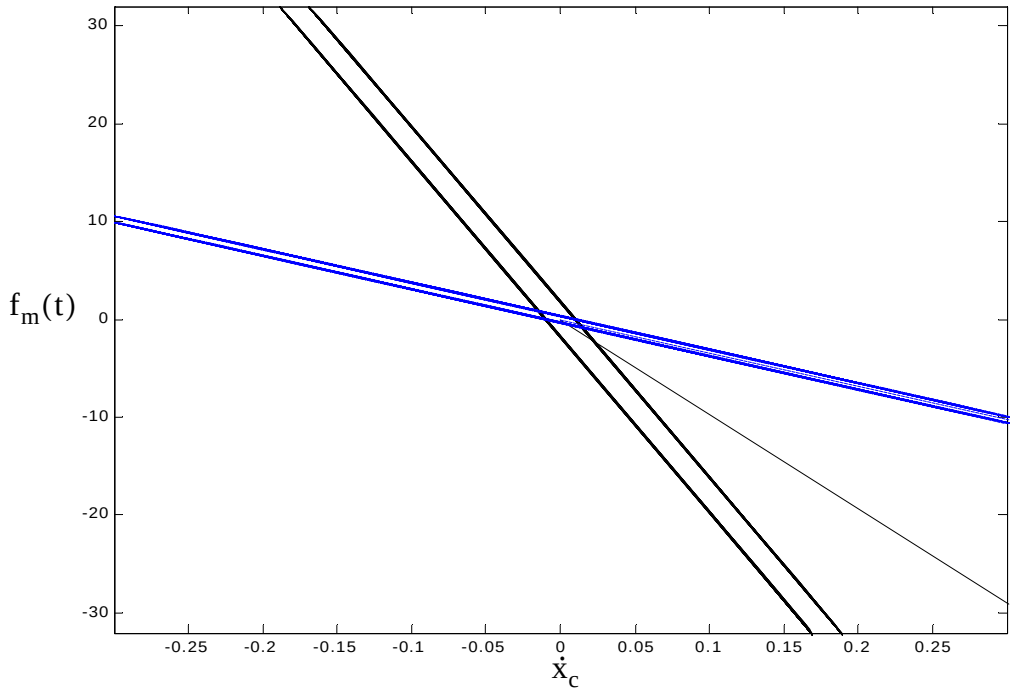

FIGURE 6-11 Force vs. velocity for a sinusoid input with V_{max} = 5 V and V_{min} = 0 V

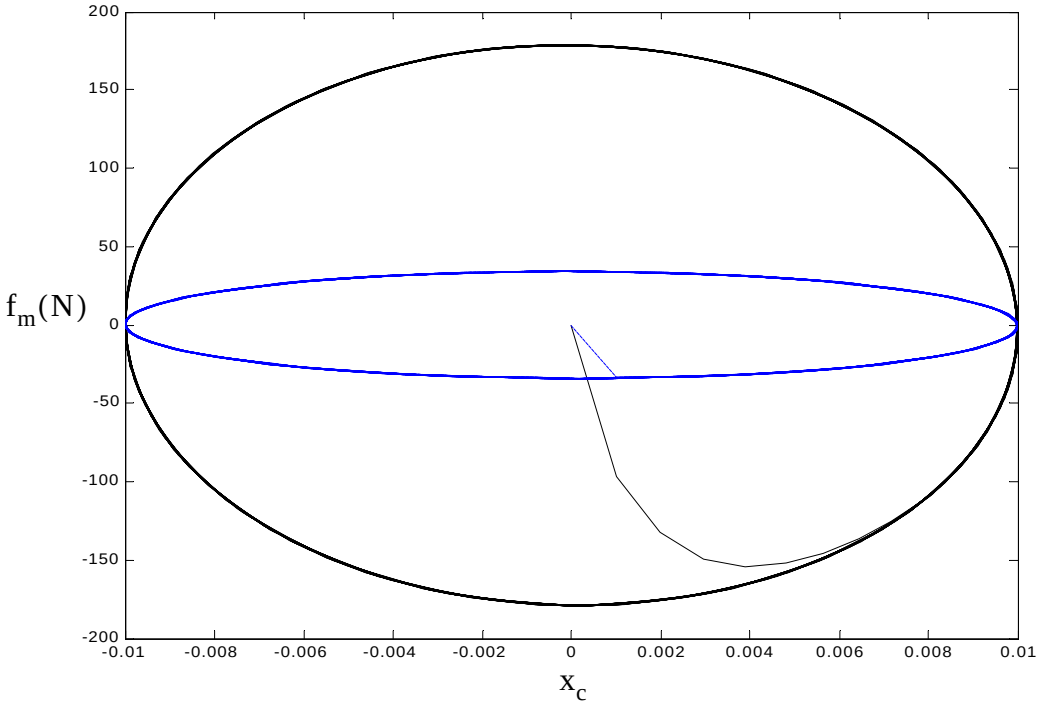

FIGURE 6-12 Force vs. displacement of a variable orifice damper for a sinusoid input with Vmax = 5 V and Vmin = 0 V

6.2.3 Q Matrix Weighting: Case Ai

The **Q** matrix from the infinite horizon cost function is defined in Chapter 3 in Eq. 3-8 where the weights a_1 are on displacements, u_1, u_2, and the weights a_2 are on absolute accelerations, $\ddot{u}_{1a}, \ddot{u}_{2a}$. Since the unweighted case for the VO damper, $a_1 = a_2 = 0$ results in the "passive off" case with $f(t) \neq 0$, the percent reduction of the "uncontrolled" values will be calculated based on the "uncontrolled" values for the other controllers. The percent reduction of the uncontrolled accelerations and uncontrolled displacements are calculated using Eq. 6-1. The $\log_{10}$ was calculated for the weights a_1 a_2 and each were plotted vs. the RMS values. The graphs of the response for various weights can be found in Fig. 6-13 for displacements, Fig. 6-14 for accelerations, and Fig. 6-15 maximum desired force for the VO damper.

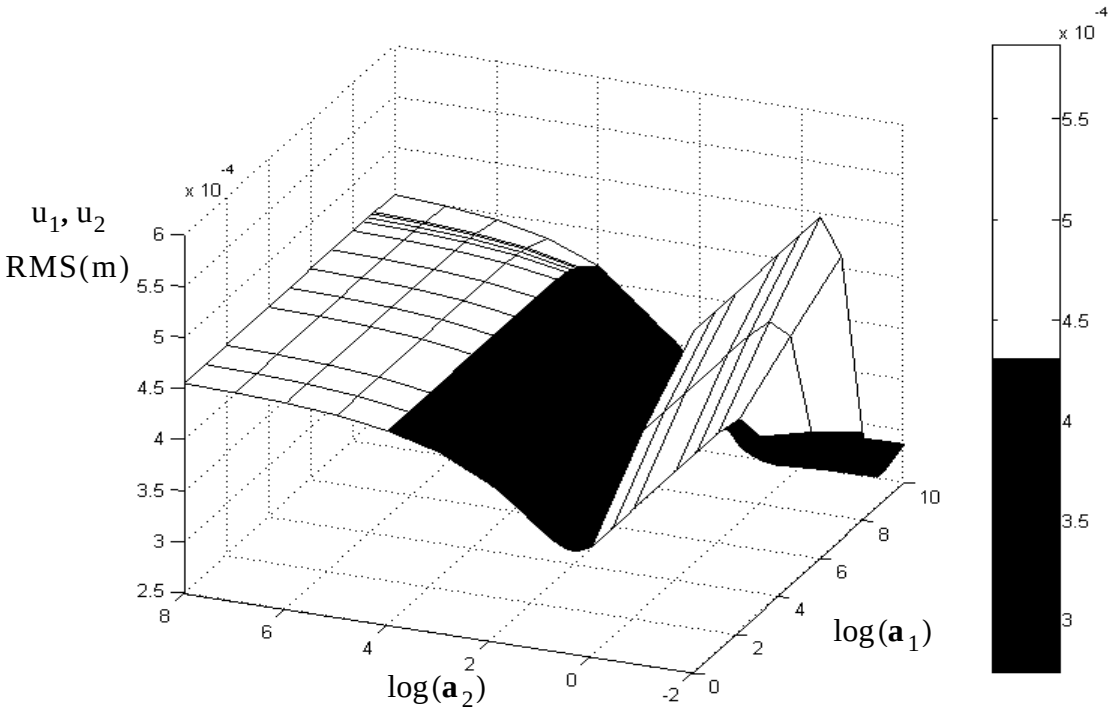

FIGURE 6-13 VO damper displacements RMS vs. weights a_1, a_2 for Case Ai

6.2.4 Selection of Q Matrix Weightings for Varying CG Cases

The best reduction for each individual parameter, u_1, u_2, $\ddot{u}_{1a}$, $\ddot{u}_{2a}$, are tabulated in Table 6-6, Table 6-7, Table 6-8, and Table 6-9 along with the best over all case for Case i and each of the CG locations. The two selection processes used for the best case performance can be found in Section 4.2.3 and Section 6.14. This will be referred to as the "best overall" performance case. It will be used for comparison with other controllers in Chapter 7.

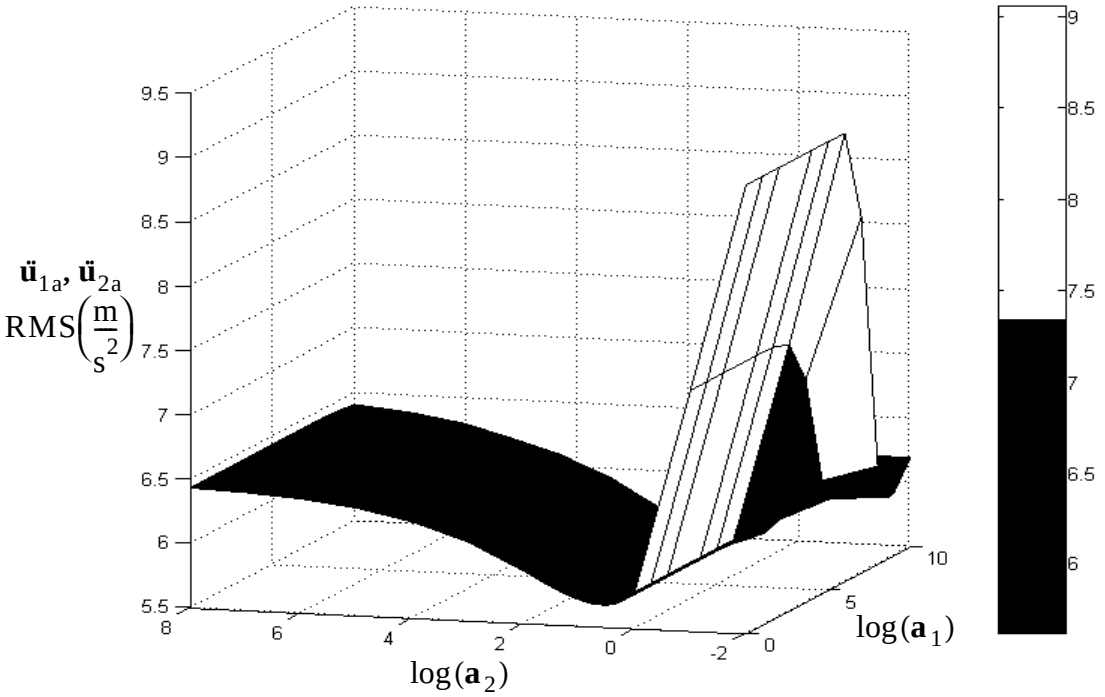

FIGURE 6-14 VO damper absolute acceleration RMS vs. weights $\mathbf{a}_1$, $\mathbf{a}_2$ for Case Ai

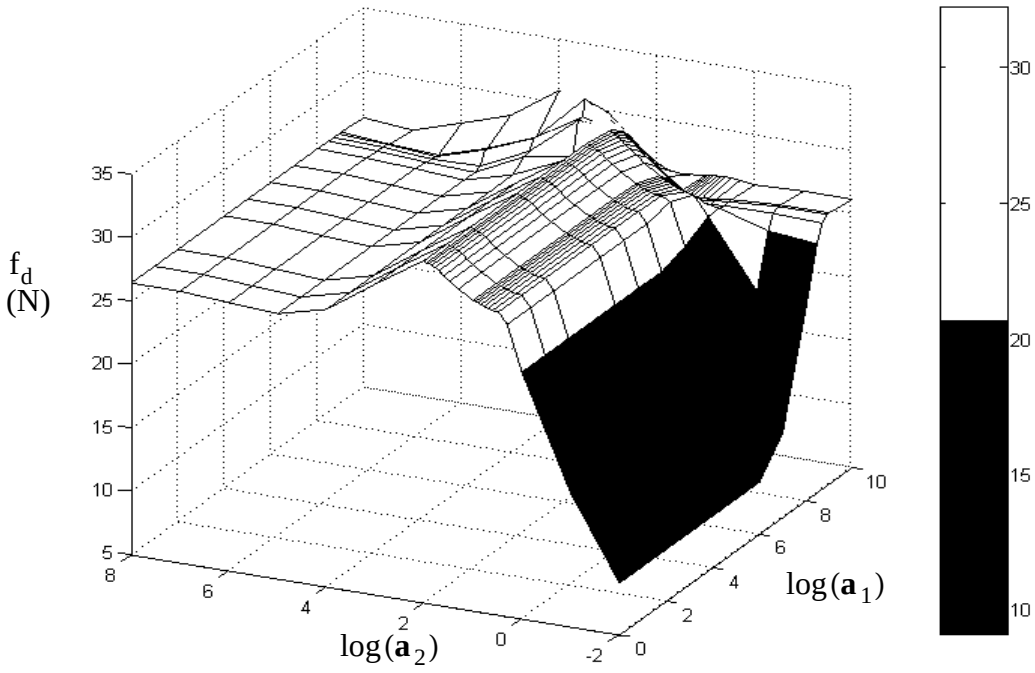

FIGURE 6-15 VO damper maximum desired control force RMS vs. weights $\mathbf{a}_1$, $\mathbf{a}_2$ for Case Ai

TABLE 6-7 VO Damper Performance: Case Ai

Case Ai	Maxu_c (N)	u_c (N)RMS	u_1 u_2 q_1 (mm)RMS	$\ddot{u}_{1a}$ $\ddot{u}_{2a}$ $\ddot{q}_{1a}$ $\left(\frac{m}{s^2}\right)$RMS
"passive-off"	9.1446	2.4706	0.5866	9.0552
$a_1 = 10^{10}$, $a_2 = 7$	26.1904	5.7900	**0.2753**	5.9126
$a_1 = 8\times10^8$, $a_2 = 20$	*27.4738*	*5.5119*	*0.3254*	***5.6182***

TABLE 6-8 VO damper performance: Case Bi

Case Bi	u_c (N) MAX	u_c (N) RMS	u_1 (mm) RMS	u_2 (mm) RMS	q_1 (mm) RMS	$\ddot{u}_{1a}$ $\left(\frac{m}{s^2}\right)$RMS	$\ddot{u}_{2a}$ $\left(\frac{m}{s^2}\right)$RMS	$\ddot{q}_{1a}$ $\left(\frac{m}{s^2}\right)$RMS
"passive-off"	9.6671	2.4044	0.4175	1.0452	0.7163	13.479	13.888	9.3445
$a_1 = 10^8$ $a_2 = 1$	*28.903*	*4.9581*	*0.2626*	*0.6420*	*0.4475*	*8.8722*	*8.4229*	*6.0957*
$a_1 = 10^{10}$ $a_2 = 40$	27.112	5.3482	0.2651	**0.5934**	0.4067	9.4867	8.1189	5.8953
$a_1 = 0$ $a_2 = 5$	28.322	4.5356	0.2799	0.7383	0.5251	**8.4336**	9.2026	6.6344
$a_1 = 10^{10}$ $a_2 = 30$	26.697	5.4360	0.2672	0.5805	0.3939	9.7535	**8.1052**	5.8664

6.2.5 Parametric Study for Control Device Location

Thirty-six different control force locations were considered in a parameter study to find the control force location that would give the best performance in the VO semi-active control system. The graphs of the four responses: u_1, u_2, $\ddot{u}_{1a}$, and $\ddot{u}_{2a}$ versus the different control force locations are shown in Fig. 6-16, with the weights $a_1 = 10^3$ and $a_2 = 10^3$. It is no surprise that the displacements, u_1 and u_2 are reduced significantly when the damper is placed on the corresponding side. However, this is only true for the absolute accelerations of the left end, $\ddot{u}_{1a}$. The results in the table show the best acceleration

TABLE 6-9 VO damper performance: Case Ci

Case Ci	u_c (N) MAX	u_c (N) RMS	u_1 (mm) RMS	u_2 (mm) RMS	q_1 (mm) RMS	$\ddot{u}_{1a}$ $\left(\frac{m}{s^2}\right)$RMS	$\ddot{u}_{2a}$ $\left(\frac{m}{s^2}\right)$RMS	$\ddot{q}_{1a}$ $\left(\frac{m}{s^2}\right)$RMS
"passive-off"	10.274	2.3889	0.5689	1.6338	1.1857	14.621	13.473	10.367
$a_1 = 10^9$ $a_2 = 20$	29.000	4.8741	**0.3571**	1.0530	0.7770	9.9458	8.5144	6.8013
$a_1 = 10^9$ $a_2 = 0.1$	29.911	5.6819	0.4125	**0.8466**	0.6009	11.287	7.5123	6.1765
$a_1 = 0$ $a_2 = 2$	*24.531*	*4.6753*	*0.3644*	*1.0942*	*0.8049*	***9.7774***	*8.8743*	*6.9953*
$a_1 = 8\times10^8$ $a_2 = 1$	30.201	5.6274	0.3951	0.8549	0.6125	10.971	**7.4574**	6.1433

TABLE 6-10 VO damper performance: Case Di

Case Di	u_c (N) MAX	u_c (N) RMS	u_1 (mm) RMS	u_2 (mm) RMS	q_1 (mm) RMS	$\ddot{u}_{1a}$ $\left(\frac{m}{s^2}\right)$RMS	$\ddot{u}_{2a}$ $\left(\frac{m}{s^2}\right)$RMS	$\ddot{q}_{1a}$ $\left(\frac{m}{s^2}\right)$RMS
"passive-off"	9.4480	2.3076	1.0550	2.3487	2.0497	14.522	12.496	11.317
$a_1 = 10^{10}$ $a_2 = 80$	25.733	5.3511	**0.6257**	1.3315	1.1640	10.400	7.3007	6.7858
$a_1 = 3\times10^8$ $a_2 = 0$	27.719	5.63	0.6658	**1.2582**	1.0930	10.818	7.1657	6.6819
$a_1 = 0$ $a_2 = 1$	*22.821*	*4.8422*	*0.6801*	*1.4839*	*1.2964*	***9.9056***	*7.9663*	*7.2767*
$a_1 = 5\times10^8$ $a_2 = 5$	27.713	5.5868	0.6460	1.2659	1.1021	10.648	**7.1344**	6.6543
$a_1 = 10^{10}$ $a_2 = 30$	27.919	5.5560	0.6572	1.2616	1.0973	10.737	7.1413	6.6589

reduction for the left end, $\ddot{u}_{2a}$, is consistently near Case iii when c is at or near c = 0.2286. Any control force location further in the positive x-direction, leads to large increases in accelerations of the right end for Case B and C. The best overall performance is Case ii, where the trade off between reducing the parameters of the left and right ends is balanced for all four CG locations. These findings will be considered for the best performance cases comparison in Chapter 7.

TABLE 6-11 VO damper performance for different control force locations

	c	u_c (N) MAX	u_1 (mm) RMS	u_2 (mm) RMS	$\ddot{u}_{1a}$ $\left(\frac{m}{s^2}\right)$RMS	$\ddot{u}_{2a}$ $\left(\frac{m}{s^2}\right)$RMS
Case A a = 0.1524	c(19) = 0.1524	25.8992	**0.2737**	**0.2739**	**5.7366**	**5.7366**
Case B	c(21) = 0.1676	26.2063	**0.2619**	0.5062	10.1020	7.3020
a = 0.1905	c(28) = 0.2209	22.9009	0.6923	**0.3995**	23.5318	8.5335
	c(1) = 0.0152	14.8661	0.3499	2.1285	**8.3615**	27.0675
	c(24) = 0.1905	25.4672	0.3224	0.4299	11.8802	**6.7551**
Case C	c(24) = 0.1905	27.6606	**0.3270**	0.5902	11.1111	5.6689
a = 0.2286	c(19) = 0.2739	25.8992	0.2737	**0.2739**	5.7366	5.7388
	c(38) = 0.3525	22.0363	1.1402	0.3525	**36.4021**	5.4994
	c(29) = 0.2286	27.6552	0.3875	0.4484	13.2676	**5.2183**
Case D	c(30) = 0.2362	23.3039	**0.3805**	0.5253	11.2661	5.0483
a = 0.2667	c(38) = 0.2971	25.9081	0.5182	**0.3957**	16.1089	5.9725
	c(1) = 0.0152	23.8102	0.5195	1.3157	**8.8920**	7.5578
	c(28) = 0.2209	23.7988	0.3900	0.5844	10.9052	**5.0088**

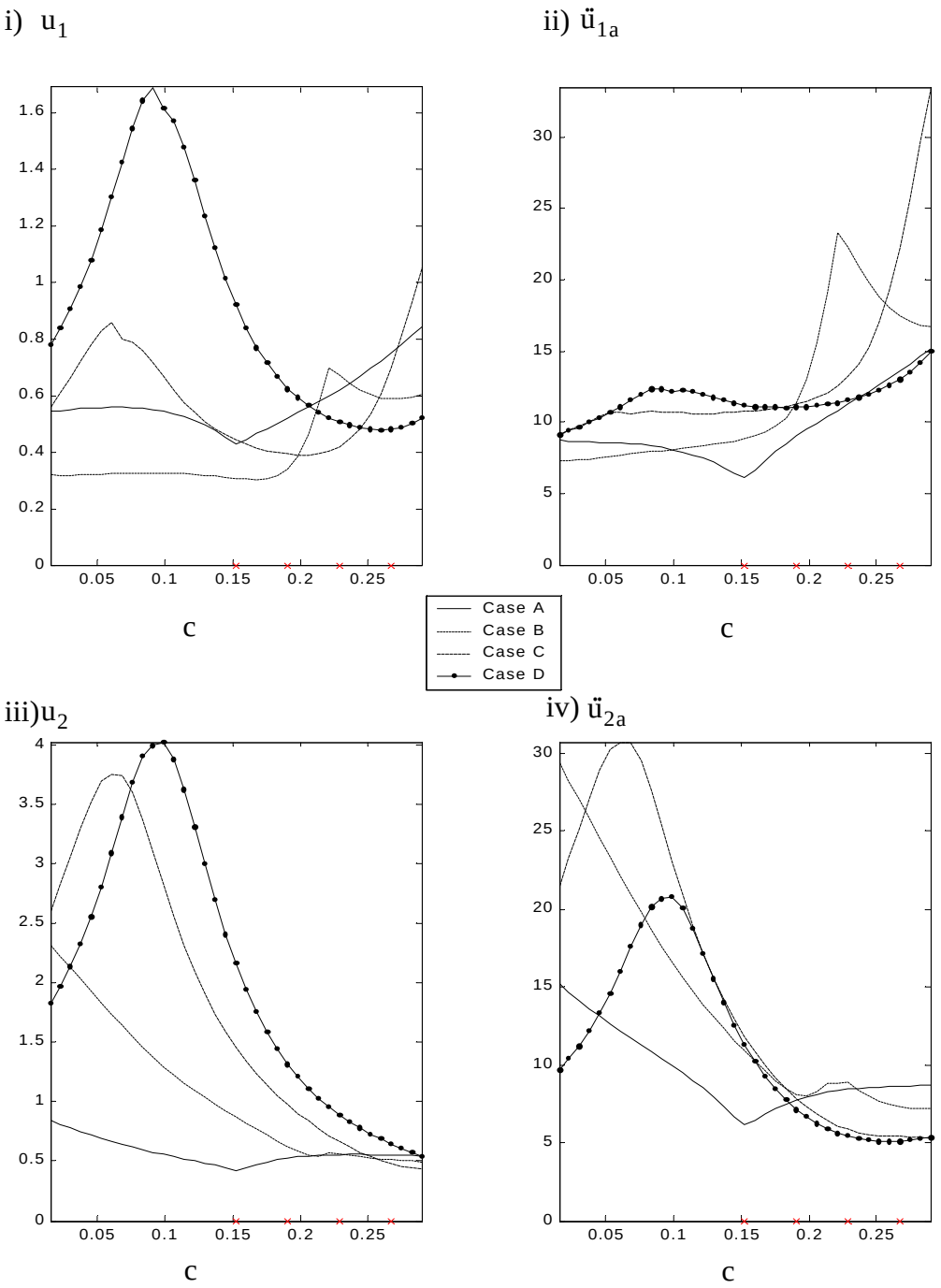

FIGURE 6-16 Control force location vs. i) u_1, ii) $\ddot{u}_{1a}$, iii) u_2, and iv) $\ddot{u}_{2a}$ for each CG location case
Note:(CG location denoted by x on origin)

The performance of the VO for different control force and CG cases are in Table 6-13 with the weights $a_1 = 10^3$ and $a_2 = 10^3$. The most reduced response is in **bold**. The "best overall" performance for two different sets of weights are in Table 6-14. The performance resulting from the weights $a_1 = 10^3$ and $a_2 = 10^3$ are in *italics*. The tables are included to illustrate the subjective nature of the "best overall" performance selection. The rule kept in the selection was to select the control force and weight with the lowest $\ddot{u}_{1a}$.

TABLE 6-12 VO damper control system performance

	u_c (N) MAX	u_1 (mm) RMS	u_2 (mm) RMS	$\ddot{u}_{1a}$ $\left(\frac{m}{s^2}\right)$RMS	$\ddot{u}_{2a}$ $\left(\frac{m}{s^2}\right)$RMS
Case Ai	*28.0919*	***0.4289***	***0.4305***	***6.1139***	***6.1139***
Case Bi	*23.2816*	***0.3068***	*0.8701*	***8.8652***	*10.8933*
Case Bii	30.5486	0.3383	0.6236	11.3381	**8.1180**
Case Biii	24.6503	0.6716	0.5637	22.2896	8.8568
Case Biv	21.2352	0.5859	**0.5118**	17.4890	7.3348
Case Ci	*24.3580*	*0.4412*	*1.4580*	***10.7531***	*11.8438*
Case Cii	24.2459	**0.3919**	0.9739	11.2788	7.8755
Case Ciii	30.8888	0.4198	0.6630	13.2173	5.8477
Case Civ	26.0065	0.6975	**0.4780**	22.1991	**5.4085**
Case Di	20.4362	0.9183	2.1614	11.2262	11.3054
Case Dii	*24.7176*	*0.6246*	*1.3158*	***11.0612***	*7.1477*
Case Diii	25.5943	0.5054	0.8896	11.5715	5.4536
Case Div	25.2355	**0.4801**	**0.6446**	13.0184	**5.1278**

TABLE 6-13 VO damper "best overall" performance

	u_c (N) MAX	u_c (N) RMS	u_1 (mm) RMS	u_2 (mm) RMS	$\ddot{u}_{1a}$ $\left(\frac{m}{s^2}\right)$RMS	$\ddot{u}_{2a}$ $\left(\frac{m}{s^2}\right)$RMS
Case Ai $a_1 = 8\times10^8$ $a_2 = 20$	27.4738 *(29.499)*	5.5119 *(4.8101)*	0.3254 *(0.4272)*	0.3254 *(0.4272)*	5.6182 *(6.1139)*	5.6182 *(6.1139)*
Case Bii $a_1 = 10^8$ $a_2 = 1$	25.0758 *(30.549)*	5.6851 *(4.9134)*	0.3302 *(0.3383)*	0.4253 *(0.6236)*	12.1744 *(11.338)*	6.8132 *(8.1180)*
Case Ciii $a_1 = 10^9$ $a_2 = 20$	27.6483 *(30.889)*	5.6114 *(5.0714)*	0.3771 *(0.4198)*	0.4992 *(0.6630)*	12.7182 *(13.217)*	5.2765 *(5.8477)*
Case Div $a_1 = 10^{10}$ $a_2 = 30$	25.1496 *(25.236)*	5.7615 *(5.1607)*	0.4100 *(0.4801)*	0.4428 *(0.6446)*	25.1496 *(13.018)*	5.7615 *(5.1278)*

6.3 Summary

In this chapter, results were presented for studies performed to characterize the behavior of the MR damper and the variable orifice damper. Parameter studies investigated were the parameters of the device, control force locations, CG locations, and weighting of the regulated outputs. These were done in order to find a "best overall" performance case presented in this chapter for each controller. The results indicate the "best overall" performance for the VO damper is achieved with the control force location: Case i. This was not true for the MR damper which had the best overall reductions for Cases Ai, Bii, Ciii, and Div. These and other findings from this chapter will be included in the final comparison of the five devices in the next chapter.

Chapter 7

Comparison of Performance

The chapter is a summary and discussion of the numerical results for the “best overall” performance case for each controller developed in Chapters 3-6: ideal active force actuator, viscous damper, ideal semi-active damper (ISA), magnetorheological (MR) damper, and the variable orifice (VO) damper. The discussion will focus on the comparison of the largest absolute acceleration reductions; within the 32 N control force limit; and the displacements noted. Although the “best overall” results are subjective, the same procedure in the selection was followed. The largest accelertion reductions for both accelerations were found. If there was a situation where two controller designs had accelerations of one end were slightly lower than the other, then the controller design with higher reductions of $\ddot{u}_{1a}$ were selected. For this study, the CG cases moved the CG from the origin towards the positive x-direction. Thus, the uncontrolled accelerations of the left end, $\ddot{u}_{1a}$, were higher than the uncontrolled accelerations of the right end, $\ddot{u}_{2a}$. For the purposes of this study, it is sufficient to say the “best overall” cases presented demonstrate the capabilities of each controller.

In this chapter, the absolute acceleration results of the “best overall” case will be provided in bar graphs and tabulated. The tables include a ranking of controller performance with respect from one another. Also included in the tables will be the percent reductions of each

absolute acceleration of the uncontrolled accelerations, i.e., no control force. The trade studies for the control force locations have indicated the most simultaneous acceleration reductions, $\ddot{u}_{1a}, \ddot{u}_{2a}$, is achieved when the control force is located at the origin, Case i, except for the MR damper. The MR damper achieved more acceleration reductions when the control force was located at or near the CG location, i.e., Case Ai, Bii, Ciii, Div. Therefore, all the control devices are located at Case i, with the exception of the MR damper. Frequency domain results will also be provided for $\ddot{u}_{1a}$ to demonstrate the ability of the controllers to reduce the peaks in the power spectra. Finally, there will be a few concluding remarks and future research in Chapter 8.

7.1 Best Overall Performance

The results in this section focus on the "best overall" performance case for each of the CG location cases (A,B,C and D). The two methods used to identifying this case are described in detail in sections 4.2.3 and 6.2.1. Many parameter studies were performed for the various controllers and the trade-offs in controller designs and parameters were discussed. In some cases, particularly semi-active cases, reducing the accelerations results in significant increase in the displacement responses. Thus, the discussion will revolve around the highest simultaneous acceleration reductions, $\ddot{u}_{1a}, \ddot{u}_{2a}$, ensuring the displacements are within a reasonable limit (<1.5 RMS mm), and the maximum control force is below the 32 N limit. If the percent reductions of the uncontrolled case are within 1% of each other they are given the same ranking. The results are graphed in Fig. 7-1 and tabulated in Table 7-1.

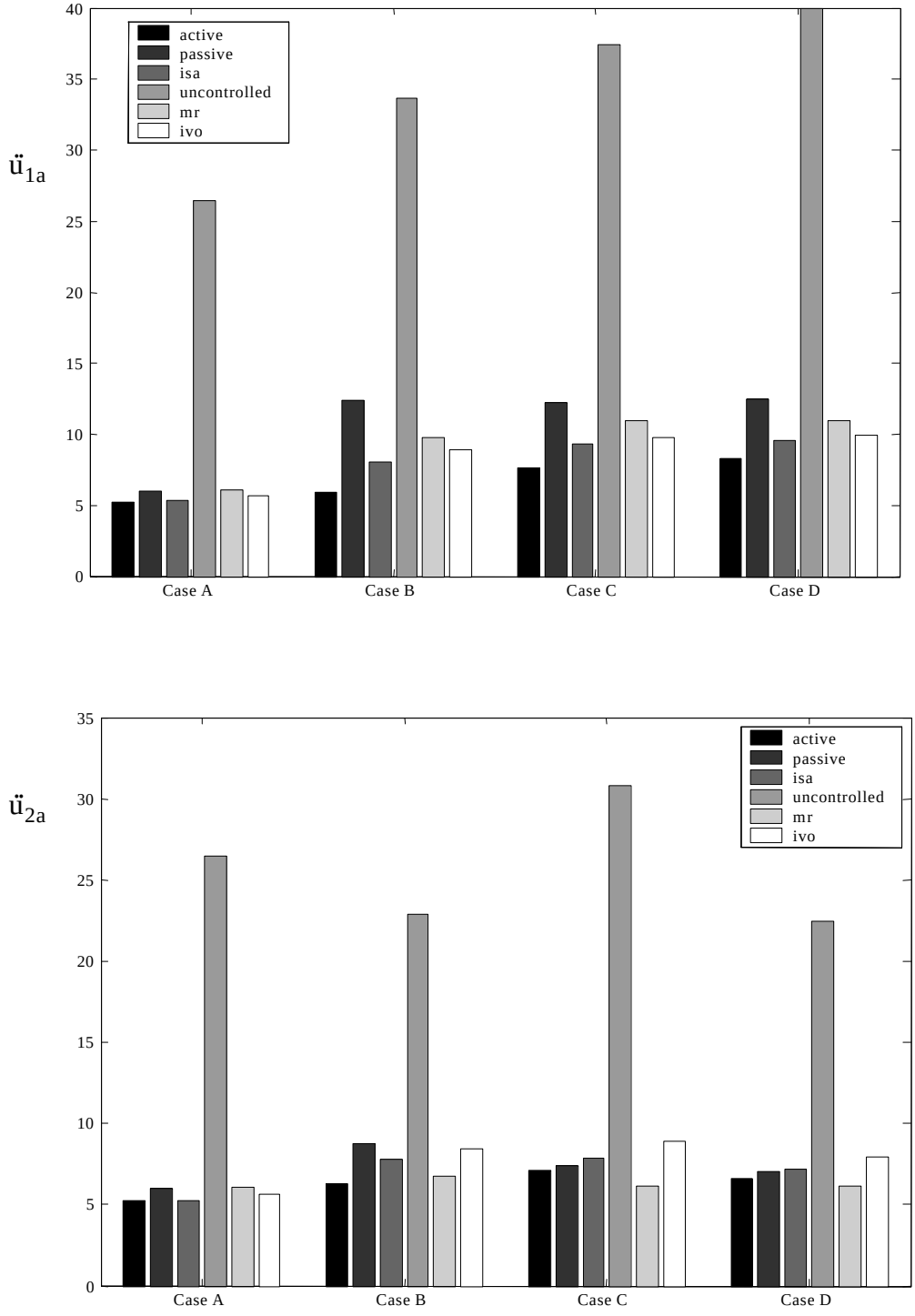

FIGURE 7-1 Comparison of best overall performance absolute accelerations

TABLE 7-1.Best overall performance case comparison: Cases Ai, Bi, Ci, and Di

		Active	Passive	ISA	MR	VO
Case Ai	$\ddot{u}_{1a}$	**2 [80.24%]**	**5 [77.39%]**	**2 [80.01%]**	**5 [77.08%]**	**3 [78.76%]**
	$\ddot{u}_{2a}$	**2 [80.24%]**	**5 [77.39%]**	**2 [80.01%]**	**5 [77.08%]**	**3 [78.76%]**
Case Bi	$\ddot{u}_{1a}$	**1 [82.34%]**	**5 [63.17%]**	**2 [76.03%]**	**4 [71.16%]**	**3 [73.67%]**
	$\ddot{u}_{2a}$	**1 [72.40%]**	**5 [61.66%]**	**3 [65.98%]**	**2 [70.50%]**	**4 [63.20%]**
Case Ci	$\ddot{u}_{1a}$	**1 [79.63%]**	**5 [67.40%]**	**2 [75.05%]**	**4 [70.70%]**	**3 [73.83%]**
	$\ddot{u}_{2a}$	**2 [76.98%]**	**3 [75.84%]**	**4 [74.57%]**	**1 [80.01%]**	**5 [71.17%]**
Case Di	$\ddot{u}_{1a}$	**1 [79.33%]**	**5 [68.89%]**	**2 [76.01%]**	**4 [72.57%]**	**3 [75.21%]**
	$\ddot{u}_{2a}$	**2 [70.62%]**	**4 [68.69%]**	**4 [68.02%]**	**1 [72.71%]**	**5 [64.47%]**

The response power spectra of the accelerations was also compared. The power spectral density (PSD) for the "best overall" performance for the active, passive, and ideal semi-active are in Fig. 7-2 i. and for the MR and VO dampers are in Fig. 7-2 ii, for Case Ai. Included in the figures are the PSDs of the uncontrolled accelerations and the input. Notice the PSD of the input remains relatively constant in the frequency range of interest 0-200 Hz.

Finally, the CG Cases B, C, and D, for this study, moved the CG in the positive x-direction. The uncontrolled accelerations of the left end, $\ddot{u}_{1a}$, were always higher than the uncontrolled accelerations of the right end, $\ddot{u}_{2a}$. Therefore, only the power spectra of the acceleration response of $\ddot{u}_{1a}$ was included for each controller for Cases Bi, Ci, and Di in Fig. 7-3, Fig. 7-4, and Fig. 7-5, respectively.

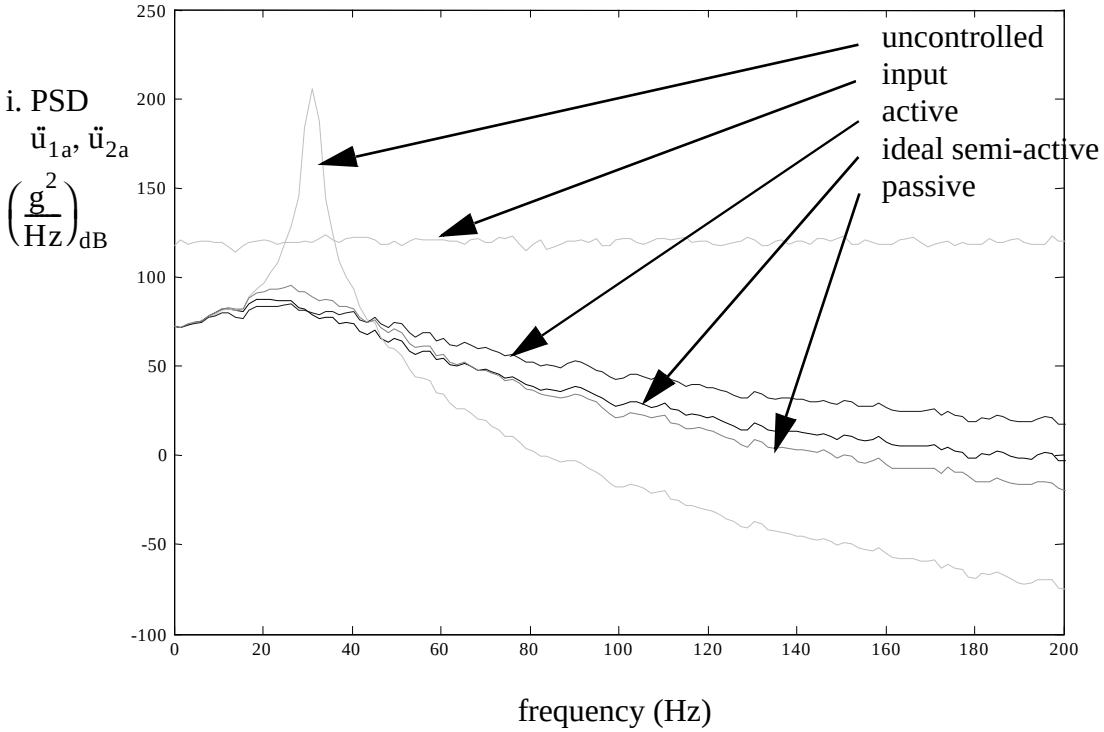

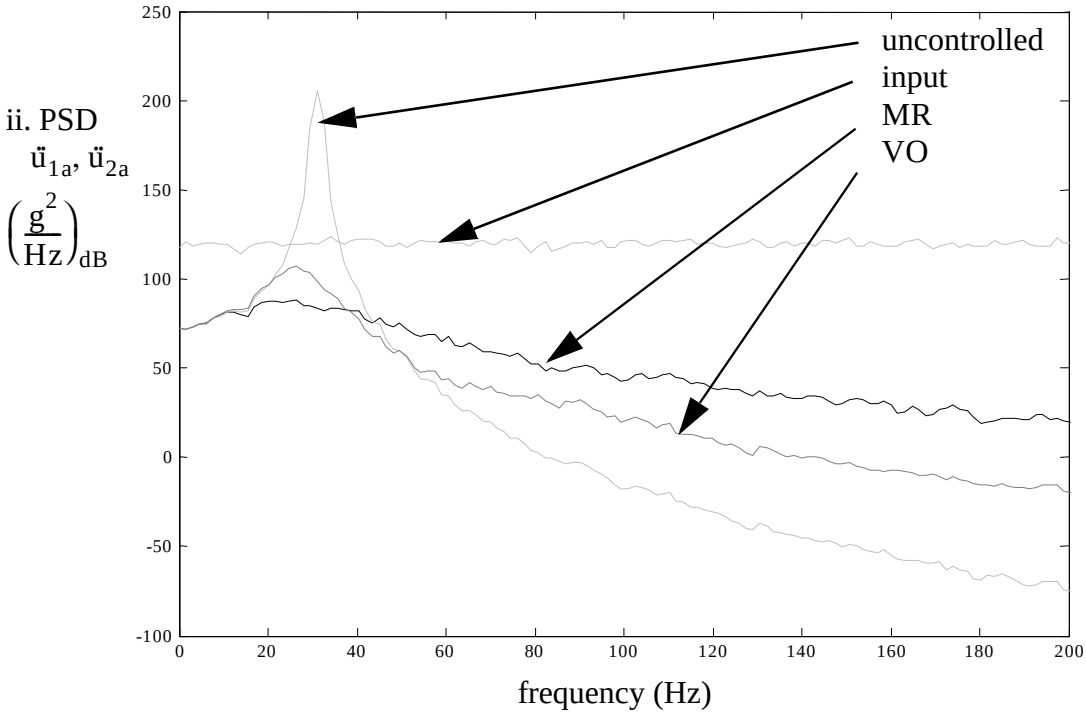

FIGURE 7-2 PSD for input, uncontrolled and controlled Case Ai: i. active, passive, and ideal semi-active ii. MR and VO dampers

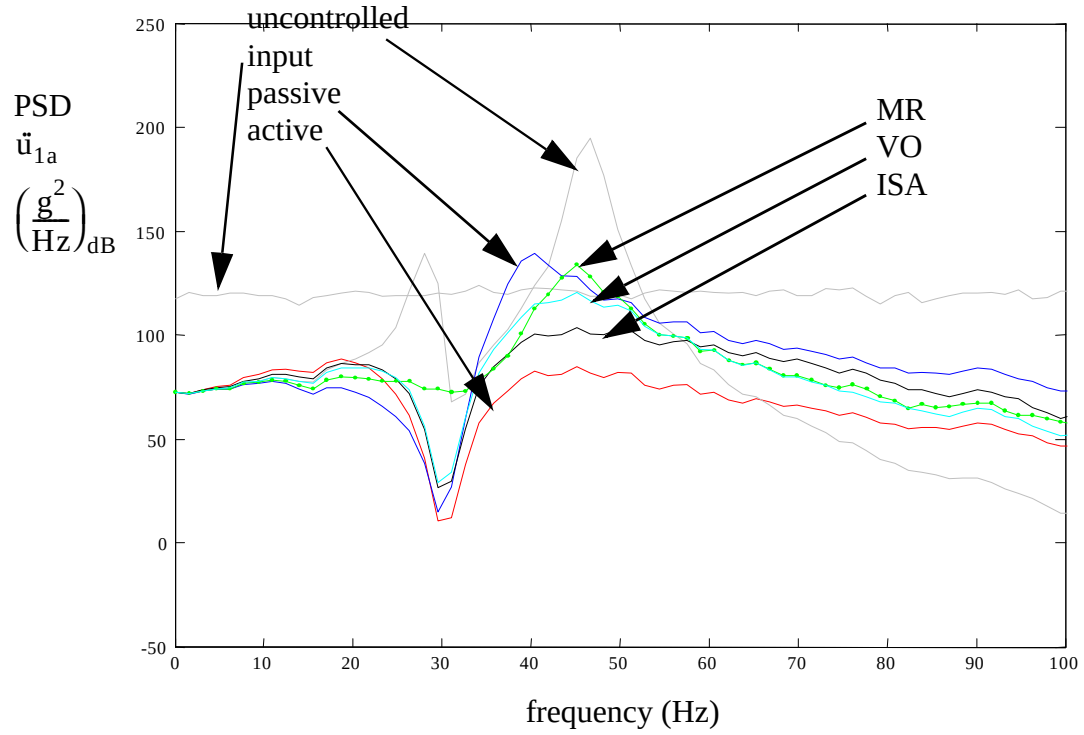

FIGURE 7-3 PSD for input, uncontrolled and controlled: Case Bi

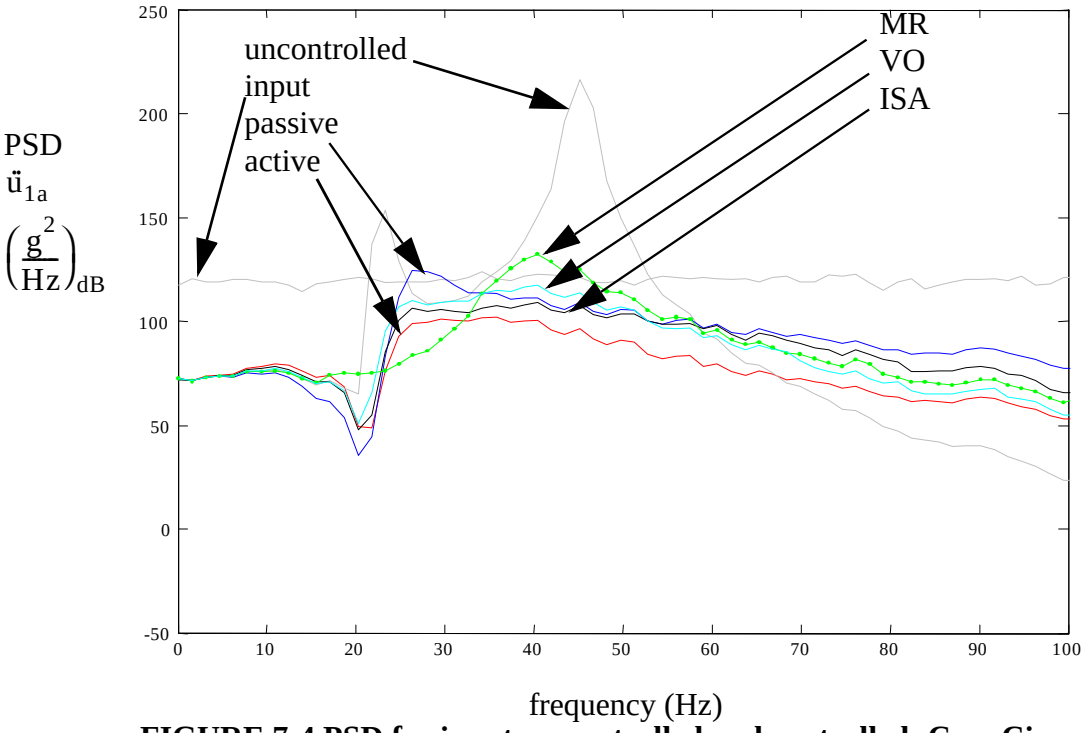

FIGURE 7-4 PSD for input, uncontrolled and controlled: Case Ci

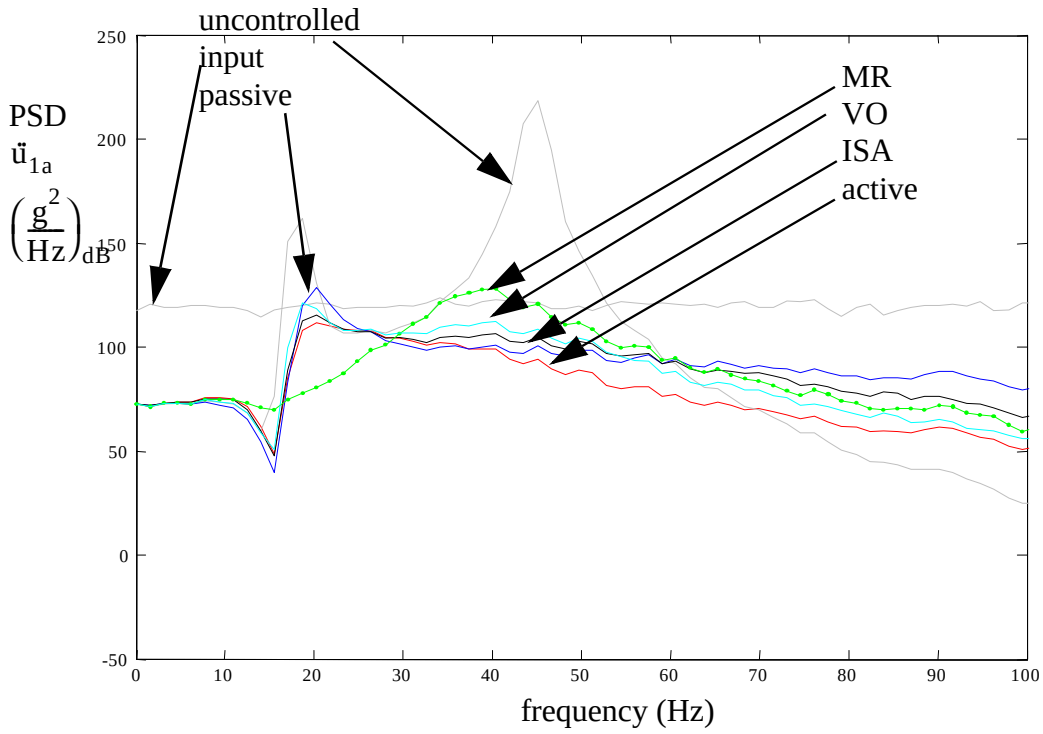

FIGURE 7-5 PSD for input, uncontrolled and controlled: Case Di

7.2 Summary of Numerical Study Results

Discussion of the results in this section will be limited to “the percent reduction” of accelerations of the “uncontrolled” case. The percentage reductions (%red.) will follow the device that produced the reductions with the notation: (%red. $\ddot{u}_a$) when the accelerations of the left and right end are equal; and (%red. $\ddot{u}_{1a}$,%red. $\ddot{u}_{2a}$) for when the accelerations of the left and right ends differ. A summary of the results for each CG location follows:

For Case A all five devices achieved similar results, with the performance varying by only 3.16%. Case A is when the CG is located at the origin. Only one mode, the translational mode is excited. Therefore, the similar acceleration reductions of all the devices for this case was expected. A reduction of up to 80% of the uncontrolled accelerations can be

achieved by the ideal active and ISA damper. The VO damper achieved 79% reductions while the viscous and the MR damper achieved 77% reductions. However, in the frequency domain plots, notice at the peak resonant frequency, the active and ideal semi active was much lower than the uncontrolled and the passive peak in Fig. 7-2 i, and the MR damper reduced the peak more than the VO damper in Fig. 7-2 iii.

In Case B, the active (82%, 72%) achieved the best overall performance. The ideal semi-active (76%, 66%), VO (73%, 63%), and MR (71%) dampers achieved about the same reductions. The previous devices slightly outperformed the passive (63%,62%) damper. The PSD shows the highest reduction of the rotational response was achieved by the active and the highest reduction of the translational response from the passive damper.

For Cases C and D, the highest numerical acceleration reductions for both $\ddot{u}_{1a}$, $\ddot{u}_{2a}$ was achieved by the active device (80%, 77%) and (79%, 71%) respectively. The performance of the semi-active devices were similar for Case C and D: the MR damper (71%, 80%) and (73%), the semi-active device (75%) and (76%, 68%), the VO damper (74%, 71%) and (75%, 65%). Finally, the passive device consistently achieved the least overall reductions (67%, 76%) and (69%, 69%). The MR damper achieved the highest reduction in the PSD translational response. The passive damper had the lowest reduction in the translational PSD response. The active achieved the highest reduction in the rotational response and the MR damper had the lowest reduction in the translational response.

Overall, the active device outperformed the other devices in acceleration reductions. Numerically, the MR damper, ideal semi-active, and VO damper achieved about the same acceleration reductions. All four devices consistently outperformed the passive device, with the exception of Case A. The ideal devices consistently ranked in the same order with the ideal force actuator having similar or better performance than the ideal semi-active, and then the passive for all of the CG location cases. The MR damper demonstrated it could perform as well as, and in a couple cases, better than the ideal devices, numerically.

Chapter 8

Final Remarks

8.1 Summary

Recently, “overcrowding” issues have begun to emerge regarding the limited space in the avionics bays for existing high performance aircraft. With the advances in technology, there is a desire to add more components to these “fixed” spaces. The research presented herein is to test the efficacy of implementing a control system to the avionics thereby, allowing lighter and smaller components. Semi-active controllers control devices do not require a large power supply, do not add much heat or weight, or do not introduce reliability issues, and do not need significant space for the devices and the associated hardware. Due to the nature and environment of the high performance vehicles, these semi-active devices are an attractive choice for this avionics applications.

A two-degree-of-freedom model of the avionics was formed. Models of the five control devices considered were adopted for the avionics systems for numerical comparisons. The five control devices consisted of three ideal device models: active force actuator, a linear viscous device, and an ideal semi-active device, and two actual device models: the MR

and VO dampers. The baseline comparison showed the semi-active actual device models performed as well as, and in some cases better than, ideal active, semi-active and passive models numerically in acceleration reductions. These results indicate that “smart damping” is a good candidate for the control system of avionics packages with the lower natural frequency and further investigations should be made.

8.2 Conclusions

The conclusions from the comparison of the results are as follows: high acceleration reductions can be made compared to the “uncontrolled” case for all five devices. The active consistently achieved the highest acceleration reductions for all four CG location cases. The next best performance was achieved by the ISA damper. The VO and MR dampers achieved similar results and achieved more reductions in accelerations than the passive dampers. The actual device models performed, as well as, and in some cases better than the ideal models.

For Case Ai, all the devices performed about the same in acceleration reductions, but this was expected since only one mode of vibration was excited. The “best overall” acceleration reductions, for the other CG cases, was achieved by active controller. However, for existing active control devices they require a large supplemental power supply. This requirement alone disqualifies it as a serious candidate for the avionics control system.

Overall, the semi-active controllers performed similarly in the amount of acceleration reductions, and the MR damper achieved higher acceleration reductions is a couple cases than the active controller. The semi-active models all outperformed the passive device. Recall, all the models were of ideal devices and control algorithms except for the MR and VO dampers. An ideal model is expected to have better results numerically than actual models, however, this was not the case for this study. This indicates the MR and VO

dampers results should be compared to the devices with more of the dynamics of the physical devices included. Numerical studies that include the dynamics of the ideal devices should be investigated experimentally and compared to the findings in this study.

The parametric studies performed for the highest acceleration reductions of the individual outputs indicated better performance may be achieved simultaneously by multiple controllers. Also, the results indicate the semi-active dampers can achieve much higher reductions at the different control force locations than the passive device. Therefore, multiple controllers should be implemented in the numerical studies to investigate if the acceleration reductions can be achieved simultaneously.

The control force Case i, with the exception of the MR damper, achieved the most acceleration reductions of both ends simultaneously. The MR damper, numerically achieved better acceleration reductions for both ends when the control force was located at or near the CG location for the Cases Ai, Bii, Ciii, and Div. Thus, this finding should be experimentally verified.

8.3 Future Research

Future research should focus on the experimental verification and comparison with the numerical results presented herein. A prototype of a 7 lb (31.137 N) magnetorheological (MR) damper from Lord corporation has been successfully tested, modeled, and verified in the Washington University Structural Control and Earthquake Engineering Laboratory by Yi and Dyke (2001) for Seismic Response Control in Civil Engineering Applications. The limiting maximum control force for this study was selected based on this device. The device will be used in the experimental verification of the numerical studies. An experimental apparatus has been designed and constructed for initial testing of the two degree of freedom system in Chapter 2 and shown in Fig. 8-1.

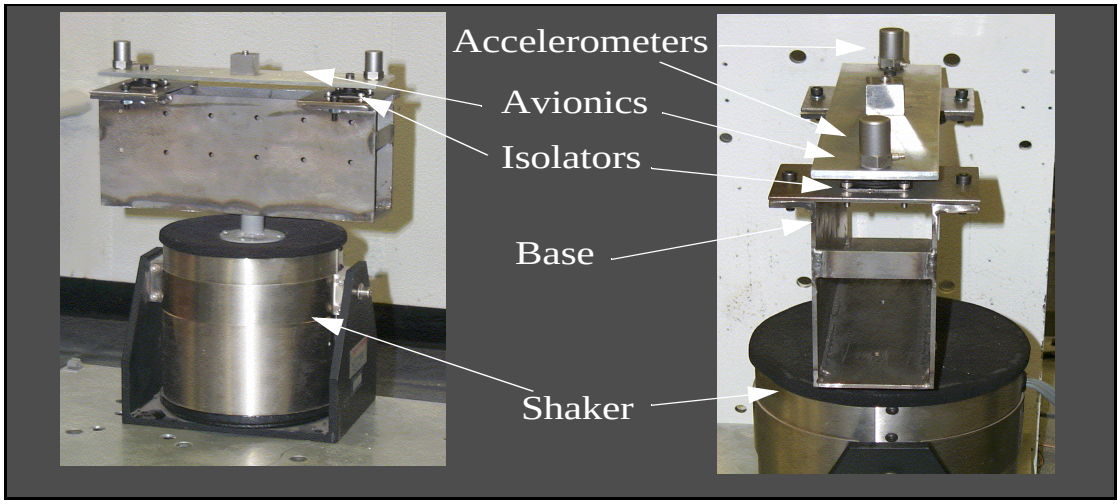

FIGURE 8-1 Experimental apparatus for 2DOF avionics

This design are the location of the center of mass and the control force can be varied. The "top" mass is bolted to the "bottom" mass various attachment locations have been included in the design. The location of the controller can also be varied. Holes were drilled at different locations allowing the control force attachment to be varied. Two accelerometers were placed on each end of the avionics to measure the accelerations. The steel plate and top mass represent the avionics. The accelerations of the avionics are measured with accelerometers. The total mass of the avionics is 1.5876 kg. The control device will be placed in parallel with the existing isolation mounts. Two lightly damped isolators (donated by Lord Corporation) were selected, each with stiffness of k1 = 12 N/ mm and k2 = 12 N/mm, to produce a natural frequency of 19 Hz in the vertical mode. Highly damped isolators (donated by Barry Controls) will be used in the experimental verification for comparison of the passive numerical results. (The force to weight ratio is 2)

The 100 lb-f electrodynamic shaker is attached directly to the base. The base acts as the racks in the avionics bays and the isolators are attached directly to the bays and to the

avionics. The shaker imparts the random exogenous vibrations to the avionics. Control will be achieved using a real-time DSP-based control system available in the laboratory.

The numerical results have indicated high acceleration reductions can be achieved with “smart damping”. Thus, the performance presented herein will be compared with experimental verification. After which, six-degree-of-freedom model will be experimentally and numerical developed and tested. Other steps in the research should include the dynamics in the ideal devices for a more realistic future numerical comparisons. Also, numerical and experimental studies should be performed for multiple control devices and compared. Larger and heavier avionics models should also be investigated.

References

[1] Brogan, W.L. (1991). *Modern Control Theory*, Prentice Hall, Englewood Cliffs, New Jersey.

[2]. K. Burnham, D. M. Pitt, D. A. Henderson and R. W. Moses, An Advanced Buffet Load Alleviation System , *42nd AIAA/ASME/ASCE/AHS/ASC Structures, Structural Dynamics, and Materials Conference*, Seattle, Washington, AIAA 2001-1666, April 16-19, 2001, pp. 10, (2.1MB PS, 1.3MB PDF).

[3] Chopra, Anil, K. (1995). Dynamics of Structures, Prentice Hall, Upper Saddle River, New Jersey.

[4] Constantinou, M.C., Symans, M.D. Tsopelas, P. and Taylor, D.P., "Fluid Viscous Dampers in Applications of Seismic Energy Dissipation and Seismic Isolation**,**" Proceedings, ATC-17-1 *Seminar on Seismic Isolation, Passive Energy Dissipation, and Active Control.* March 1993. San Francisco. CA.

[5] Dyke, S.J., Spencer Jr., B.F., Quast, P., Sain, M.K., Kaspari Jr., D.C. and Soong, T.T. (1996a). "Acceleration Feedback Control of MDOF Structures," *J. of Engrg. Mech., ASCE*, Vol. 122, No. 9, pp. 907–918.

[6] Dyke, S.J., Spencer Jr., B.F., Quast, P., Kaspari Jr., D.C., and Sain, M.K. (1996b). "Implementation of an AMD Using Acceleration Feedback Control," *Microcomputers in Civil Engrg.*, Vol. 11, pp. 305–323.

[7] Dyke, S.J., Spencer Jr., B.F., Sain, M.K., and Carlson, J.D. (1996e). "Experimental Verification of Semi-Active Structural Control Strategies Using Acceleration Feedback," *Proc. of the 3rd Intl. Conf. on Motion and Vibr. Control*, Vol. 3, pp. 291–296, Chiba, JAPAN, September.

[8] Dyke, S.J. and Spencer Jr. B.F. (1997). "A Comparison of Semi-Active Control Strategies for the MR Damper," *Proc. of the IASTED Intl. Conf. on Intelligent Info. Systems*, pp. 580–584, Bahamas, December 8–10.

[9] Dyke, S.J., Spencer Jr., B.F., Sain, M.K., and Carlson, J.D. (1998). "An Experimental Study of MR Dampers for Seismic Protection," *Smart Materials and Structures: Special Issue on Large Civil Structures*, Vol. 7, pp. 693–703.

[10] Jansen, L.M. and Dyke, S.J. (1999). "Investigation of Nonlinear Control Strategies for the Implementation of Multiple Magnetorheological Dampers," *Proceedings of the 1999 ASCE Engineering Mechanics Conference*, Baltimore, Maryland, June 16, 1999.

[11] Jansen, L.M. and Dyke, S.J. (2000). “Semi-Active Control Strategies for MR Dampers: A Comparative Study,” *J. Engrg. Mechanics.*

[12] Kawashima, K., (1992). “Experiments on Dynamics Characteristics of Variable Damper’, *Proc. Japan Nat. Symp. on Struc. Resp. Cont.*, pp.121.

[13] Kurata, N, Kobori, T., Takahashi, M., Niwa, N., and Midorikawa, H. (1999). “Actual Seismic Response Controlled Building with Semi-Active Damper System,” *Earthquake Engineering and Structural Dynamics*, 28, 1427-1447.

[14] Kwakernaak, H., and Sivan, R. (1972), *Linear Optimal Control Systems*, John Wiley & Sons Publishing, Edison, New Jersey.

[15] Lopez, Donald S. (1995) (in association with the National Air and Space Museum), Washington, D.C. *Aviation - A Smithsonian Guide*. A Prentice Hall Macmillan Company. New York, New York.

[16] MATLAB (1999). The Math Works, Inc. Natick, Mass.

[17] Meirovitch, Leonard (1996). *Elements of Vibration Analysis*, McGraw-Hill.

[18] Mizuno, T., Kobori, T., Hirai, J., Matsunaga, Y., and Niwa, N. (1992). “Development of Adjustable Hydraulic Damper for Seismic Response Control of Large Structure,” *ASCE PVP Conf.*, Vol. 229, pp. 163-170.

[19] Moses, R.W., Huttsell, L., “Fin Buffeting Features of an Early F-22 Model,” *AIAA 2000-1695, 41st AIAA/ASME/ASCE/ASC Structures, Structural Dynamics, and Materials Conference and Exhibit*, Atlanta, GA, April 2000.

[20] Moses, R.W., Carol D. Wieseman, Aaron A. Bent and Alessandro E. Pizzochero, Evaluation of New Actuators in a Buffet Loads Environment , *SPIE's 8th International Symposium on Smart Structures and Materials*, Newport Beach, California, March 4-8, 2001, (805KB PS, 463KB PDF).

[21] Nitzsche, F., Zimcik, D., Ryall, T., Moses, R., Henderson, D., (1999). “Control Law Synthesis for Vertical Fin Buffeting Alleviation Using Strain Actuation,” *40th AIAA/ASME/ASCE/AHS/ASC Structures, Structural Dynamics, and Materials Conference*, St. Louis, Missouri, AIAA 99-1317, April 12-15,1999.

[22] Patten, W.N., Mo, C., Kuehn, J., and Lee, J. (1998a). “A Primer of Design of Semi-active Vibration Absorbers (SAVA)’, *Journal of Enginering Mechanics,* ASCE 124(1), 61-68.

[23] Patten, W.N. (1998b). “The I-35 Walnet Creek Bridge: An intelligent highway bridge via semi-active structural control’, *Proc. of 2nd World Conf. on Structural Control*, Vol. 1, pp. 427-436.

[24] Oh, H-U., Onoda, J., and Minesugi, K. (2000). “Characteristics of a Liquid-Crystal Type ER-Fluid Variable Damper for Semiactive Vibration Suppression,” *ASME Journal of Vibration and Acoustics*, Vol. 122, October, pp.412-419.

[25] Onoda, J., Endo, T., Tamaoki, H., and Watanabe, N. (1991). “Vibration Suppression by Variable Stiffness Members,” *AIAA Journal*, Vol. 29, No. 6, June, pp. 977-983.

[26] Onoda, J. and Minesugi, K. (1996). “Semi-Active Vibration Suppression by Variable Damping Members,” *AIAA Journal*, Vol. 34, No. 2, February, pp. 335-361.

[27] Onoda, J., Oh, H-U., and Minesugi, K. (1997). “Semi-Active Vibration Suppression of Truss Structures by Electrorheological-Fluid,” *Acta Astronautical Journal*, Vol. 40, No. 11, pp. 771-779.

[28] Onoda, J., Oh, H-U., and Minesugi, K. (1997). “Semi-Active Vibration Suppression with Electrorheological-Fluid Dampers,” *AIAA Journal*, Vol. 35, No. 12, December, pp. 1844-1852.

[29] Onoda, J., Oh, H-U., and Minesugi, K. (2000), “Improved Electrorheological-Fluid Variable Damper for Semi-Active Vibration Suppression,” *AIAA Journal*, Vol. 38, No. 9, September, pp. 1736- 1742.

[30] Sack, R.L. and Patten, W. (1994). “Semiactive Hydraulic Structural Control.” *Proceedings of the International Workshop on Structural Control*, USC Publication Number CE-9311, pp. 417–431.

[31] Ramallo, J.C., Johnson, E. A., and Spencer, B.F., Jr. (2001). “Smart” Base Isolation Systems,” *ASCE Journal of Engineering Mechanics (submitted)*.

[32] SIMULINK. The Math Works, Inc. Natick, Mass.

[33] Spencer Jr., B.F., Dyke, S.J., and Sain, M. K.,(1995), “Experimental Verification of Acceleration Feedback Control Strategies for Seismic Protection,” *Proceedings of the Japanese Society of Civil Engineers 3rd Colloquium on Vibration Control of Structures,* Tokyo, Japan, August 7-8, 1995, Part A, pp. 259-265.

[34] Spencer Jr., B.F., Dyke, S.J., Sain, M.K., and Carlson, J.D., (1997c). “Phenomenological Model for Magnetorheological Dampers, “*Journal of Engineering Mechanics*, ASCE, Vol. 123, No. 3, pp 230-238.

[35] Spencer Jr., B.F. and Sain, M.K. (1997). "Controlling Buildings: A New Frontier in Feedback," *IEEE Control Systems Magazine: Special Issue on Emerging Technologies* (Tariq Samad Guest Ed.), Vol. 17, No. 6, pp. 19-35.

[36] Stavrodou, V. (1999). "Provably Dependable Software Architectures for Adaptable Avionics," *Proceedings of the 18th Digital Avionics Systems Conference.*

[37] Symans, M.D. and Constantinou, M.C. (1995). "Development and Experimental Study of Semi-Active Fluid Damping Devices for Seismic Protection of Structures," *Technical Report NCEER-95-0011*.

[38] Yi, F., Dyke, S.J., Caicedo, J.M., and Carlson, J.D. (Nov. 2001). "Experimental Verification of Multi-Input Seismic Control Strategies for Smart Dampers," *Journal of Engineering Mechanics*.

[39] Yoshioka, O., S.J. Dyke (2001). "Seismic Control of a Nonlinear Benchmark Building Using Smart Dampers," (*submitted*).

VITA

Suzy M. Hyun

EDUCATION

University of Illinois- Urbana-Champaign, *Urbana-Champaign, Missouri*, B.S. Aeronautical and Astronautical Engineering (December, 1999)

Washington University, *St. Louis, Missouri*, M.S. Civil Engineering (December, 2001)

AWARDS

Research for Undergraduates Experience (REU) Award from National Science Foundation (NSF)

Graduate Research Assistanship, Washington University, 2000-2001.

Affiliations

American Institute of Aeronautical and Astronautical Engineering (AIAA)

American Society of Civil Engineering (ASCE)

Earthquake Engineering Research Institute (EERI)

December 2001

Short Title: Control Development for Avionics Suzy M. Hyun, M.S. 2001